ALEPH 90-189
PHYSIC 90-116
L. Rolandi et al.
19.12.1990

Measurement of the cross section and forward backward asymmetry for the process

$$e^+e^- \rightarrow \tau^+\tau^-$$

G. Apollinari, G. Bagliesi, I. Ferrante, B. Gobbo, P.S. Marrocchesi,
L. Rolandi, L. Silvestris

December 19, 1990

Abstract

We discuss the measurement of the cross section and forward backward (F-B) asymmetry for the process $e^+e^- \rightarrow \tau^+\tau^-$ on the 1990 data. The statistical error of both measurements at the peak is 1.6%. The systematic error on the cross section due to the background subtraction is 0.5% and the systematic error on the efficiency is 0.8%. The selection has an acceptance of 0.858 and an efficiency of 0.854 inside this acceptance. The systematic error on the F-B asymmetry at the peak is 0.3%. With the same program we have also recalculated the cross sections and the F-B asymmetries on the 1989 data.

1 Introduction

In this note we describe the analysis done to measure the cross section of the process $e^+e^- \rightarrow \tau^+\tau^-$ and its F-B asymmetry. In section 2 we list the cuts used to select $\tau^+\tau^-$ events and we count the events at the 7 energy points of the 1990 scan around the Z peak. In section 3 we discuss the background subtraction and in section 4 the determination of the selection efficiency. In section 5 we compute the cross sections. The measurement of the F-B asymmetry is discussed in section 6.

The list of the Data files used in this analysis is given in Appendix.

2 Definitions, cuts and $\tau^+\tau^-$ events selection

The $e^+e^- \rightarrow \tau^+\tau^-(\gamma)$ events are selected from the "common lepton" sample. The selection is done in two steps: first we define an almost pure sample of $Z \rightarrow l^+l^-$ events (the "common lepton sample"), then we apply specific cuts to eliminate $Z \rightarrow e^+e^-$ and $Z \rightarrow \mu^+\mu^-$ events.

The cuts are listed at the end of this section and are numbered from 1 to 15.

The acceptance of the selection si defined by the cuts on the acollinearity (cut 4) and on the scattering angle (θ^*) of the τ^- with respect to the electron computed in the reference frame of the centre-of-mass of the two incident particles (cut 5). This angle is computed in the assumption that at most one hard photon is emitted from the initial lines; in this case it depends only on the polar angle of the two τ's measured in the laboratory frame:

$$\cos\theta^* = \cos\frac{1}{2}(\theta_- + \pi - \theta_+) \;/\; \cos\frac{1}{2}(\theta_- - \pi + \theta_+), \qquad (1)$$

The polar angles of the τ's cannot be measured since they decay very close to the production vertex. We measure instead the "jets" of the charged particles produced in their decay and we approximate the τ scattering angle with the "jet" scattering angle. This approximation does not introduce any important error in the evaluation of the cross section , but introduces a correlation between the "acceptance" and the "selection efficiency" since the decay product of the τ's not always can be detected. A fraction of about 1.2% of the events with the τ's produced inside the acceptance is lost because we do not detect the decay product of one of the τ's. This is discussed in section 4.3.

The angular acceptance of the TPC (cut 1) does not reduce the acceptance defined by cuts 4 and 5 since the largest possible value of $\cos\theta$ for an event with $|\cos\theta^*| < .9$ and $\cos\eta < -0.9397$ is 0.94 and cut 1 corresponds $|\cos\theta| < 0.96$.

The common lepton sample is defined using a set of cuts designed to eliminate hadronic events and $\gamma\gamma$ events. The hadronic events are rejected by the requirement of low charged track multiplicity (cut 2) and collimation of the reconstructed "jets" (cut 6). The $\gamma\gamma$ events are rejected by a set of kinematical cuts (cuts from 7 to 10) and also by the acollinearity cut. Cosmic rays are rejected by requiring the timing with the ITC and excluding events with large impact parameter respect to the known beam's position (cuts 11 and 12). Fig from 1 to 2 show some plots of the relevant variables used in the common lepton selection.

To separate $e^+e^- \rightarrow \tau^+\tau^-$ we reject e-pair and μ-pair events. We have tried to design a selection using the minimum number of cuts in order to simplify the study of the sistematics. The main cut is cut n. 14, the missing mass cut (see fig 6): we identify tau events through the invariant mass of the two (unseen) neutrinos produced in the decay of the two tau's which is large. Moreover we use only charged tracks. μ-pair and e-pair events have missing mass $\sim$0 also when one radiative photon is present in the initial or final state.

The cut on the sum of the energies of the charged tracks (cut 13) provides a guarantee that we do not fake large missing mass in events with bad measured tracks. Fig. 7 shows the correlation between the missing mass cut and the sum of the energies for events that pass the common lepton selection at $\sqrt{s} = M_z$. We notice that events with measured energy much larger than $\sqrt{s}$ can have large missing mass. This cut rejects only 3 events among $\sim$ 4000 $\tau^+\tau^-$ candidates.

A consistent fraction of e^+e^- events has two photons in the final state. These events can have large missing mass. To reduce this background to a neglegible level we introduce the cut on the total ECAL energy (cut 15).

These cuts are applied to class-15 events. The influence of class 15 cuts on the selection is discussed in section 4.

1. A track must have at least 4 coordinates measured in the TPC (this cut limits the geometrical acceptance to $\sim| \cos\theta |< 0.96)$, have momentum exceeding 0.1 GeV/c, and originate from the beam-crossing within $\pm$10 cm along the beam direction and 5 cm in the transverse direction.(This cut is superseeded by the class 15 cut of 2 cm in the transverse direction).

2. The event is required to have more than one and less than seven tracks.

$$\mathbf{2} \leq N_{track} \leq \mathbf{6}$$

3. The event, divided into two hemispheres by a plane perpendicular to the thrust axis, has to have at least one track in each hemisphere. We call "jet" the set of the tracks in each hemisphere. With this definition all events are two-jets events.

4. The angle η between the vector sums of the momenta in each emisphere has to be larger than 160°.

$$\cos\eta \leq \mathbf{-0.9397}$$

5. The event has to satisfy $-0.90 < \cos\theta^* < 0.90$.

6. Events are rejected if any of the tracks makes an angle θ_{jt} with the vector sum of the track momenta in the same hemisphere, that gives

$$\cos\theta_{jt} \leq \mathbf{0.95}$$

.

7. At least one track must have a momentum larger than 3 GeV/c.

$$P_{max} \geq 3$$

8. The transverse momentum relative to the beam of the vector sum of the tracks in each hemisphere (the jet transverse momentum) must be larger than 2.5 GeV/c in at least one of the two hemispheres.

$$\mathbf{P^{\perp}_{max} \geq 2.5}$$

9. In two-track events with both momenta below 6 GeV/c, the ratio of transverse momenta with respect to the beam has to differ from unity by more than 15%.

10. The centre-of-mass energy of the reconstructed charged tracks W, calculated assuming pion masses, has to be larger than 4.5 Gev

$$\mathbf{W \geq 4.5}$$

11. In two-track events at least one track has to originate from the beam-crossing within 1 cm in the transverse direction and 5 cm in the direction along the beam.

$$d0_{min} < 1.\text{AND.} \mid Z0_{min} \mid < 5$$

12. The sum of the ITC coordinates associated to all tracks must be larger than 3.

13. The sum of the energies of the tracks (assuming pion masses) has to be smaller than $100(2 * E_{beam}/M_Z)$GeV.

14. The square of the missing mass calculated from the tracks (assuming pion masses) and the known centre-of-mass energy is required to exceed 400GeV^2 .

$$\mathbf{MM^2 \geq 400\frac{4E_{beam}^2}{M_Z^2}GeV^2}$$

15. The ECAL energy, measured with the wires (PEWI bank) must be smaller than 55Gev.

$$\mathbf{E_{wires} \leq 55\frac{2E_{beam}}{M_Z}GeV}$$

Those cuts have been applied to the 1990 data (the run list is given in the appendix) and the number of selected events are reported in table 1.

3 Background subtraction

The various background contributions are discussed in the following subsections. Here the final results in the tables 2 and 3 are summarized. The number of events at each energy point after the background subtraction are listed in the tables 4 and 5. The main background is due to $Z \rightarrow$ *hadrons* events. This has been studied comparing data and Monte Carlo prediction as described in section 3.2.

Table 1: Number of events selected by the common-lepton and by the tau selections at each energy. The error on the luminosity is statistical.

$\sqrt{s}$ (GeV)	common lepton	tau	$\mathcal{L}^{\rm int}$ $\rm nb^{-1}$
88.2	589	68	479±4
89.2	955	158	517±4
90.2	1375	302	444±4
91.2	15435	4144	3629±12
92.2	1608	449	552±5
93.2	1064	257	593±5
94.2	820	203	637±5

Table 2: Background events to be subtracted from tau selection at each energy.

$\sqrt{s}$	$\gamma\gamma$	$q\bar{q}$	cosmic	e^+e^-	$\mu^+\mu^-$	total
88.2	4.7± 0.9	1.3± 0.4	0.3± 0.3	3.3± 0.8	0.1± 0.1	9.8± 1.3
89.2	5.1± 1.0	2.5± 0.7	0.3± 0.3	4.9± 1.2	0.3± 0.2	13.1± 1.7
90.2	4.4± 0.8	4.7± 1.3	0.5± 0.3	5.2± 1.2	0.5± 0.3	15.4± 2.0
91.2	35.6± 6.8	61.6±17.0	3.8± 1.0	45.0± 6.4	6.6± 4.4	152.5± 20.0
92.2	5.5± 1.0	6.2± 1.7	0.5± 0.3	5.6± 1.2	0.7± 0.4	18.5± 2.4
93.2	5.9± 1.1	4.6± 1.3	1.0± 0.5	5.5± 1.3	0.5± 0.3	17.5± 2.2
94.2	6.3± 1.2	2.9± 0.8	0.5± 0.5	4.2± 0.9	0.3± 0.2	14.3± 1.8

Table 3: Background events to be subtracted from common lepton selection at each energy.

$\sqrt{s}$	$\gamma\gamma$	$q\bar{q}$	cosmic	total
88.2	4.7± 0.9	1.5± 0.4	0.3± 0.3	6.5± 1.0
89.2	5.1± 1.0	2.9± 0.8	0.3± 0.3	8.3± 1.3
90.2	4.4± 0.8	5.4± 1.4	0.5± 0.3	10.3± 1.7
91.2	35.6± 6.8	69.8±18.7	3.8± 1.0	109.2± 19.9
92.2	5.5± 1.0	7.0± 1.9	0.5± 0.3	13.0± 2.2
93.2	5.9± 1.1	5.2± 1.4	1.0± 0.5	12.1± 1.9
94.2	6.3± 1.2	3.3± 0.9	0.5± 0.5	10.1± 1.6

Table 4: Number of $Z \rightarrow \tau^+\tau^-$ background subtracted at each energy.

$\sqrt{s}$	tau	bkg	tau bkg subtracted
88.2	68	9.8± 1.3	58.2± 8.3
89.2	158	13.1± 1.7	144.9± 12.7
90.2	302	15.4± 2.0	286.6± 17.5
91.2	4144	152.5± 20.0	3991.5± 67.4
92.2	449	18.5± 2.4	430.5± 21.3
93.2	257	17.5± 2.2	239.5± 16.2
94.2	203	14.3± 1.8	188.7± 14.4

Table 5: Number of common-lepton events background subtracted at each energy.

$\sqrt{s}$	common lepton	bkg	common lepton bkg subtracted
88.2	589	6.5± 1.0	582.5± 24.3
89.2	955	8.3± 1.3	946.7± 30.9
90.2	1375	10.3± 1.7	1364.7± 37.1
91.2	15435	109.2± 19.9	15325.8± 125.8
92.2	1608	13.0± 2.2	1595.0± 40.2
93.2	1064	12.1± 1.9	1051.9± 32.7
94.2	820	10.1± 1.6	809.9± 28.7

3.1 $\gamma\gamma$ background

The following background cross sections are obtained by applying the common-lepton selection procedure on the Monte Carlo files:

	Selected events	Cross section (pb)
$e^+e^- \to e^+e^-e^+e^-$	29	5.3 ± 1.0
$e^+e^- \to e^+e^-\mu^+\mu^-$	53	5.5 ± 0.8
$e^+e^- \to e^+e^-\tau^+\tau^-$	35	0.9 ± 0.1
$e^+e^- \to e^+e^-q\bar{q}$ (u,d)	1	~ 0
$e^+e^- \to e^+e^-q\bar{q}$ (s)	0	~ 0
$e^+e^- \to e^+e^-q\bar{q}$ (c)	1	~ 0

The contribution of $e^+e^- \to e^+e^-q\bar{q}$ is negligible. The total contribution of $e^+e^- \to e^+e^-l^+l^-$ is 11.7 ± 1.3 pb , where the error is only the Monte Carlo statistical error. The tau selection accepts all the remaining background events.

Before studing the consistency between Monte Carlo prediction and data we have to verify the efficiency of the trigger on $\gamma\gamma$ events. This has been done on all events passing cuts 1, 2 and 3. We define a trigger flag for each jet. This is done by computing the entry points of the good tracks in each jet both in ECAL and HCAL and looking for a match between the fired ECAL (or HCAL) trigger segment and the geometrically corresponding ITC segment. The presence of this match sets the trigger flag for the jet to which the track belongs.

Fig. 10 summarizes the trigger information as a function of W. As can be seen, there are events where apparently none of the jets trigger fired. Those events are actually triggered by a "bad" track (i.e. a track failing cut 1) that does not fall within our "jet trigger" definition. Anyhow, these events are concentrated at low values of W and do not affect our selection. There is a considerable number of events where only one of the jets fires the trigger.

Fig. 11 shows the ratio between events in which both jets triggered and the total number of events as a function of W. A cut at $W > 4.5$ GeV assures a very high efficiency. In particular, in the region $4.5 < W < 10$ GeV we have a trigger efficiency of 97.8% (2693 "jet triggered events" out of a total of 2814).

In order to verify the Monte Carlo simulation, we compared Monte Carlo predictions and data in a region of the phase-space where the $\gamma\gamma$ production is dominant. First we define a sample of data that includes essentially all $\gamma\gamma$ and leptonic events. This is done by applying the cuts 1,2,3,5,6,11 and 12.

$$\text{CUT A} = 1.\text{and}.2.\text{and}.3.\text{and}.5.\text{and}.6.\text{and}.11.\text{and}.12.\text{and}.10$$

By adding cut 10 ($W > 4.5$ GeV) we can assume that the trigger efficiency is $\sim 100\%$. To add this cut is also important because the Monte-Carlo files have been generated with W>4 GeV. This enables us to compare data and Monte Carlo predictions without any correction for trigger efficiency and for partial simulation.

In addition to these cuts, the following cuts are applied to reject the leptonic events and the remaning hadronic events:

$$\text{CUT B} = \text{W.lt.25 .and. } N_{\text{track}}\text{.eq.2 .and. } E_{\text{wires}}\text{.lt.15}$$

The Monte Carlo computed efficiency of CUT B is 91% for $e^+e^-e^+e^-$ final state, 97% for $e^+e^-\mu^+\mu^-$ and 70% for $e^+e^-\tau^+\tau^-$. The total efficency of CUT B on the $\gamma\gamma$ sample is $\sim$ 92% Since these efficiencies are high, the bias introduced by these additional cuts is small.

Fig 12 shows the Monte Carlo predicted cross sections as a function of $\cos\eta$ for $\gamma\gamma$ and Z events after A*B. The background to the $\gamma\gamma$ production in the region $\cos\eta > -0.95$ is predicted to be very small ($\leq 1\%$) and to be due to $Z \to \tau^+\tau^-$ only.

Fig 13 shows the measured cross section for the cuts

$$\text{A.and.B.and.}\cos\eta > -0.95$$

at 7 centre-of-mass energies. The fit of a constant to the measured cross sections gives a χ^2/dof of 2.1 . The measured cross section of 128 ± 4 pb is to be compared with the Monte Carlo prediction of 143 ± 4 pb. Fig 14 shows the angular distribution of the selected events and the prediction of the Monte Carlo. No particular bias is observed.

In order to study the trend of the simulation at small values of $\cos\eta$, we compared Monte Carlo predictions with data taken at 88.28, 89.28 and 94.28 GeV (corresponding to a luminosity of $\sim$ 1616 nb^{-1}). Here the Z background is smaller. Fig 15 shows the number of events passing the previous selection as a function of $\cos\eta$ together with the Monte Carlo prediction for $\gamma\gamma$ events and for Z decays. In the first bin ($\cos\eta < -0.95$) there are 136 events in the data. The Monte Carlo predicts 102 events from $\gamma\gamma$ and 54 events from Z decays. The predicted cross section for $\gamma\gamma$ is 63 ± 2 pb and the measured cross section , after the subtraction of the Z decays, is 51 ± 7 pb. The agreement is at 1.5 standard deviations.

Another test was performed to check the effect of the remaining cuts applied in the common-lepton selection against $\gamma\gamma$ events . The common-lepton selection has been modified inverting cut 4 ($\cos\eta > -0.95$) and requiring in addition CUT B. This procedure tests all cuts except cut 4. The cross section was measured using the data taken at 88.28, 89.28 and 94.28 GeV is 54 ± 6 pb. The Monte Carlo predicts a cross section of 63 ± 3 pb. Also in this case the agreement is rather good.

The ratio DATA/SIMULATION in these three tests is 0.89 ± 0.04 , 0.81 ± 0.11 and 0.86 ± 0.10. We decided to reduce the background subtraction computed with Monte Carlo by a factor 0.85 and to assign to it a systematic error of 15%.

The $\gamma\gamma$ contamination to be subtracted to the measured cross-section is then :

$$9.9 \pm 1.1_{\text{stat}} \pm 1.5_{\text{syst}} \text{ pb} = 9.9 \pm 1.9 \text{ pb}$$

It is not clear why the Monte Carlo shows this discrepancy with the Data: it is a pure QED Monte Carlo and it should be rather well understood. One possible explanation is that we have correlated trigger iniefficiency that would not be spotted by our method used to determine the trigger efficiency. Fig 16 shows the number of events at 88.2,89.2 and 93.2 events passing the $\gamma\gamma$ selection described before as function of W. We notice that indeed there is a lack of events at values of W close to the threshold (4.5 GeV) while the agreemennt is better at higher walues of W.

3.2 $q\bar{q}$ background

The $Z \rightarrow q\bar{q}$ background is obtained by applying the standard selection procedure on the Monte Carlo files. Out of 54.000 $q\bar{q}$ Monte Carlo events 33 are selected by the common-lepton selection and 29 by the tau selection. They correspond to cross sections of

$$\sigma_{q\bar{q}} = \frac{33}{54000} \; 20.8 * \sigma_{\tau^+\tau^-} = (1.27 \pm 0.22)\% \sigma_{\tau^+\tau^-}$$

$$\sigma_{q\bar{q}} = \frac{29}{54000} \; 20.8 * \sigma_{\tau^+\tau^-} = (1.12 \pm 0.21)\% \sigma_{\tau^+\tau^-}$$

The 4 events have been rejected by the E_{wires} cut of the tau selection.

Scanning these events we have noticed that they have typically more than 3 tracks and that they are typically generated with low charge multiplicity. They have a rather flat distribution in $\cos\theta$ (see fig 17).

Fig 18 shows the plot of the number of events as a function of $\cos\theta_{jt}$ from Data and Monte Carlo, with all the cuts applied except for $\cos\theta_{jt}$ and requiring in addition $N_{track} > 3$. The common-lepton selection cuts in the region $\cos\theta_{jt} > 0.95$. The $q\bar{q}$ Monte Carlo extrapolates rather smoothly into this bin while the remaining cross sections are much steeper. In the region $\cos\theta_{jt} < 0.95$ we count 104 events to be compared to a Monte Carlo prediction of 74 ± 12 events from $q\bar{q}$ and 34 ± 3 from other processes. We can test the $q\bar{q}$ Monte Carlo to the level of:

$$\frac{\text{DATA}}{\text{MONTECARLO}} = \frac{70 \pm 10}{74 \pm 12} = 0.94 \pm 0.20$$

In conclusion we add a 20% systematic error to the Monte Carlo prediction and we obtain the following background cross sections:

$$\sigma_{q\bar{q}} = (1.27 \pm 0.34)\% \sigma_{\tau^+\tau^-} \quad \text{common} - \text{lepton}$$
$$\sigma_{q\bar{q}} = (1.12 \pm 0.31)\% \sigma_{\tau^+\tau^-} \quad \text{tau}$$

We notice that the error on this background subtraction, that is the dominant background subtraction, is limited by the Monte Carlo statistics. With more Monte Carlo we could reduce this error to $\sim 0.15\%$.

3.3 Cosmic rays background

The cosmic rays are rejected by cuts 11 ($d0_{min}$) and 12 (number of associated ITC hits). We have selected events with cuts 1,2 and 3 only to study the association of ITC hits to the TPC tracks. We have required in addition $N_{track} = 2$. This has been done separathely for the period at the end of the data taking when the ITC had some problems (KRUN > 9040).

Fig 19 shows the plots of $d0_{min}$ in events with 0 ITC hits for the two sets of data. Plot a) is rather flat at an average level of 9.5 ± 0.6 tracks/2 mm. The first bin contains 19 events, which have been scanned. 14 ± 4 are consistent with cosmic rays, 5 of them

Table 6: Cosmic-ray events to be subtracted to the common-lepton and tau selections at each energy.

$\sqrt{s}$	events
88.2	0.25±0.25
89.2	0.25±0.25
90.2	0.5 ±0.35
91.2	3.75±1.0
92.2	0.5±0.35
93.2	1.0±0.5
94.2	0.5±0.35

are beam-beam events with a track spiraling inside the ITC, both tracks with very low momenta. Probably there are no linked ITC coordinates because of the single hit electronics of the ITC. None of these 5 events pass the common-lepton selection (this cut excluded). Excluding these 5 events there remain 14 events in the first bin to be compared with 9.5 (average of the other bins). We conclude that there is no evidence of malfunctioning of the ITC with respect to this cut.

Fig 19 b) shows the same plot for the runs following run number 9040 (first run with problems in the ITC in the last data taking period of August 1990). Again the absence of an over-population in the first bin of the distribution provides sufficient indication of the good behaviour of the ITC with respect to this cut.

Fig 20 shows the $d0_{min}$ distribution of events passing all the cuts of the common lepton selection except for cut 11. The flat distribution for events with $d0_{min} > 1$ cm confirms the presence of a small residual cosmic background. The estimation of cosmic events below the peak of beam-beam events is based on an extrapolation from events with $d0_{min} > 1$ cm. The number of events of cosmic-ray background to subract from the selected events at each energy point is listed in table 3.3

3.4 $Z \rightarrow e^+e^-$ background

This background is due to events where the electrons radiate two photons producing a large missing mass and, at the same time, part of the electromagnetic energy is lost because of the ECAL cracks or because the radiation is collinear with the initial electrons.

There are three possible cases: two photons from the final lines (including also the radiation of the final state electron with the material of apparatus), one from initial line and one from final line, two from initial lines. The latter contribution is small and is computed with an analytical formula [1] as discussed at the end of this section. The acollinearity cut limits the amount of radiation which can be obtained from the initial lines. This is at most 50% of the beam energy when only one photon is emitted (this happens at $|\cos\theta^*| = 0.9$). Since we require less than 55 GeV seen in ECAL we conclude that in case 1 and 2 we can accept an e^+e^- event only if one of the electrons or the photons goes into an ECAL crack. In case 1 the two photons are almost back to

back: if one goes into a crack, also the other is lost.

The initial state radiation is larger than in the $\mu^+\mu^-$ events because of the presence of the t channel exchange. The Monte Carlo simulation of the initial state radiation is not adequate and does not contemplate the possibility of the radiation of two hard photons. The events with large missing mass produced by the Monte Carlo have at least one photon produced in the interaction of the final electron with the apparatus.

The background is therefore evaluated from the data at each energy point using the e^+e^- selection program written by the Bhabha group [2]. This program has a high efficiency for e^+e^- events and a quite small contamination of $\tau^+\tau^-$. Two different procedures are followed.

In the first (direct) procedure we evaluate the efficiency of the e^+e^- selection ϵ_a in the region $MM^2 > 400GeV^2$ and $E_{wires} < 55GeV$ from e^+e^- Monte Carlo. We obtain

$$\epsilon_a = 0.64 \pm 0.21 \quad \text{barrel}$$

$$\epsilon_a = 0.57 \pm 0.28 \quad \text{overlap}$$

$$\epsilon_a = 0.52 \pm 0.11 \quad \text{endcaps}$$

Where barrel stands for $|\cos\theta| < 0.7$, overlap indicates $0.7 < |\cos\theta| < 0.8$ and endcaps indicates $0.8 < |\cos\theta| < 0.9$. In each region we count the events, N_{ee}, that pass the e^+e^- selection in our sample of tau candidates and from $\tau^+\tau^-$ Monte Carlo the contamination of $\tau^+\tau^-$ to this electron selection, N_{tt}, normalized to the same luminosity as the data. We compute the background subtraction as

$$N_{bkg} = (N_{ee} - N_{tt})/\epsilon_a$$

At the peak , where the tau selection selects ~ 4000 $\tau^+\tau^-$ candidates , the results for the three angular region are as follows:

$$\frac{19 \pm 4.4 - 15.9 \pm 2.0}{0.64 \pm 0.21} = 5 \pm 8 \quad \text{barrel}$$

$$\frac{10 \pm 3.2 - 2.6}{0.57 \pm 0.28} = 13 \pm 8 \quad \text{overlap}$$

$$\frac{16 \pm 4.0 - 2.0}{0.52 \pm 0.21} = 27 \pm 14 \quad \text{endcaps}$$

The total subtraction amounts to 45 ± 18 events and corresponds to $(1.1 \pm 0.5)\%$. This method relies on Monte Carlo for the calculation of the efficiency of the e^+e^- selection in the very small region of the phase-space selected by the tau selection.

The other procedure assumes that the cuts on MM^2 and E_{wires} are not correlated in the different angular regions. It is important to distinguish different angular regions since the probablity to have one particle into the craks changes as a function of theta and also the probability to radiate two photons changes as function of theta. This hypothesis is not completely correct since there is a small correlation between large missing mass and small ECAL energy: in the events with large missing mass the probability to loose energy is larger because there are two photons in the final state. The Monte Carlo confirmed that this effect is small (see later).

In this procedure we count the background events as :

$$N_{bkg} = \frac{N_{ee}(E_{wires} > 75.and.MM^2 > 400)}{N_{ee}(E_{wires} > 75)}(N_{ee}(E_{wires} < 55) - N_{tt}(E_{wires} < 55))/\epsilon_b$$

Where the terms N_{ee} are the events selected by the e^+e^- selection program inside the indicated cuts and N_{tt} is evaluated with Monte Carlo. The first term is the probability to produce a large Missing mass, the second is the number of events which lost energy because of the cracks.

In this formula ϵ_b is the efficiency of the e^+e^- selection in for $E_{wires} < 55GeV$; we have neglected the terms for the efficiency and the tau contamination of the e^+e^- selection for $E_{wires} > 75GeV$ since they are respectively $\sim 100\%$ and ~ 0 (from Monte Carlo).

To check the hypothesis of the non-correlation between the two cuts we have computed the ratio between the number of events with
$MM^2 > 400.and.E_{wires} < 55$ and the number of events predicted using the previous formula using Monte Carlo events. The result for the three angular regions is: 1.1 ± 0.3, 0.7 ± 0.3 and 1.1 ± 0.2. The fact that these ratios are close to 1 indicates that the correlation is small.

In our formula we measure the probability to produce large missing mass with a cut at 75 GeV on Ecal . Moving the cut at 65 GeV this probability changes by less than 10 %.

The efficiency ϵ_b of the e^+e^- selection for $E_{wires} < 55$ Gev is measured with Monte Carlo and is :

$$\epsilon_b = 0.94 \pm 0.06 \quad \text{barrel}$$
$$\epsilon_b = 0.92 \pm 0.10 \quad \text{overlap}$$
$$\epsilon_b = 0.87 \pm 0.06 \quad \text{endcaps}$$

.

By applying this procedure we find the following results, at the peak, for the three angular regions respectively:

$$\frac{208}{3426}\ \frac{166 \pm 13 - 35.6}{0.94} = 8 \pm 1 \quad \text{barrel}$$
$$\frac{81}{617}\ \frac{77 \pm 9 - 6.7}{0.92} = 10 \pm 2 \quad \text{overlap}$$
$$\frac{183}{1486}\ \frac{150 \pm 12 - 4.5}{0.87} = 21 \pm 2 \quad \text{endcaps}$$

These values are consistent with the previous ones, but have much smaller errors. This method relies much less on the evaluation of the $\tau^+\tau^-$ contamination to the e^+e^- selection and is also less sensitive to the Monte Carlo measurement of the efficiency of the e^+e^- selection. A 15% systematic error has to be added in quadrature to take into account the uncertainty on the assumption that the two cuts are not correlated. In this case the subtraction at the peak is 38 ± 6 events and corresponds to $(1.0 \pm 0.2)\%$.

Table 7: e^+e^- events to be subtracted to the tau selection at each energy. 15 % of the subtraction has to be added in quadrature all errors

$\sqrt{s}$	barrel	overlap	endcaps	total
88.2	0.3±0.2	0.4±0.3	1.6±0.6	2.4±0.7
89.2	0.7±0.3	1.2±0.6	2.0±0.7	3.9±1.0
90.2	0.6±0.2	0.6±0.3	3.2±0.9	4.4±1.0
91.2	8.4±1.0	9.2±1.7	20.6±2.1	38.2±2.9
92.2	2.1±0.6	0.4±0.3	2.2±0.8	4.6±1.0
93.2	1.2±0.5	0.7±0.5	2.4±0.9	4.4±1.1
94.2	1.0±0.4	0.6±0.4	1.4±0.6	3.0±0.8

The number of e^+e^- to subtract from the events selected by the tau selection for each energy point and for the three angular region is listed in table 7.

This subtraction does not yet include the events with radiation of two photons from the initial lines. The cross section for the process $e^+e^- \to e^+e^-\gamma\gamma$ with the two photons along the initial lines has been computed with the program MIBA [1] with the following cuts:

- $\cos\eta < -0.9397$
- Both final electrons inside the region $-0.9 < \cos\theta < 0.9$
- Sum of the energies of the electrons smaller then 55 Gev
- Product of the energies of the photons larger the 100 Gev**2 (this is equivalent to missing mass larger then 400 Gev**2)
- Invariant mass of the two final state electrons larger then 4 GeV.

This cross section is 1.95 ± 0.05 pb and has to be subtracted from the data. Since these events have a total ecal energy + total momentum in the final state less then 110 GeV they do not pass the selection program of the Bhabha group and there isn't any problem of double-counting.

3.5 $Z \to \mu^+\mu^-$ background

This background is evaluated from the data using the $\mu^+\mu^-$ selection program based on the digital readout of HCAL [3]. Events with less then 7 good tracks have been preselected requiring in addition 2 muons identified with HCAL with momentum larger then 3 GeV/c and $\cos\eta < -.9397$. This procedure selects a good fraction of $Z \to \mu^+\mu^-$ events (the inefficiency is due to the HCAL identification) and some $Z \to \tau^+\tau^-$ events. This analysis has been performed on a fraction ($\sim 80\%$) of the events taken at the peak and 2648 events have been selected.

A cut requiring $\mathrm{ABS}(\mathrm{Ecal_{wire}} - \mathrm{Ecal_{pads}}) < 1\mathrm{GeV}$ has been applied to reject events with noise in ECAL (see fig 21 and in addition HCAL energy is required to be below 15 GeV (see fig 21) to reduce the $Z \to \tau^+\tau^-$ since sometimes the hadronic shower of the

hadrons from tau decay fakes a muon in the selection procedure. Moreover it has been required that the scalar sum of the momenta (later called TPC energy) be less then 100 GeV/c. 2272 events remain. Among the events with TPC energy larger then 100 GeV (34 events) those with missing mass larger then 400 GeV^2 (10 events) have been scanned and found to be cosmic rays candidates. All events with Hcal energy larger then 40 GeV have been scanned and found to be $Z \rightarrow \tau^+\tau^-$ candidates.

Fig. 22 show the plots of ϕ and $\cos\theta$ of the thrust axis of the events after the preselection and after these additional cuts have been applied. These distributions are standard and show that we do not bias the events with the additional requirements.

Fig. 23 show TPC energy vs ECAL energy for the selected events. One can see three families. $\mu^+\mu^-$ events with or without radiation , some $\mu^+\mu^-$ events with high bremssthralung in ECAL (those events at TPC energy of 91 GeV and with some Ecal energy) and $\tau^+\tau^-$ events that show up with almost zero ECAL energy and TPC energy smaller than $\sim$ 80 GeV. The events with TPC energy smaller then 60 GeV and ECAL energy between 3 and 30 GeV (14 events) have been scanned. They are all $Z \rightarrow \tau^+\tau^-$ candidates. 5 of them have one tau decaying into hadronic final state and the remaining ones with two muons and one γ in the final state.

Fig. 24 show the distribution of TPC energy + ECAL energy for data and Monte Carlo. We call $Z \rightarrow \mu^+\mu^-$ events those with the energy sum larger then 70 GeV. They are 2171 events. Fig. 25 show the Missing mass distribution for events with energy sum larger then 70 GeV and lower then 70 GeV separathely. 5 events with energy sum larger then 70 GeV have missing mass larger then 400 GeV^2. One of them is a $Z \rightarrow \tau^+\tau^-$ with one of the tau decaying into three pions, three of them are $Z \rightarrow \mu^+\mu^-$ with two photons in the final state and one is ambiguos since none of the muon candidates reaches the muon chamber. The HCAL energy of this event is 14 GeV, which is quite unlikely for a two muon event.

Another check has been performed by plotting the maximum momentum of the selected muons. This is shown in fig. 26 separathely for energy sum larger or smaller than 70 GeV. The events with energy sum larger then 70 GeV and maximum momentum lower then 35 GeV (2 events) belong to the sample of missing mass larger then 400 GeV^2. There are three events with energy sum smaller then 70 GeV and pmax larger then 35 GeV. Two of them have one muon with energy comparable with beam enery, one γ in the final state and missing mass smaller then 200 GeV^2. The third has one particle of 37.9 GeV, the second of 27 GeV and no photons in the final state.

In conclusion, on a sample of 2171 $Z \rightarrow \mu^+\mu^-$ events there are 3 ± 2 events with missing mass larger then 400 GeV^2. We assume that the efficiency of the remaining cuts for $Z \rightarrow \mu^+\mu^-$ events is 100% within the angular acceptance. The background cross section is then:

$$\sigma_{\rm bkg} = \frac{3 \pm 2}{2171}\ 0.8752\ \sigma_{\tau^+\tau^-} = (0.12 \pm 0.08)\%\ \sigma_{\tau^+\tau^-}$$

Where 0.872 is the angular acceptance of the $\tau^+\tau^-$ selection.

4 Efficiency

Three components are involved in the determination of efficiency : trigger efficiency, tracking efficiency and selection efficiency.

The three topics are discussed in the following subsections. The final result is that the efficiency is given by:

$$\epsilon_{tau} = (1.0000 \pm 0.0005)(0.9985 \pm 0.0005)(0.7301 \pm 0.0034)(1.004 \pm 0.007)$$

where the four terms are : trigger efficiency, tracking efficiency, acceptance and selection efficiency determined through Monte Carlo, systematic effects on the selection efficiency. They give:

$$\epsilon_{tau} = (73.19 \pm 0.61)\%$$

The angular acceptance is ~ 0.858 and the selection efficiency within this angular region is ~ 0.853 .

4.1 Trigger efficiency

The trigger efficiency has been studied estensively in [4]. They determine a single arm efficiency on tau events of $(99.30 \pm 0.7)\%$. In our sample of events we find among 4092 events 4034 with double arm trigger and 58 with single arm trigger at the peak. This figure corresponds to a trigger efficiency for a tau pair of $\sim 100\%$ with an error smaller then 0.05%.

4.2 Tracking efficiency

The tracking efficiency has been studied using Bhabha event selected with ECAL [5], we have repeated the same study obtaining similar results. Applying the corrections for TPC crack inefficiency to Monte Carlo and data, for TPC inefficiency due to problems in the electronics and for TPC reconstruction inefficiency in Monte Carlo and data, we conclude that the tracking efficiency is

$$\epsilon_{tracking} = (99.85 \pm 0.05)\%$$

Furthermore, we have searched events with one good track in the TPC, ITC activity opposit to it and no cluster associated in ECAL. No evidence of inefficiency has been found for track at momenta lower then Bhabha events.

4.3 Selection efficiency

The selection efficiency has been studied on a Monte Carlo file (VDET in) of ~ 20.000 events. Table 8 summarizes the effects of the different cuts. In this table the selection is divided in 5 logical steps. The first 3 are discussed in this section and the remaining 2 in the next section.

Table 8: Number of events passing the various cuts in cascade in the selection , absolute and relative efficiencies. All efficiencies are given in %.

step	cut	selected events	efficiency relative to the previous cuts	absolute efficiency
	No cuts	19995	100	100
	Angular acceptance	17114	85.59±0.27	85.59±0.27
A	$N_{track} \geq 2$	16902	98.76±0.08	84.53±0.28
B	$\cos\eta \leq -.9397$	16683	98.70±0.09	83.44±0.29
C	$N_{track} \leq 6$	16591	99.45±0.06	82.98±0.29
D	common lepton	16153	97.36±0.12	80.78±0.31
E	tau	14599	90.38±0.24	73.01±0.34

The first three steps reduce the number of $e^+e^- \rightarrow \tau^+\tau^-$ that pass the acceptance cuts by $\sim$ 2%. The systematic effects of these cuts are studied by comparing Monte Carlo with data. The other two steps further reduce the number of $e^+e^- \rightarrow \tau^+\tau^-$ by $\sim$ 12% . The systematic effects of these cuts is studied using data alone.

In the previous table "angular acceptance" indicates that the event has passed cuts 1,2,and 5 (at least one track per emisphere and $|\cos\theta^*| < 0.9$) or , if it has only one reconstructed track, this track has $|\cos\theta| < 0.9$. If we calculate the angular acceptance from the integral of $(1+\cos^2\theta)$ between -0.9 and 0.9 (since it is symmetric we can neglect the $\cos\theta$ term in the angular distribution) we obtain an acceptance of 85.79%. This is not strictly correct since, due to the acollinearity cut, our angular distribution does not follow exactly $(1 + \cos^2\theta)$, but the deviation is small. Assuming the value of 85.79%, we expected to find 17139 ± 50 events that pass the 1st cut. We found 17114 events. This acceptance could have a systematic error due to possible systematic effect in the measurement of the angle inside the TPC. We have not yet studied all the possibilities. One contribution comes from the systematic error on the drift velocity. This error is $\Delta v/v \sim 10^{-3}$ [6]. This corresponds to an error $\Delta\cos\theta = 1.7\ 10^{-4}$ for $\cos\theta = 0.9$ and gives an error on the acceptance of $\Delta\epsilon \sim 2\ 10^{-4}$.

The first loss of efficiency comes from the request for one track per emisphere (step A). Among 17114 events having at least one track inside the acceptance, 212 events have only one track. Fig 27 shows the angular distribution of these 212 events in two plots. Plot (a) is done for events with less then 4 "any-track" (for this purpose, no request is applied on the track parameters) and plot (b) for those having more then 3 "any-track". This cut enriches the second sample with the events where one of the decay products of the tau interacts inside the apparatus producing many tracks that do not satisfy the track-cuts (cut 1).

In this sample we expected $\sim$ 21 events with one track lost because of the cracks [5]. This are in plot (a) at large values of $|\cos\theta|$. Plot (b) does not follow the $(1 + \cos^2\theta)$ distribution since tracks at small angles cross more material and have a larger interaction probability.

We scanned 70 events of this sample in the region $|\cos\theta| < 0.7$. 24 have an interaction, 36 have one track at very low momentum that is not reconstructed (9 of them

have ECAL activity opposite to the reconstructed track , indicating a tau decay with neutrals, 3 are lost because of pattern recognition problem and 7 for different resons that could not be classified into these cathegories. We have not checked the systematic of this cut with data. We have to assume that the interactions are correctly simulated (and this is verified by the distribution of e^+e^- pairs in hadronic events compared with the Monte Carlo). Moreover we have to assume that the momentum spectra of the tau decay products is correctly simulated at the low momenta. This is supported by the momentum spectra of the different decay modes studied for the polarisation.

The second cut (step B) is studied using fig. 2 that shows the distribution of $\cos\eta$ in the selected tau events. Also in this case the agreement between data and Monte Carlo is very good. When moving the cut to $\cos\eta < -0.72$ the ratio DATA/MONTECARLO changes by 0.2%. This provides an extimate of the systematic error of this cut.

The third cut (step C) is studied using fig. 1 that shows the distribution of the good tracks in the selected tau events. When we move the cut to include events up to 8 charged tracks (doing that we include more hadronic events than τ's !!!) the ratio DATA/MONTECARLO (the Monte Carlo prediction includes also the qq contribution) changes by 0.2%.This provides an extimate of the systematic error of this cut.

The combined effects of acollinearity and angular cuts changes as a function of $\sqrt{s}$. The quoted efficiency is for $\sqrt{s} = M_z$. This variation has been evaluated with KORALZ producing $\mu^+\mu^-$ events [7] and counting how many follow inside the acceptance defined by these two cuts at the different centre-of-mass energies. The acceptance is maximal at the peak and changes at most by 3.7%(this happens at -3 GeV).

The other cuts are studied from the data using a special selection procedure as described in the next sub-section.

The effect of class-15 cuts has also been studied with Monte Carlo. Only one Monte Carlo event among $\sim$ 16000 would have been selected by the common lepton selection and NOT by class 15. This is due to differences in track-counting. We should notice that this is not a complete test since the variables used by class 15 to compute the cuts are calculated according to the Aleph reference system, while those of the common lepton selection are calculated according to the measured position of the beams. In the Monte Carlo the beams are always along the z axis and the two definition coincide. Since the cuts are very loose one does not expect to find big differences, but this has not been tested yet.

4.4 Determination of the selection efficiency from the data

In order to check the efficiency of the selection procedure we have produced from the data an almost-umbiassed sample of tau events combining two taus from different events. This is done on a preselected sample with cuts that correspond roughly to the steps 1-3 of table 8; we can only study the effects of steps D and E.

In these procedure we loose the spin correlation existing in $Z \rightarrow \tau^+\tau^-$ events. and we have to check that this effect does not bias our result.

Events are selected with a multiplicity cut at 7. The event is divided into two emispheres with a plane perpendicular to the thrust axis and at least one good track per emisphere is required. The acollinearity is required to be $\cos\eta$ <-0.5. Cosmic

rays are rejected with the standard procedure. Then futher cuts are applied to one emisphere.

- TPC energy is required to be larger then 8 GeV .
- If there is only one track, the sum of TPC+ECAL+HCAL energy is required to be smaller then 35 GeV.
- If there are 2 or 3 charged tracks the sum of TPC+ECAL energy is required to be smaller then 35 GeV and the invariant mass of the tracks to be smaller then 2 GeV.

When all these conditions are fulfilled, the event is taken as a tau-candidate and the other emisphere contains an almost-umbiassed sample of tau. Only this half-event is taken. The half-events are binned in 12 ϕ bins and 10 $\cos\theta$ bins (120 in total) according to the direction of the thrust axis of the original event.

Two half-events belonging to opposite ϕ and $\cos\theta$ bins are randomly paired to produce an event. Each half-event is used only once. One of the two half-event is rotated in order to align the direction of its original thrust axis to the one of the other half-event.

The efficiency of these selection and the contaminations have been evaluated with Monte Carlo data. The efficiency in selecting an half-event is $\sim$ 30% and the contamination in the half-events sample is less then 5%. Since the the events are randomly paired, we assume that this contamination does not bias the conclusions.

The effect of the spin correlation has been studied by applying the same procedure to Monte Carlo events. In this case, the events have been divided and binned without any selection and then randomly paired. Figures from 28 to 31 show the comparison between paired-half-events and standard Monte Carlo events. The fits of standard Monte Carlo events to the paired-half-events are very good, typically giving a χ^2/dof of 1 except for the acollinarity distribution that in the paired-half-events is sligthely broader than in the standard Monte Carlo events, probably due to the alignment procedure. These distributions match standard Monte Carlo events where the correlation due to the tau polarisation is taken into account. We conclude that we can apply this procedure to the data to evaluate the efficiency.

The distributions of half-paired events from data and their comparison with standard Monte Carlo events are shown in figs. from 32 to 34. The agreement is very good and also in this case the fit gives typically a χ^2/dof of 1.

With these events we can test steps D and E of the selection (see table 8). Before step D we have 1390 events; applying step D we remain with 1341 events. 1215 events survive after the tau selection (step E). The corresponding efficiencies are

$$\text{STEP D} \quad \epsilon_D = (96.47 \pm 0.50)\%$$

$$\text{STEP E} \quad \epsilon_E = (90.60 \pm 0.80)\%.$$

These two efficiencies are compared with the Monte Carlo value in column 4 of table 8. The ratio DATA/MONTECARLO is 0.991 ± 0.005 for ϵ_D and 1.002 ± 0.009 for ϵ_E. The agreement is not perfect but still rather good.

Another possibilty is to pair each event with all events in the opposite ϕ and $\cos\theta$ bin. In this case we have to take into account the correlations between the half-events that are used more than once. The statistical gain is not considerable and is a function of the efficiency of the cut. The reduction of the error respect to the previous case (when one half-event is used only once) is plotted in fig 35 and is typically 0.5.

In this case, before step D we have 52016 events, 50390 after step D and 45797 after step E. The corresponding efficiencies, taking into account the reduction of the error, are :

$$\epsilon_D = 0.9687 \pm 0.0030 \quad \epsilon_E = 0.9088 \pm 0.0052$$

The ratio DATA/MONTECARLO in this case is 0.995±0.004 for ϵ_D and 1.005±0.007 for ϵ_E. The agreement is good.

The relatively larger error ϵ_E comes mainly from the MM^2 cut that has the largest ineffiency. This cut is rather safe and can be studied also in a different way that is shown later. For this purpose it is interesting to study the effect of the E_{wires} cut alone.

From Monte Carlo we measure the efficiency of the E_{wires} and total momentum cuts after step D. It is $(95.22 \pm 0.17)\%$. From data we measure $95.97 \pm 0.54\%$ using each event only once and $(96.04 \pm 0.32)\%$ making all the combinations. In this case the ratio DATA/MONTECARLO is 1.009 ± 0.004. Also in this case we have an agreement at 2 standard deviation.

The systematics of the cut on $\mu^+\mu^-$ can be studied from the plot of the missing mass of a sample $\mu^+\mu^-$ events (selected requiring $N_{track} = 2$ and $E_{wires} < 4GeV$) shown in fig 36. The position of the peak at $MM^2 \sim 0$ could be affected by an error on the energy scale of the TPC. The upper end of the missing mass distribution in tau events has no appreciable error since it is defined by the energy scale of LEP. Fig 36 shows an enlarged view of the missing mass plot in the region $MM^2 = 0$ and fig. 37 shows the fit of the position of the peak for data and Montecarlo. The two fits give central values that differ from 0 by less then $0.1GeV^2$. Since a shift of 1 GeV^2 would produce a change of efficiency of 0.013% we conclude that the systematic error due to the energy scale of the TPC is negligible.

This study shows that we have no appreciable systematic effects linked to the energy scale of the TPC. Neverthless our simulated efficiency could be affected by wrong hypotheses on the decay of the tau, that would change the shape of the missing mass distribution. To study this effect we have computed with Monte Carlo the efficiency of the MM^2 cut after step D for the two polarization of the tau. This is important since the energy distribution of the charged tracks depend on the tau polarisation. The two efficiencies are :

$$\epsilon_{+1} = (92.95 \pm 0.31)\% \; and \; \epsilon_{-1} = (96.18 \pm 0.20)\%$$

a change in polarisation of the tau would change the efficiency of the MM^2 cut as :

$$\Delta\epsilon = (\epsilon_{-1} - \epsilon_{+1})\Delta P$$

using $\Delta P = 0.05$, that is our precision on the polarisation measurement, we obtain $\Delta\epsilon = 0.16\%$. We conclude that there is no correction to be applied for the MM^2 cut and that we can ascribe to it an error of 0.2%.

Table 9: Integrated Luminosity, Number of selected events and Background subtraction at each energy.

	1989 DATA			1990 DATA		
$\sqrt{s}$	$\mathcal{L}^{int}$	N_τ	Background	$\mathcal{L}^{int}$	N_τ	Background
88.2	108	31	4.0± 0.6	479	68	9.8± 1.3
89.2	46	18	2.0± 0.5	517	158	13.1± 1.7
90.2	72	45	3.4± 0.5	444	302	15.4± 2.0
91.0	143	154	8.3± 1.2			
91.2	137	141	7.9± 1.1	3629	4144	152.5±20.0
91.5	142	156	8.9± 1.4			
92.2	112	95	6.4± 1.1	552	449	18.5± 2.4
93.2	42	18	2.2± 0.8	593	257	17.5± 2.2
94.2	66	21	2.4± 0.4	637	203	14.3± 1.8

The global systematic effect of step D and E is then given by the product of these three numbers :

$$(0.995 \pm 0.004)\ (1.009 \pm 0.004)\ (1.000 \pm 0.002) = 1.004 \pm 0.006$$

that represent the systematic effects of step D, of the cut on E_{wires} and of the cut on MM^2.

Including the systematic errors of the other steps we reach a total systematic error of 0.7% for the selection efficiency.

5 $e^+e^- \rightarrow \tau^+\tau^-$ cross sections

Table 9 summarize the luminosity, number of events and background subtraction for the different energies , separated for 1989 and 1990 data. Tables 10 and 11 contain the cross sections for the two different data sets and combined. The first error is the statistical error, the second includes also the error in the background subtraction and the third also the error in the efficiency. No error is quoted for the Luminosity.

Fig 38 shows the number of selected $Z \rightarrow \tau^+\tau^-$ events divided by the luminosity (this is not the cross section since no background subtraction nor efficiency correction is applied) as function of time. The same plot is also shown for the "common lepton" candidates. We notice that both plots do not show any strange effect.

Fig 39 shows the plot of the $\tau^+\tau^-$ cross sections vs the hadronic cross section.

Table 10: Cross section and errors at each energy. 1st error is statistical, 2nd is statistical + background subtraction, 3rd includes also the efficiency error. No error is included for the luminosity.

	1989 DATA				1990 DATA			
$\sqrt{s}$	$\sigma_{\tau\tau}$	er1	er2	er3	$\sigma_{\tau\tau}$	er1	er2	er3
88.2	0.355	0.073	0.074	0.074	0.172	0.024	0.025	0.025
89.2	0.484	0.128	0.129	0.129	0.390	0.034	0.034	0.034
90.2	0.796	0.128	0.129	0.129	0.889	0.054	0.054	0.055
91.0	1.392	0.119	0.119	0.120				
91.2	1.327	0.118	0.119	0.119	1.503	0.024	0.025	0.028
91.5	1.415	0.120	0.121	0.122				
92.2	1.083	0.119	0.120	0.120	1.068	0.053	0.053	0.054
93.2	0.518	0.139	0.142	0.142	0.556	0.037	0.038	0.038
94.2	0.392	0.097	0.097	0.097	0.412	0.031	0.031	0.032

Table 11: Cross section and errors at each energy 1989 and 1990 combined. 1st error is statistical,2nd is statistical + background subtraction, 3rd includes also the efficiency error. No error is included for the luminosity.

$\sqrt{s}$	$\sigma_{\tau\tau}$	er1	er2	er3
88.2	0.206	0.024	0.024	0.024
89.2	0.398	0.033	0.033	0.033
90.2	0.876	0.050	0.050	0.051
91.0	1.391	0.118	0.119	0.120
91.2	1.496	0.024	0.025	0.028
91.5	1.414	0.120	0.121	0.121
92.2	1.071	0.048	0.048	0.049
93.2	0.554	0.036	0.036	0.037
94.2	0.410	0.030	0.030	0.030

6 $\tau^+\tau^-$ Forward Backward Asymmetry

At each center of mass energy, the observed angular distribution :

$$dN/dcos\theta^* = N\,(1 + cos^2\theta^* + \frac{8}{3}\,A_{\rm FB}\,cos\theta^*)$$

is studied in order to extract the value of the forward backward asymmetry $A_{\rm FB}$. The cms scattering angle θ^* is inferred from the two polar angles θ_1 and θ_2 which are defined by the vector sum of all charged tracks momenta in either hemisphere .

As it is well known, the value of the θ^* angle is uneffected by collinear initial state radiation , whereas this is not necessarily true if the direction of the τ pair is recostructed using the thrust axis . However, MC simulation indicates that the diffence θ^*-θ^τ , shown in Fig. 40 (b) is numerically small .
In the following ,we shall use θ^* as the measured direction of the τ .
The difference θ^* - θ^τ between the reconstructed cms scattering angle θ^* and the true $\tau^+\tau^-$ production angle θ^τ from Monte Carlo is plotted in Fig. 40 (a). The rms width is 24 mrad .

In addition to its direction, the charge of the lepton must be known. The total reconstructed charge in the event from the data is compared with the MC prediction in Fig. 41. The distribution is symmetrical for either charge sign and in good agreement with the prediction .
Events with non zero total charge have been studied both from data and MC . The measured charge multiplicity is plotted against the total observed charge in Fig. 42 . The extra track which is present in events with 1+2 topology (mainly the result of interactions in the apparatus) is characterized by low momentum and large impact parameter, as it can be seen in Fig. 43 , where again data and simulation show a good agreement.
A cut on total zero charge is applied with a reduction of 8.5 $\pm$ 0.4 % in the number of events.

6.1 Evaluation of the systematics

6.1.1 Bhabha background

As explained in section 3.4 , the sample of events selected for the cross section measurement at the Z_0 peak is affected by a background contamination from e^+e^- of 1.1$\pm$0.5 %. The size of the systematic error induced by this background on $A_{\rm FB}$ has ben estimated as follows .
For each pair of cos θ^* bins centered at x_i = cos θ_i^* and -x_i respectively, a differential asymmetry A_i can be defined as :

$$A_i = \frac{N_i^+ - N_i^-}{N_i^+ + N_i^-}$$

For $\tau^+\tau^-$ events we expect :

$$A_i = \frac{8}{3}\;A_{\rm FB}\;w_i$$

where :

$$w_i = \frac{x_i}{1 + x_i^2}$$

Let B_i^+ and B_i^- be the number of background events in bins x_i and -x_i , respectively and $C_i = \frac{B_i^+ + B_i^-}{N}$ where $C^{bkg} = \sum_{i=1}^{n_b} C_i$ is the total background contamination from e^+e^- pairs ; n_b is the number of bin pairs ; N is the total number of selected $\tau^+\tau^-$ events.
The systematic error on $A_{\rm FB}$ due to the background is :

$$\delta A_{\rm FB} = -\sum_{i=1}^{n_b} C_i A_i + \sum_{i=1}^{n_b} C_i A_i^{bkg} = \sum_{i=1}^{n_b} C_i (A_i^{bkg} - A_i)$$

where :

$$A_i^{bkg} = \frac{B_i^+ - B_i^-}{B_i^+ + B_i^-}$$

and :

$$A^{bkg} = \sum_{i=1}^{n_b} A_i^{bkg} \frac{(N_i^+ + N_i^-)}{N}$$

is the asymmetry in the angular distribution of the background events .

The first term in $\delta A_{\rm FB}$ is due to background events with a forward-backward symmetrical distribution (e.g.: $\gamma\gamma$ events).
It contributes a total systematic error of :

$$\delta A_{\rm FB} / A_{\rm FB} = -C^{bkg}$$

which has the effect to compress by a multiplicative $(1 - C)$ scale factor the $\sqrt{s}$ dependence of $A_{\rm FB}$.
The second term, due to asymmetrical backgrounds (e.g.: e^+e^- events) produces a *positive* shift in the measured value of $A_{\rm FB}$ of size :

$$\delta A_{\rm FB} = C^{bkg} A^{bkg}$$

Therefore, if the background is not subtracted from the data, we would expect at peak energy a value for $\delta A_{\rm FB}$ of -0.34 % to be compared with the SM prediction ($sin^2\theta_w = 0.23$) for $A_{\rm FB}$ of 0.9 % and with the current statistical error of 1.6 % .
However, we have further reduced the amount of such background by rejecting those events which are identified as e^+e^- pairs according to the criteria described in section 3.4 .
After application of these additional cuts , the remaining event sample is 99.3 % of the original one.

The efficiency of the e^+e^- rejection on the events accepted by the cross section selection has been evaluated by MonteCarlo simulation for different angular regions as shown in Fig. 44 (a)). The rather poor 50 % average efficiency for this particular class of e^+e^- events ($m_x^2 > 400\,GeV^2$, $E_{wires} < 55$ GeV) has to be compared with the average 98.4 % efficiency obtained on an unbiased e^+e^- sample . (see Fig. 44 (b)) .

If we assume an average e^+e^- rejection efficiency of 50 % for the events passing the τ selection cuts, we expect the systematic error induced by the residual e^+e^- background

on A_{FB} at the peak to be of order -0.0017 .

The uncertainty on this correction is dominated by the uncertainty on the background contamination ΔC and by the uncertainty on the asymmetry of the background ΔA^{bkg}.

The value of A^{bkg} is measured from the data by binning the angular distribution of the e^+e^- identified events in 18 bins of $cos\theta^*$ (see Fig. 45). By lowering the missing mass cut, the amount of background can be enhanced to get a statistically more accurate measurement of A^{bkg}. At the peak, we find for the identified Bhabha events :

$$A^{bkg} = 0.30 \pm 0.06$$

with ($m_x^2 > 0\, GeV^2$, $E_{wires} < 55$ GeV) while we get :

$$A^{bkg} = 0.18 \pm 0.08$$

with ($m_x^2 > 400\, GeV^2$, $E_{wires} < 55$ GeV).

The value of C^{bkg} is inferred from the data by counting the number of events flagged as e^+e^- and by assuming a background rejection efficiency of 50% . The error ΔC^{bkg} on the total background contamination C^{bkg} (see table 13) is dominated by the statistical error and by the uncertainty on the Bhabha identification efficiency.

As a consistency check, the variation of the $\tau^+\tau^-$ asymmetry as a function of the amount of e^+e^- contamination can be observed directly from the data . By varying the missing mass cut on the data at the peak, we can add to our sample a known fraction of e^+e^- background and measure its effect on the value of the asymmetry . In Fig. 46 the observed variation of δA_{FB} of the asymmetry is shown as a function of the estimated background contamination . The low value of the e^+e^- efficiency for events with missing mass $> 400\ GeV^2$ is of little consequencehere, as the largest variation of the asymmetry occurs for small values of the missing mass cut ($m_x^2 < 100\ GeV^2$) , where the e^+e^- identification efficiency is fairly high .

For each value of the missing mass cut, the value of the asymmetry is obtained by an unbinned maximum likelihood fit to the angular distribution .
However, if we do plot the data in 18 bins of $\cos\theta^*$ in the range [-0.9,+0.9] , we observe that *only* the upper bin at +0.9 gets more populated when the amount of e^+e^- background is increased by lowering the missing mass cut.

The slope from Fig. 46 is consistent with a background asymmetry A^{bkg} of 0.37 ± 0.1.

The values for the correction applied at each cms energy point for the combined fit to 1989 and 1990 data are listed in table 13 together with the estimated uncertainty on the correction .

6.1.2 $\gamma\gamma$ background

The contamination from $\gamma\gamma$ background at the peak was found to be 0.65 ± 0.12 % (see section 3.1). By assuming a FB symmetrical $(1 + cos^2\theta)/sin^2\theta$ angular distribution for

Table 12: Contamination from $\gamma\gamma$ events . Estimated correction to the measured asymmetry .

$\sqrt{s}$ (GeV)	$C_{\gamma\gamma}$ %	$\delta A_{\rm FB}^{\gamma\gamma}$ %
88.28	3.1 ± 1.3	-1.1 ± 0.5
89.28	3.2 ± 0.6	-0.3 ± 0.05
90.28	1.4 ± 0.3	-0.1 ± 0.02
91.28	0.8 ± 0.2	0.01 ± 0.002
92.28	1.2 ± 0.2	0.2 ± 0.03
93.28	2.3 ± 0.4	0.5 ± 0.1
94.28	3.1 ± 0.6	0.7 ± 0.3

Table 13: Measured values of A_{FB} vs. cms energy before and after background correction

*

$\sqrt{s}$ (GeV)	events	C^{Bhabha} (%)	$\delta A_{Bhab.}$ (%)	A_{FB}^{meas} (%)	A_{FB}^{corr} (%)
88.28	84	1.2±1.2	−1.1±0.7	−36.6±9.4	−38.8 ±9.4 ±0.9
89.28	170	0.6±0.6	−0.4±0.4	−9.9±7.5	−10.6 ±7.5 ±0.4
90.28	344	0.9±0.5	−0.5±0.3	−5.0±5.5	−5.6 ±5.5 ±0.3
91.03	168	0.3±0.4	−0.06±0.1	+8.3±7.5	+8.2 ±7.5 ±0.1
91.28	3902	0.6±0.1	−0.17±0.03	+1.3±1.6	+1.1 ±1.6 ±0.03
91.53	185	0.5±0.5	−0.10±0.1	−3.3±7.0	−3.4 ±7.0 ±0.1
92.28	481	0.8±0.4	−0.31±0.2	+14.8±4.4	+14.7 ±4.4 ±0.2
93.28	264	0.2±0.3	−0.11±0.2	+20.6±5.7	+20.1 ±5.7 ±0.2
94.28	204	0.1±0.1	−0.04±0.4	+22.2±6.6	+22.8 ±6.6 ±0.4

*

this background, the required correction to $A_{\rm FB}$ due to a total percentual contamination C^{bkg} of $\gamma\gamma$ events is :

$$\delta A_{\rm FB}/A_{\rm FB} = -C^{bkg}$$

This would result in a negligible correction of $\delta A \simeq -10^{-4}$ to the measured $A_{\rm FB}$ value at the peak . Outside the resonance, we expect the background to signal ratio to increase to about 3.1 % at $\sqrt{s} = 88.28\ GeV$.
The required correction on the asymmetry at this point would be δA = -1.1 % which has to be compared with the predicted value for the asymmetry of -27.4% and the current statistical error of 9.4 %

6.2 Fit procedure

The number of events selected per cms energy point are listed in table 13 for the combined '89 and '90 data, together with their statistical errors. An unbinned maximum likelihood fit to the angular distribution is performed for each energy as shown in

Fig. 49 . The measured values of A_{FB}, before and after the correction for the residual e^+e^- background, are listed in table 13.

The fit has been repeated , introducing an additional free parameter $\mathbf{a_2}$ for the curvature term $cos^2\theta^*$:

$$N(1 + \mathbf{a_2}\ cos^2\theta^* + \frac{8}{3}\ A_{FB}\ cos\theta^*)$$

The effect on A_{FB} at the peak is negligible : 0.0132 ± 0.016 with $\mathbf{a_2}$ as a free parameter to be compared with 0.0133 ± 0.016 with the same parameter constrained to 1.
The absence of correlation between the two parameters is shown in fig. 48 where the contour of minimum log likelihood is shown .

The values for $a_e * a_\tau$ and $v_e * v_\tau$ coupling constants are fit using the Burgers at al. procedure , as implemented by Ramon and Martinez . For the combined '89 + '90 data we get :

$$v_e * v_\tau = (0.43 \pm 0.16)\%$$

$$a_e * a_\tau = 0.352 \pm 0.005$$

References

[1] M. Martinez and R.Miquel, program MIBA. They have calculated the cross section inside the decsribed cuts.

[2] We had this program from Elizabeth Locci. There is a note in preparation that will describe it.

[3] We had this program from Fabio Bossi.

[4] G. Bagliesi and L. Silvestris, trigger efficiency in $Z \rightarrow \tau^+\tau^-$ events, note in preparation.

[5] H.Meinhard, presentation at the electroweak meeting... note in preparation.

[6] W. Wiedenmann, Aleph 90-156. Tracking with the Aleph TPC.

[7] These efficiencies were calculated by the Barcelona group.

Figure Caption

1. Events selected by the tau selection. Distribution of the number of charged tracks (This cut was excluded).
2. Events selected by the tau selection. Distribution of acollineraity ($\cos\eta$)
3. Events selected by the tau selection. Distribution of the maximun $\cos\theta_{jt}$ (thic cut was excluded).
4. Events selected by the tau selection. Distribution of the maximum momentum of the track in the event (this cut was excluded) but the plot is biassed by the Pt cut.
5. Events selected by the tau selection. Distribution of the centre-of-mass energy of the reconstructed charged tracks. This cut was excluded.
6. Events selected by the common lepton selection. Missing mass square distribution.
7. Correlation between Missing mass square and charged energy.
8. Events selected by the common lepton selection. Ecal wire energy distribution. The Monte Carlo Energy has been multiplied by 0.976 to fit the data !!
9. Ecal energy as a function of $\cos\theta$ for Bhabha candidates (see section 3.4).
10. Number of events as a function of W for (a) no associated single-arm trigger, (b) only one jet with associated single-arm trigger, (c) both jets with associated single-arm trigger.
11. Efficiency for events with both jets triggering.
12. Predicted cross section for $\gamma\gamma$ events (see text for definition) as a function of $\cos\eta$.
13. Measured cross section for $\gamma\gamma$ events (see text for definition) as a function of $\sqrt{s}$.
14. Angular distribution of the selected $\gamma\gamma$ events.
15. Mesured cross section for $\gamma\gamma$ events (see text for definition) as function of $\cos\eta$ at $\sqrt{s} = 88.2, 89.2, 94.2\text{GeV}$.
16. Number of events selected as $\gamma\gamma$ (see text for definition) as function of W at $\sqrt{s} = 88.2, 89.2, 94.2\text{GeV}$.
17. Number of events as a function of $\cos\theta$ for the $q\bar{q}$ Montecarlo events passing the tau selection.
18. Number of events as a function of $\cos\theta_{jt}$ for Data and Monte Carlo. $N_{track} > 3$ is required to enhance the $q\bar{q}$ contribution.
19. Distribution of $d0_{min}$ for events with no ITC linked coordinates. For 1990 runs before run 9040 (a) and after (b).
20. Distribution of $d0_{min}$ for events passing the common-lepton selection. The flat tail is caused by the cosmic-ray background.

21. Hcal energy (a) and difference between Ecal wire and Ecal pad energies (b) in events with two muons.

22. Angular distributions for the events with two muons

23. TPC energy vs ECAL energy in events with two muons

24. TPC+ECAL energies form Monte Carlo (a) and Data (b) in events with two muons

25. Missing mass distribution for events with TPC+ECAL energies larger (a) and smaller (b) the 70 GeV in events with two muons.

26. Maximum momentum of the muons in events with two muons for energy sum larger (a) and smaller (b) then 70 GeV.

27. $\tau^+\tau^-$ Monte Carlo events. Angular distribution for events with one charged track satisfying the "good track" criteria (cut 1). Less then 4 tracks in the TPC (a) and more then 4 tracks in the TPC (b). The latter are typically events where one of the decay products of the tau interacts in the apparatus.

28. Comparison between standard Monte Carlo events (full line) and paired-half-events from Monte Carlo (crosses). Missing mass distribution (a), Ecal wire energy (b).

29. Comparison between standard Monte Carlo events (full line) and paired-half-events from Monte Carlo (crosses). Scalar sum of the momenta of the charged tracks (a), Track multiplicity (b).

30. Comparison between standard Monte Carlo events (full line) and paired-half-events from Monte Carlo (crosses). Largest momentum of a single track (a), Maximum transverse momentum of the jet (b).

31. Comparison between standard Monte Carlo events (full line) and paired-half-events from Monte Carlo (crosses). Invariant mass of the reconstructed charged particles (a) and acollinerity (b).

32. Comparison between standard Monte Carlo events (full line) and paired-half-events from Data (dots). Missing mass distribution (a), Ecal wire energy (b).

33. Comparison between standard Monte Carlo events (full line) and paired-half-events from Data (dots). Scalar sum of the momenta of the charged tracks (a), Largest momentum of a single track (b).

34. Comparison between standard Monte Carlo events (full line) and paired-half-events from Data (dots). Invariant mass of the reconstructed charged particles (a) and acollinerity (b).

35. Ratio between the error on the efficiency obtained with multiple pairing of the events and the error obtained using each hal-event only once. It is a function of the efficiency.

36. MM^2 distribution for DATA and Monte Carlo, zoom near $MM^2 = 0$.

37. MM^2 distribution for DATA(a) and Monte Carlo(b), zoom near $MM^2 = 0$ with a gaussian fit to the central bins.

38. Ratio between selected $\tau^+\tau^-$ events and luminosity as function of time (a). Same for "common lepton" events (b).

39. Cross section for $e^+e^- \rightarrow \tau^+\tau^-$ vs cross section for $e^+e^- \rightarrow hadrons$. The streigth line fits with (a) and without (b) the constraint at the origin are shown.

40. (a) difference θ^* - θ^τ between the reconstructed cms scattering angle θ^* and the true $\tau^+\tau^-$ production angle θ^τ from Monte Carlo .
(b) difference θ^*-θ^τ between the reconstructed cms scattering angle and the direction of the τ pair from the thrust axis.

41. Number of events as a function of the total charge measured by the TPC for events passing the tau selection

42. Charged multiplicity correlations in the two hemispheres vs. the total charge measured by the TPC . Events with n charged tracks in one hemisphere and m tracks in the opposite are labelled nm in the vertical axis .

43. Impact parameter for the track with the lowest momentum per hemisphere in events with 1+2 charged multiplicity and non zero total charge.

44. e^+e^- identification efficiency from MonteCarlo for :
(a) events with $m_x^2 > 400\,GeV^2$, $E_{wires} > 75$ GeV
(b) events with $m_x^2 > 400\,GeV^2$, $E_{wires} < 55$ GeV

45. angular distribution of identified e^+e^- events at peak energy.

46. Variation of the measured value of the forward backward asymmetry as a function of the total percentage of e^+e^- background in the data .

47. Fit to the $cos\theta^*$ distribution for events $\tau^+\tau^-$ events :
(a) $\sqrt{s} = 88.28GeV$
(b) $\sqrt{s} = 81.28GeV$
(c) $\sqrt{s} = 94.28GeV$

48. Correlation between the the two parameters a_1 (asymmetry coefficient) and a_2 (curvature) in the fit of the angular distribution .

49. Measured values of the backward asymmetry A_{FB} as a function of $\sqrt{s}$ The dotted line is the result of a fit to $a_e * a_\tau$, $v_e * v_\tau$ coupling constants .

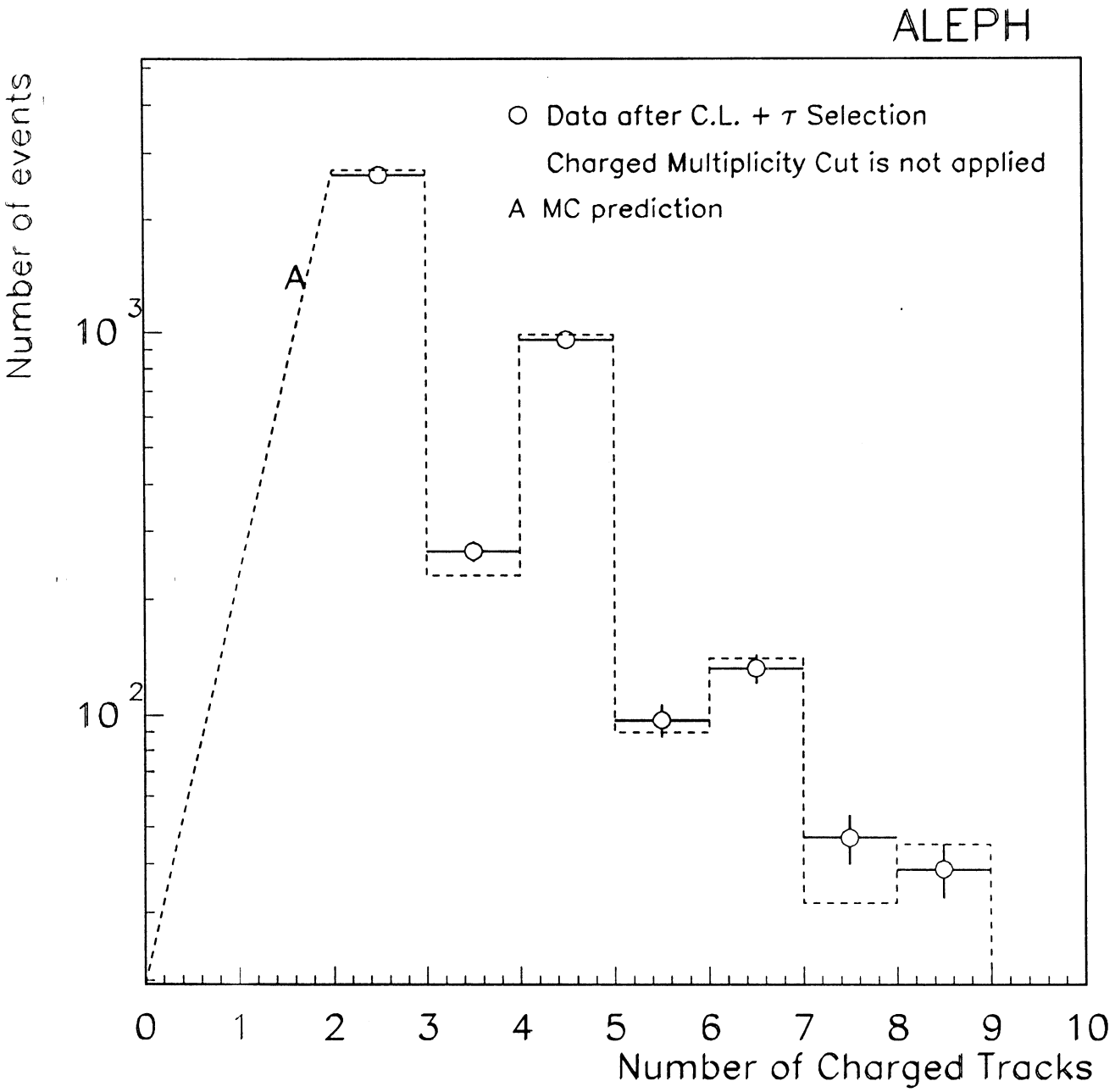
ALEPH
Data after C.L. + τ Selection
Charged Multiplicity Cut is not applied
A MC prediction
A
Number of events
10 3
10 2
0 1 2 3 4 5 6 7 8 9 10
Number of Charged Tracks

Fig. 1

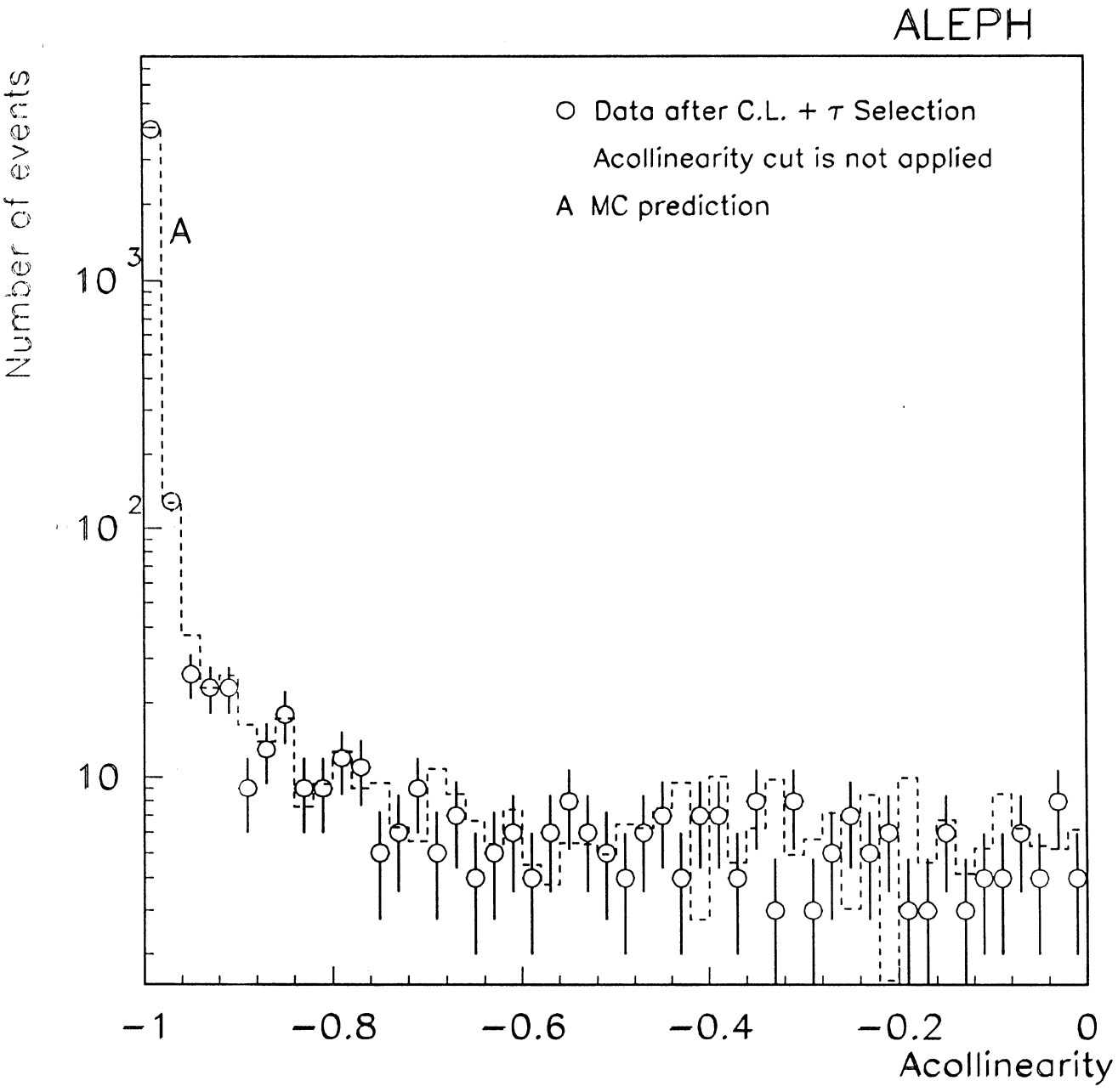
ALEPH
Data after C.L. + τ Selection
Acollinearity cut is not applied
A MC prediction
A
Number of events
10 3
10 2
10
−1
−0.8
−0.6
−0.4
−0.2
0
Acollinearity

Fig. 2

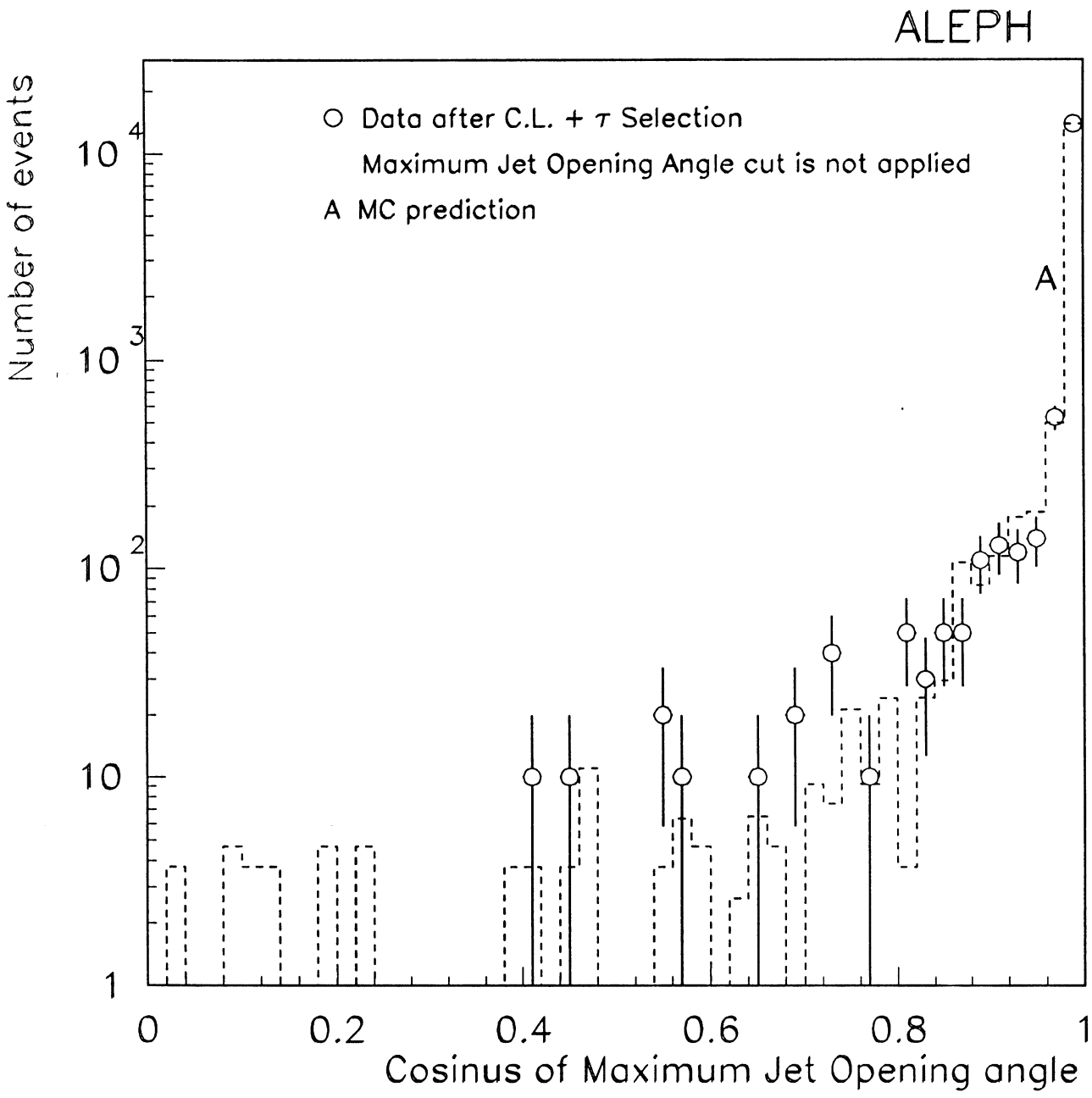
ALEPH
Data after C.L. + τ Selection
Maximum Jet Opening Angle cut is not applied
A MC prediction
A
Number of events
10^4
10^3
10^2
10
1
0
0.2
0.4
0.6
0.8
1
Cosinus of Maximum Jet Opening angle

Fig. 3

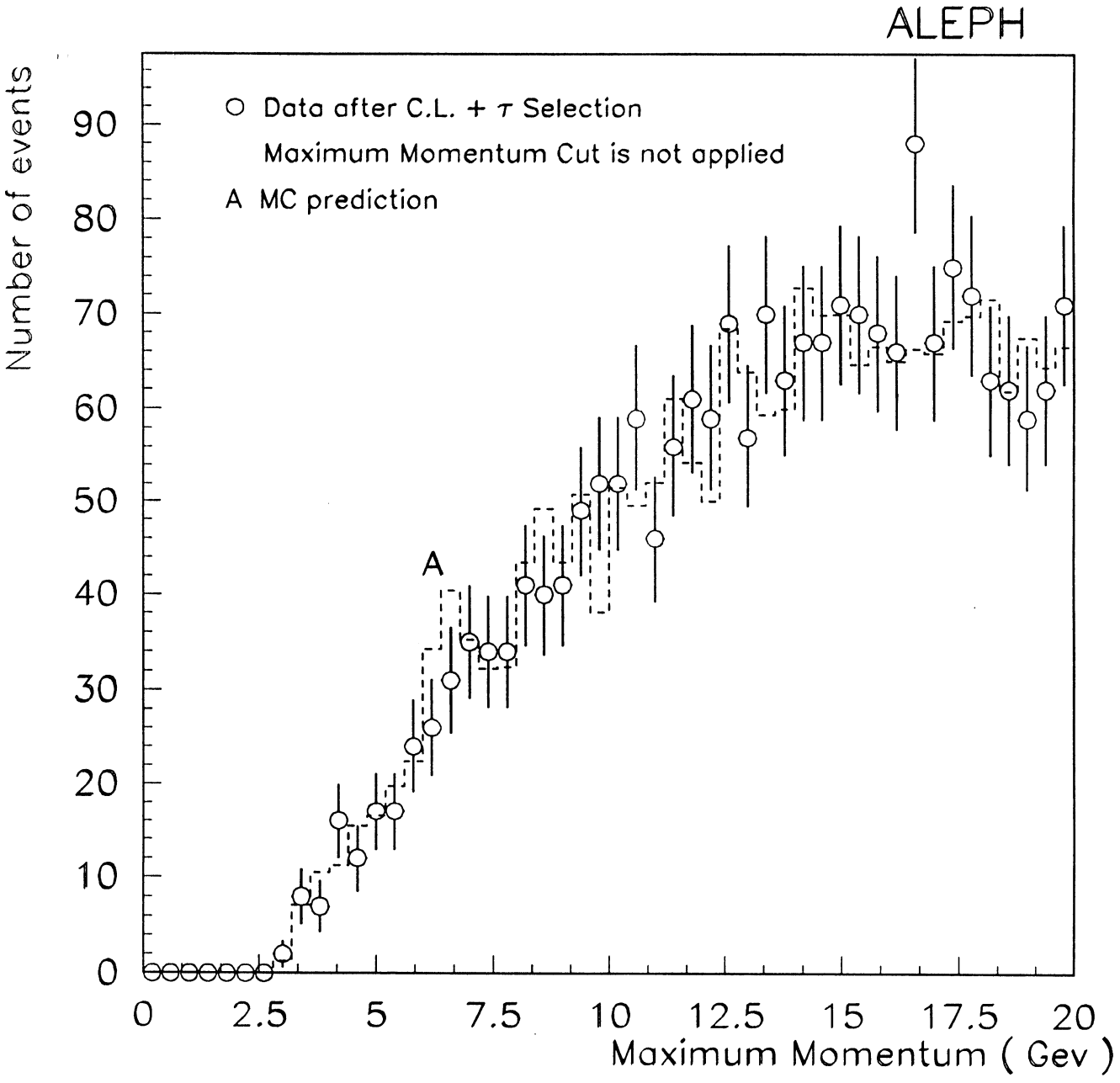
ALEPH
Data after C.L. + τ Selection
Maximum Momentum Cut is not applied
A MC prediction
A
Number of events
0
10
20
30
40
50
60
70
80
90
0
2.5
5
7.5
10
12.5
15
17.5
20
Maximum Momentum (Gev)

Fig. 4

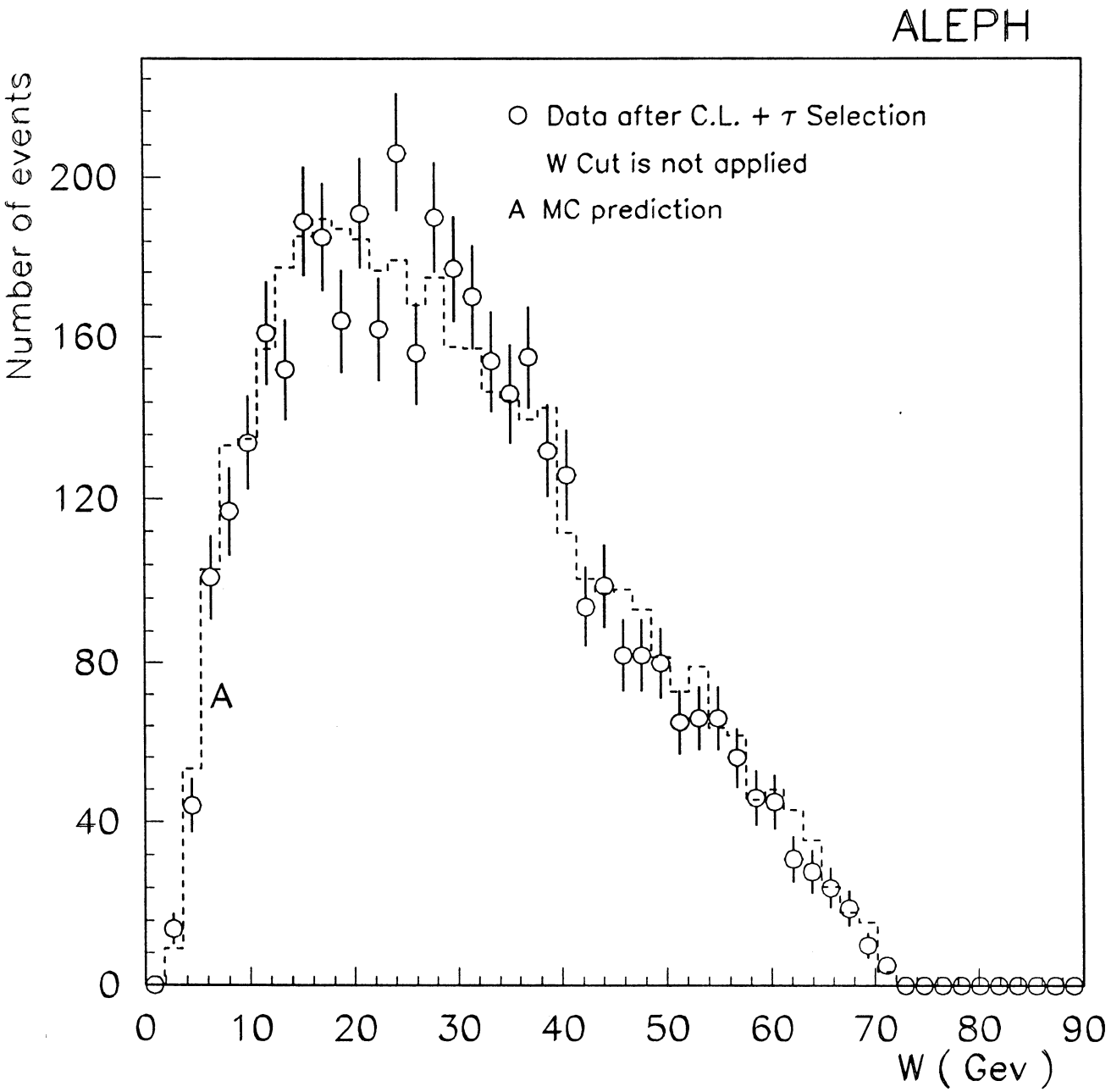
ALEPH
Number of events
Data after C.L. + τ Selection
W Cut is not applied
A MC prediction
A
0
40
80
120
160
200
0
10
20
30
40
50
60
70
80
90
W (Gev)

Fig. 5

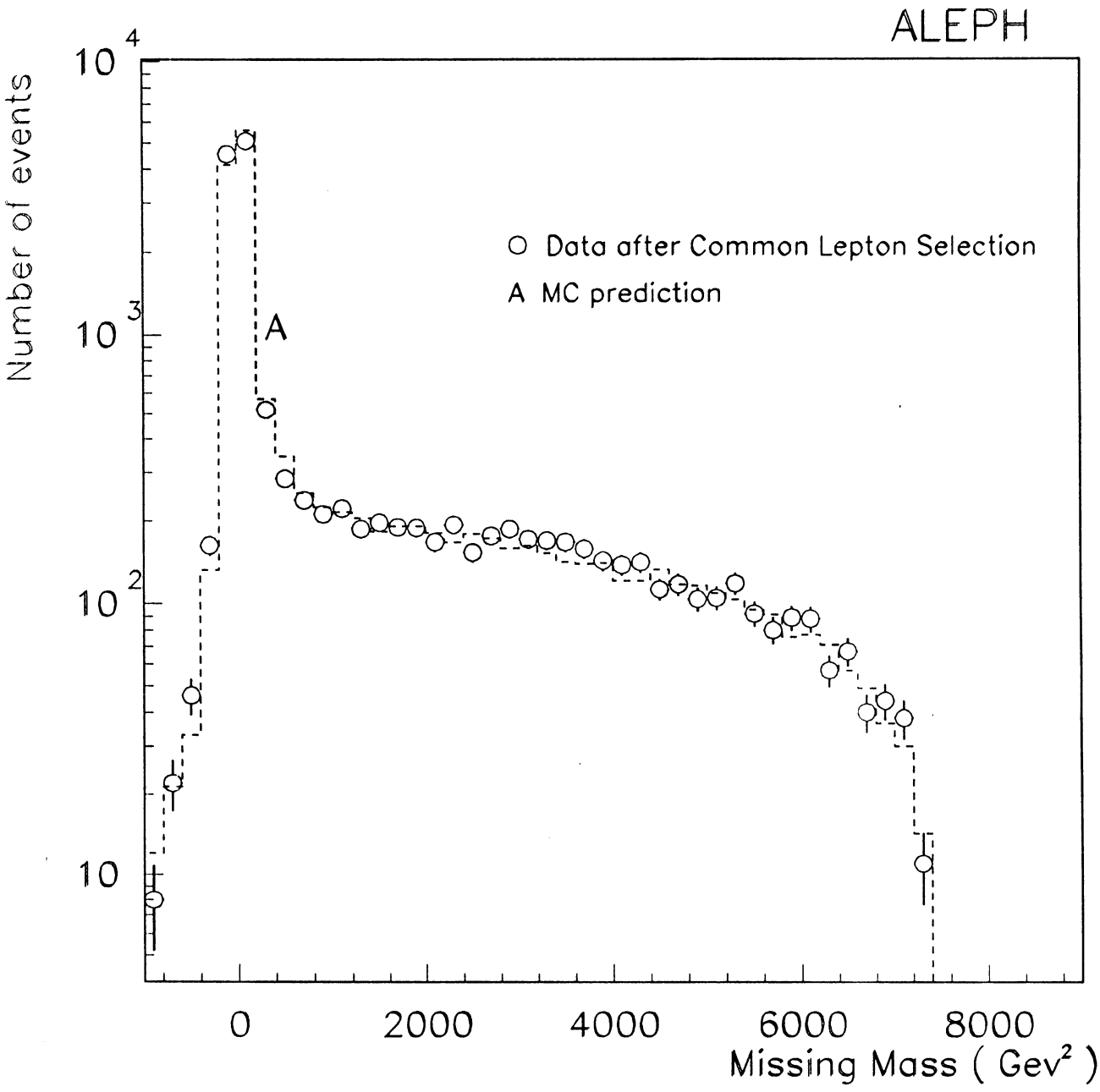
ALEPH
Number of events
10^4
10^3
10^2
10
A
O Data after Common Lepton Selection
A MC prediction
0
2000
4000
6000
8000
Missing Mass (Gev^2)

Fig. 6

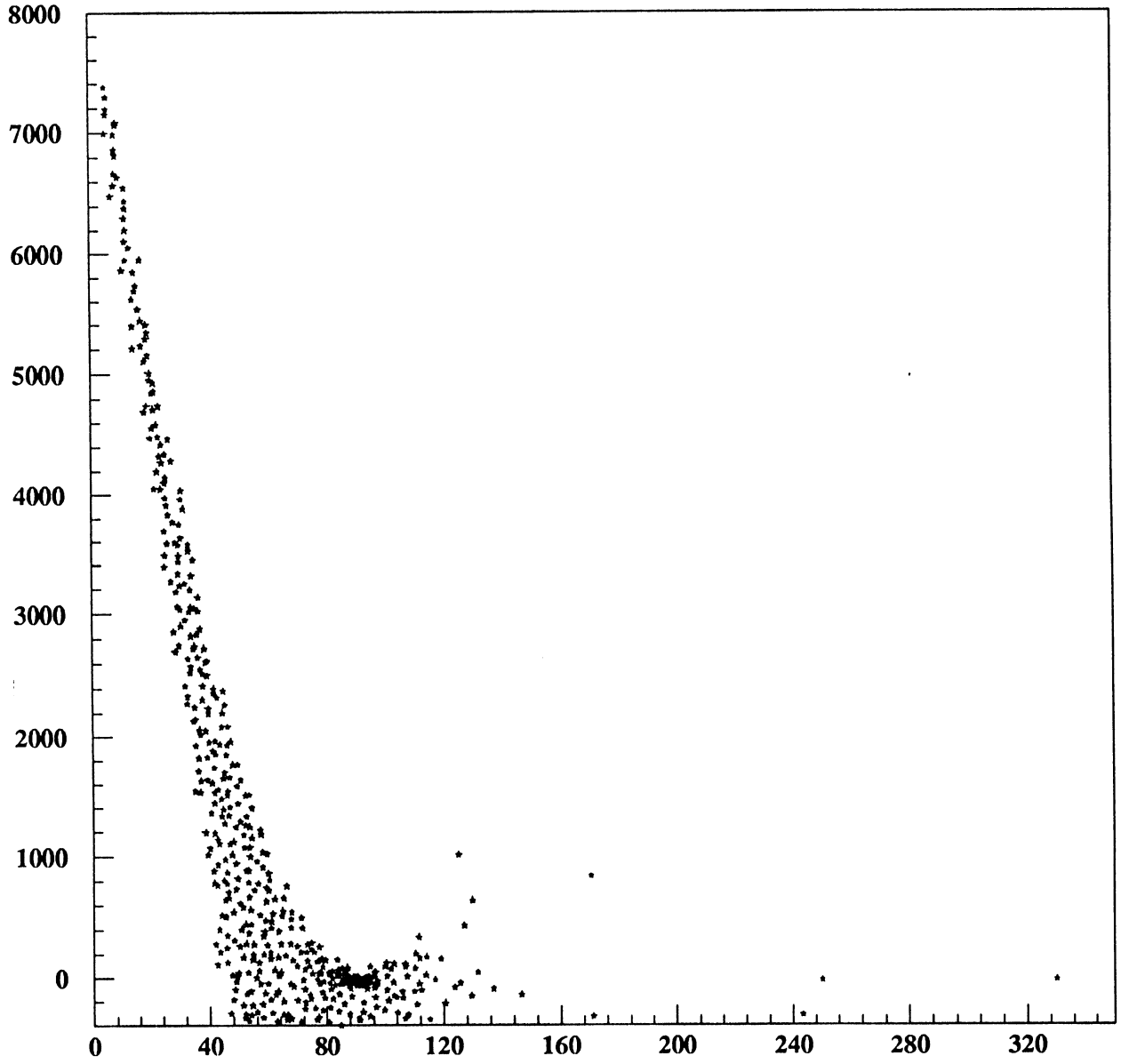

MM^2 vs Charged energy

Fig. 7

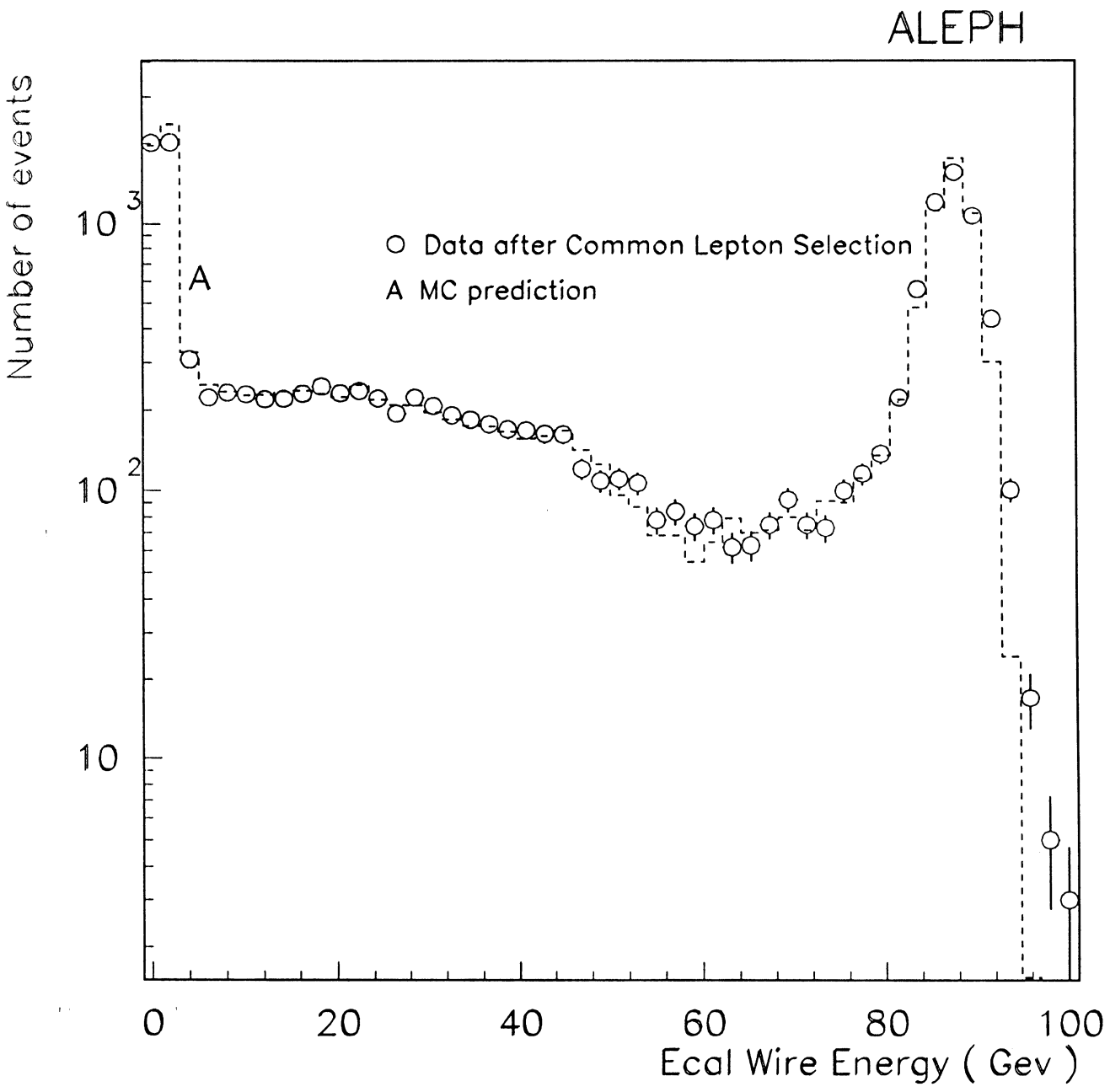
ALEPH
Number of events
10 3
10 2
10
A
Data after Common Lepton Selection
A MC prediction
0
20
40
60
80
100
Ecal Wire Energy (Gev)

Fig. 8

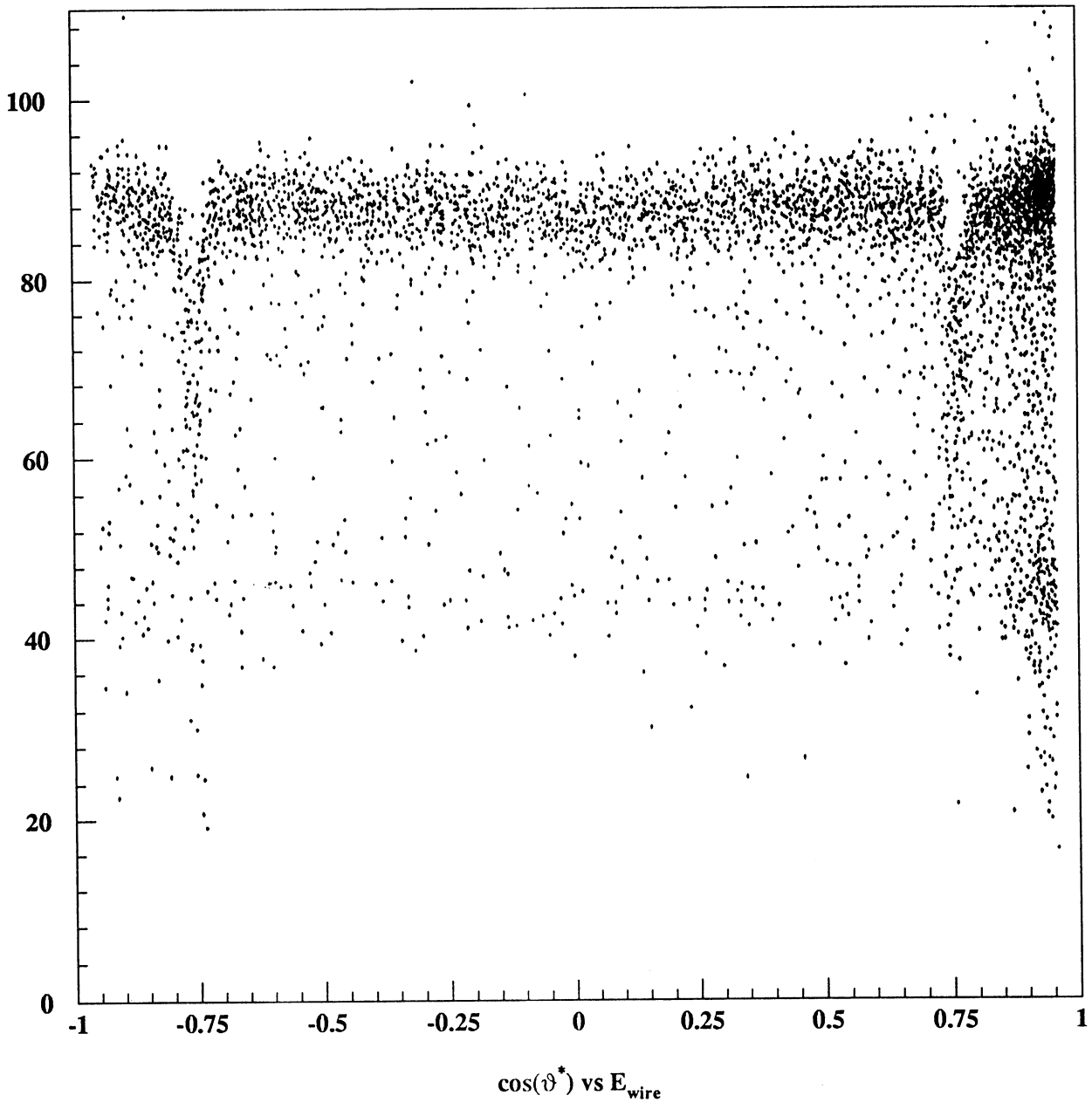

Fig. 9

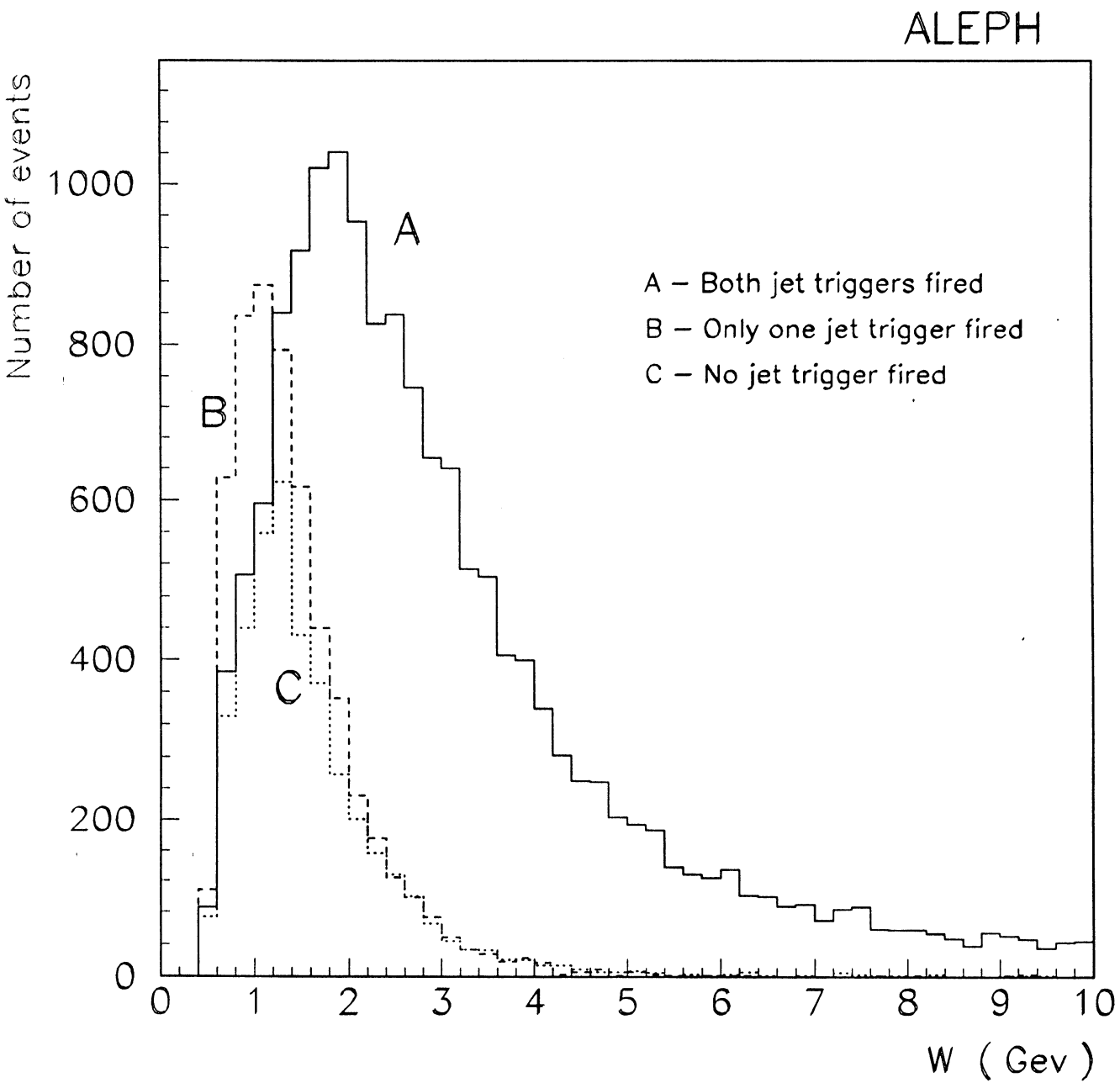
ALEPH
Number of events
1000
800
600
400
200
0
A
B
C
A – Both jet triggers fired
B – Only one jet trigger fired
C – No jet trigger fired
0
1
2
3
4
5
6
7
8
9
10
W (Gev)

Fig. 10

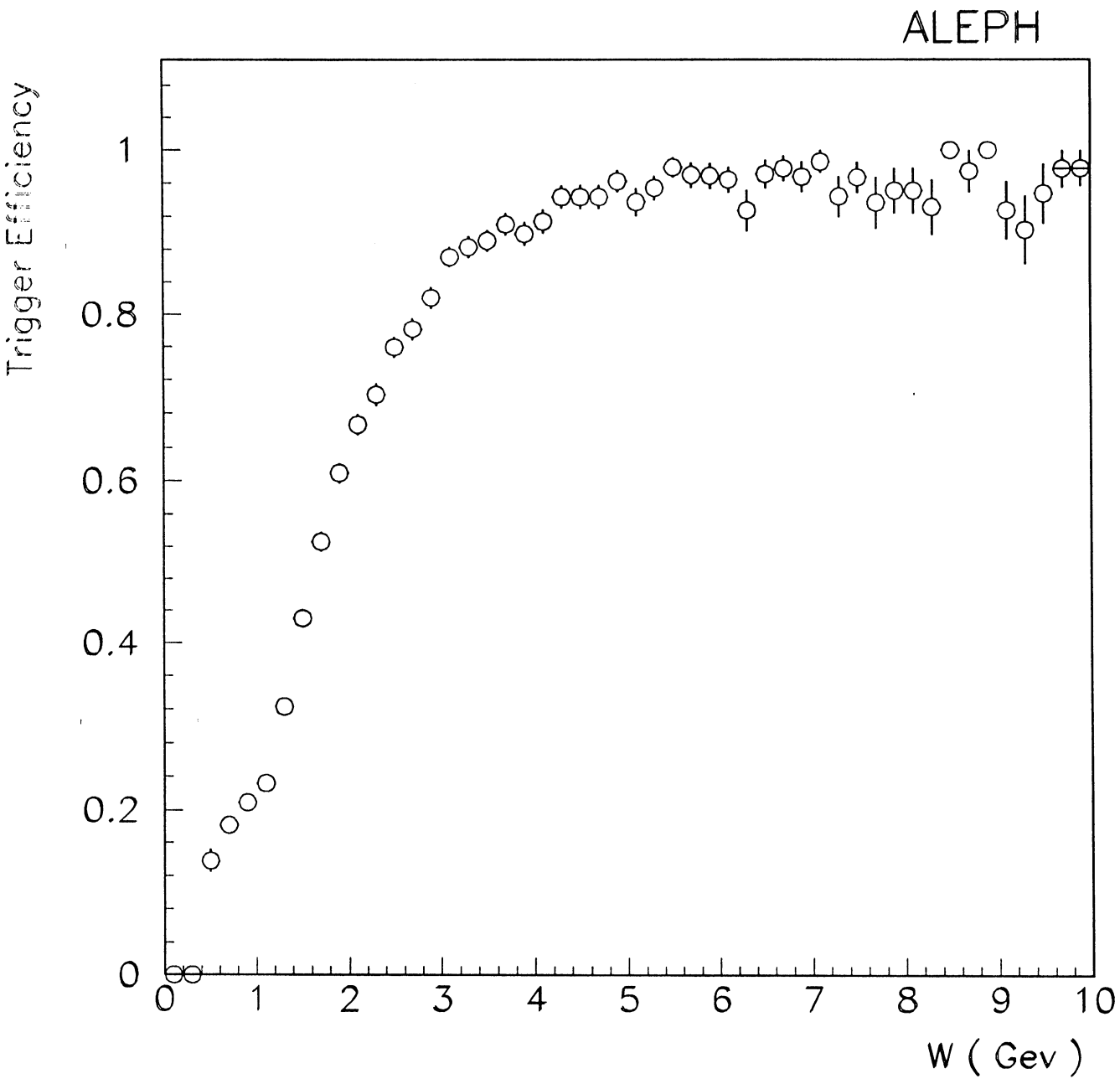

Fig. 11

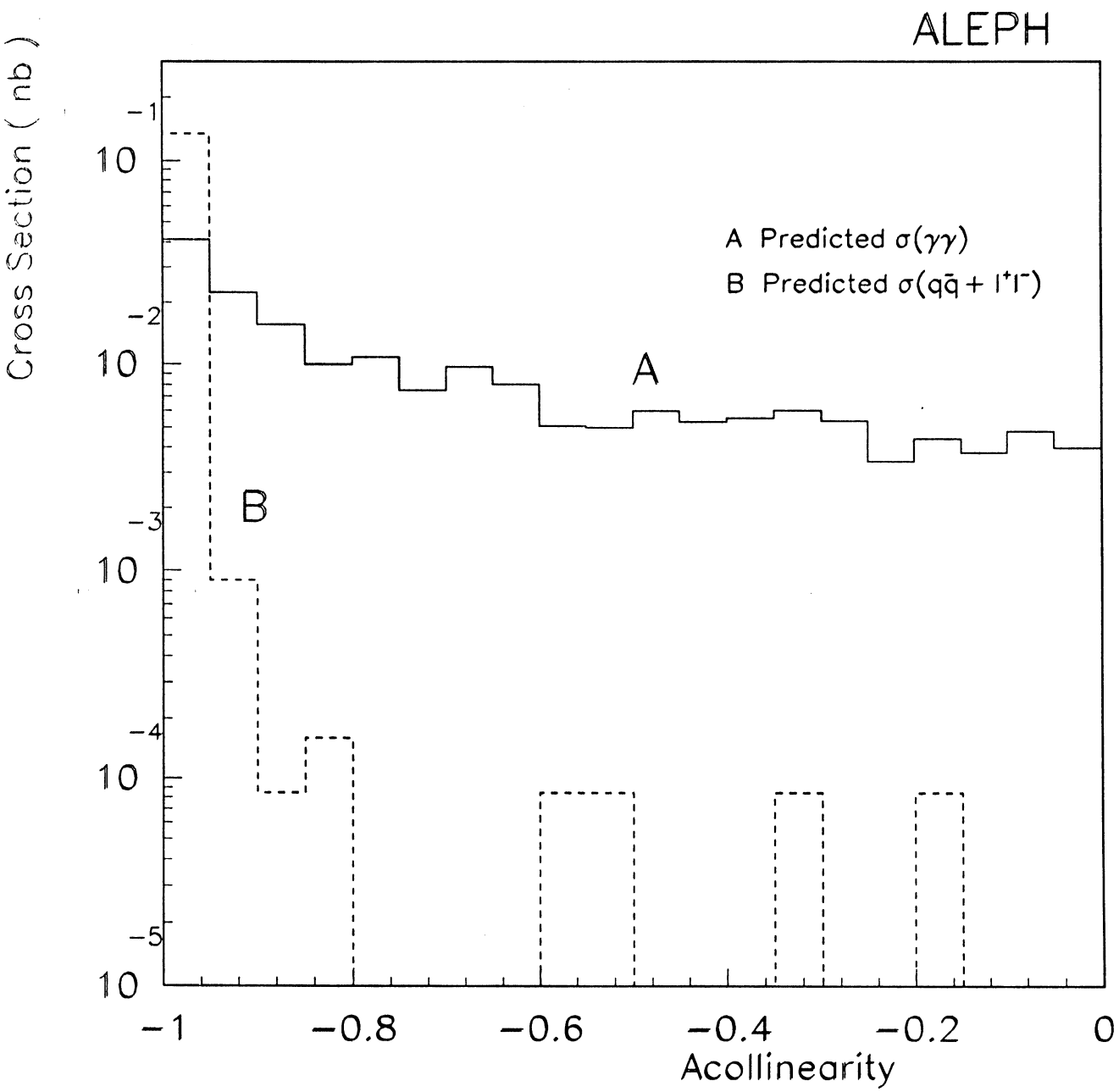
ALEPH
Cross Section (nb)
A Predicted σ(γγ)
B Predicted σ(qq̄ + l⁺l⁻)
A
B
10^-1
10^-2
10^-3
10^-4
10^-5
−1
−0.8
−0.6
−0.4
−0.2
0
Acollinearity

Fig. 12

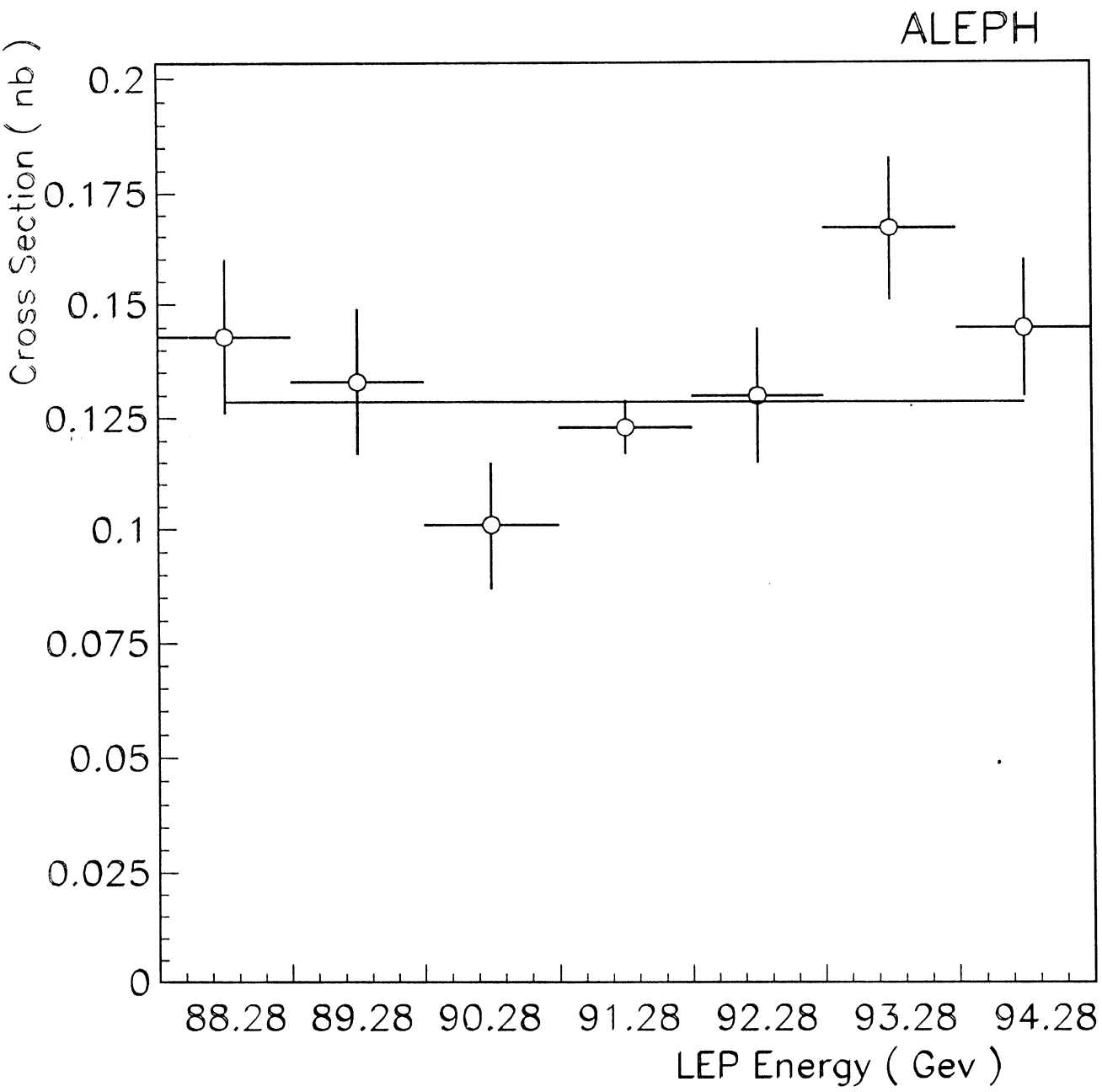
ALEPH
Cross Section (nb)
0.2
0.175
0.15
0.125
0.1
0.075
0.05
0.025
0
88.28
89.28
90.28
91.28
92.28
93.28
94.28
LEP Energy (Gev)

Fig. 13

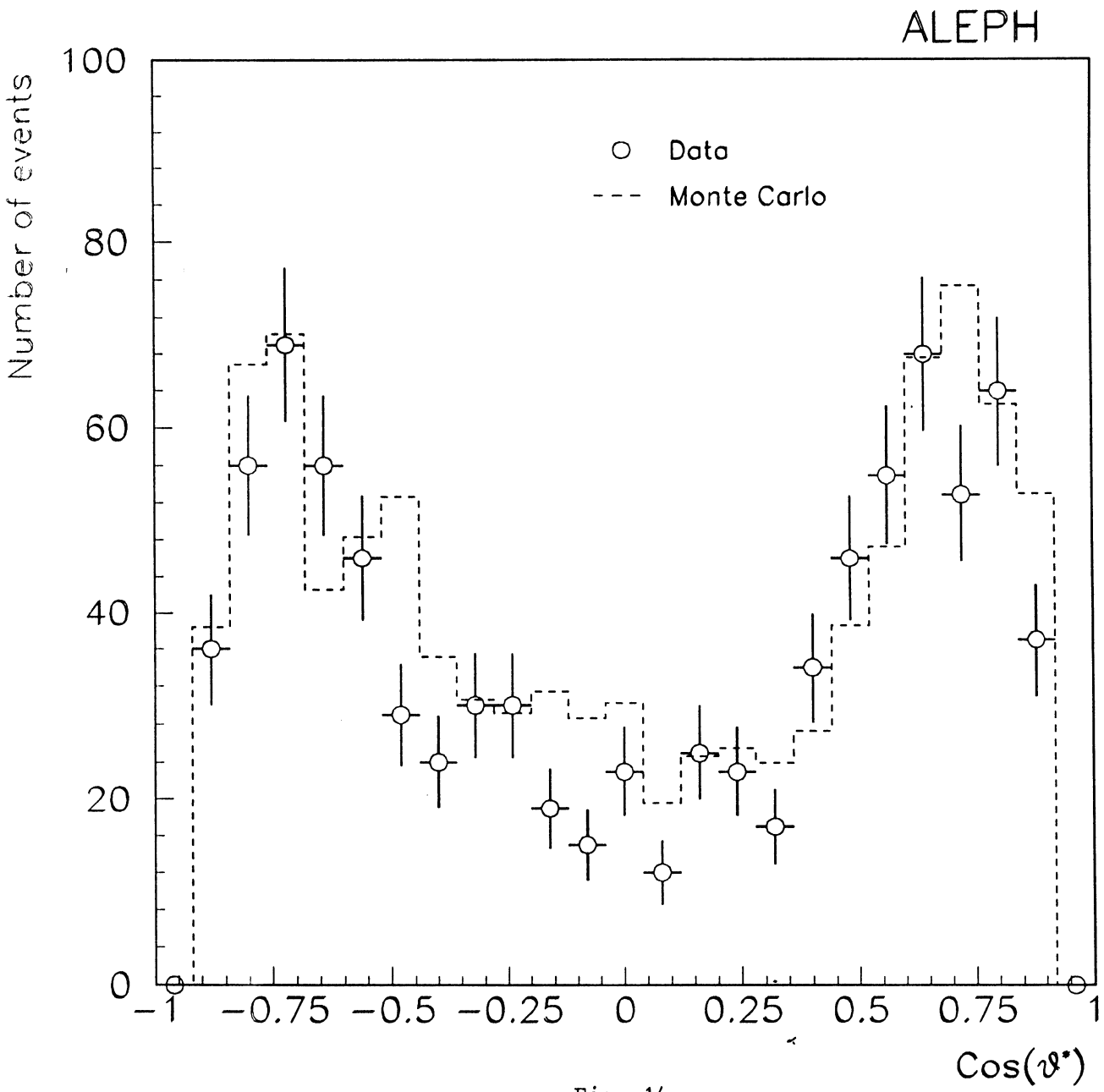
ALEPH
Data
Monte Carlo
Number of events
100
80
60
40
20
0
−1
−0.75
−0.5
−0.25
0
0.25
0.5
0.75
1
Cos(ϑ*)

Fig. 14

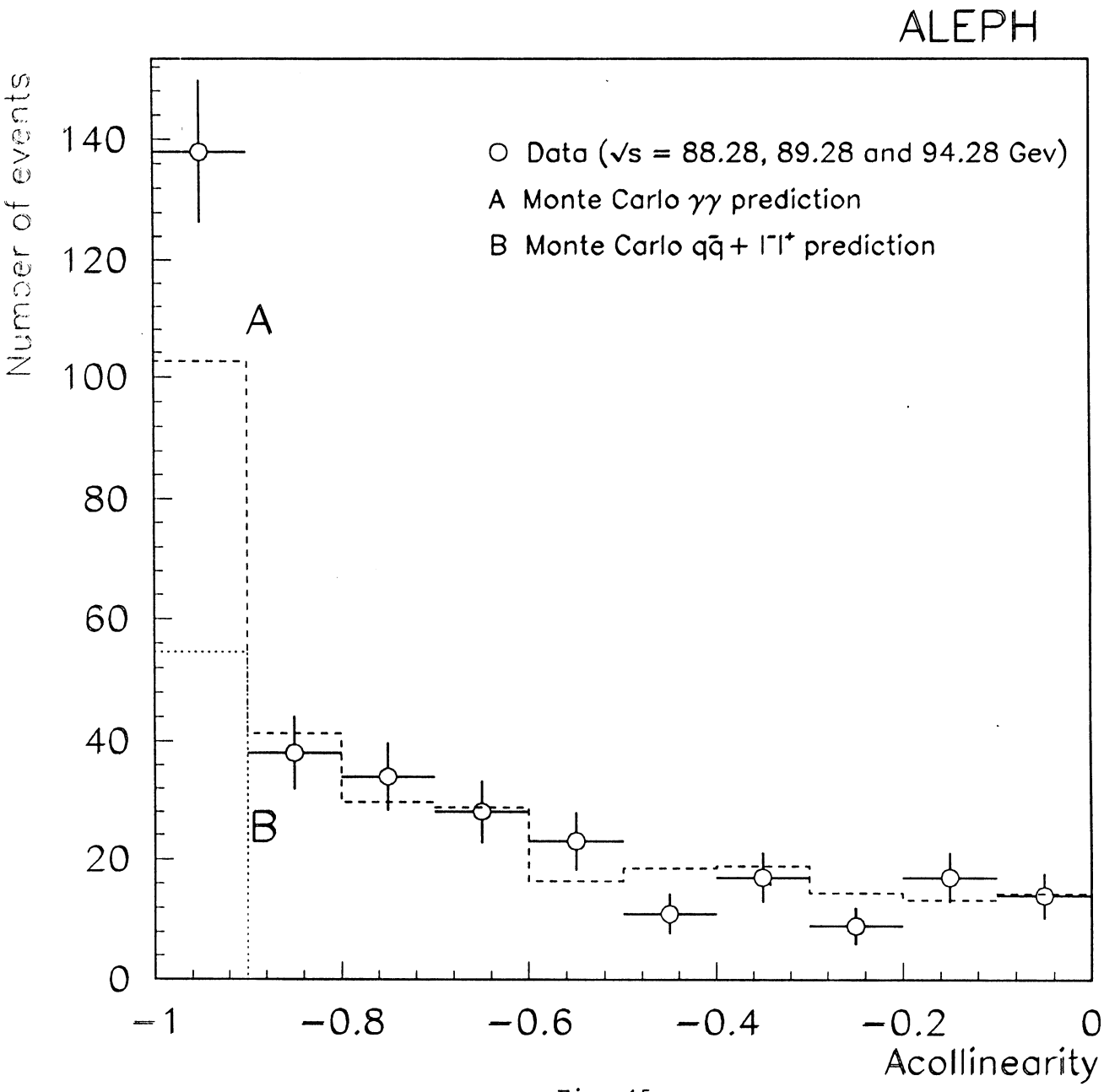
ALEPH
Number of events
140
120
100
80
60
40
20
0
−1
−0.8
−0.6
−0.4
−0.2
0
Acollinearity
O Data (√s = 88.28, 89.28 and 94.28 Gev)
A Monte Carlo γγ prediction
B Monte Carlo qq̄ + l⁻l⁺ prediction
A
B

Fig. 15

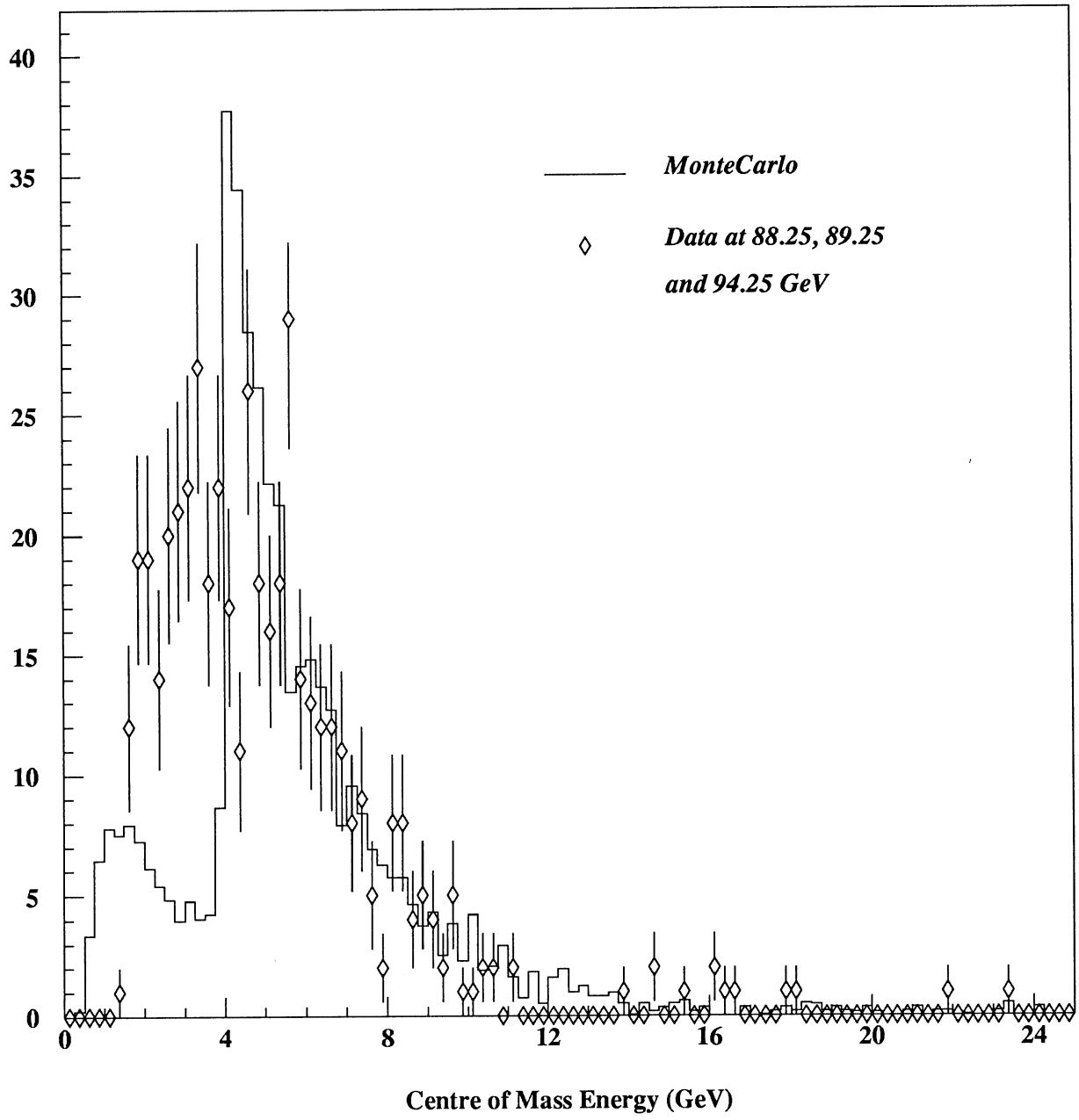
40
35
30
25
20
15
10
5
0
0
4
8
12
16
20
24
MonteCarlo
Data at 88.25, 89.25
and 94.25 GeV
Centre of Mass Energy (GeV)

Fig. 16

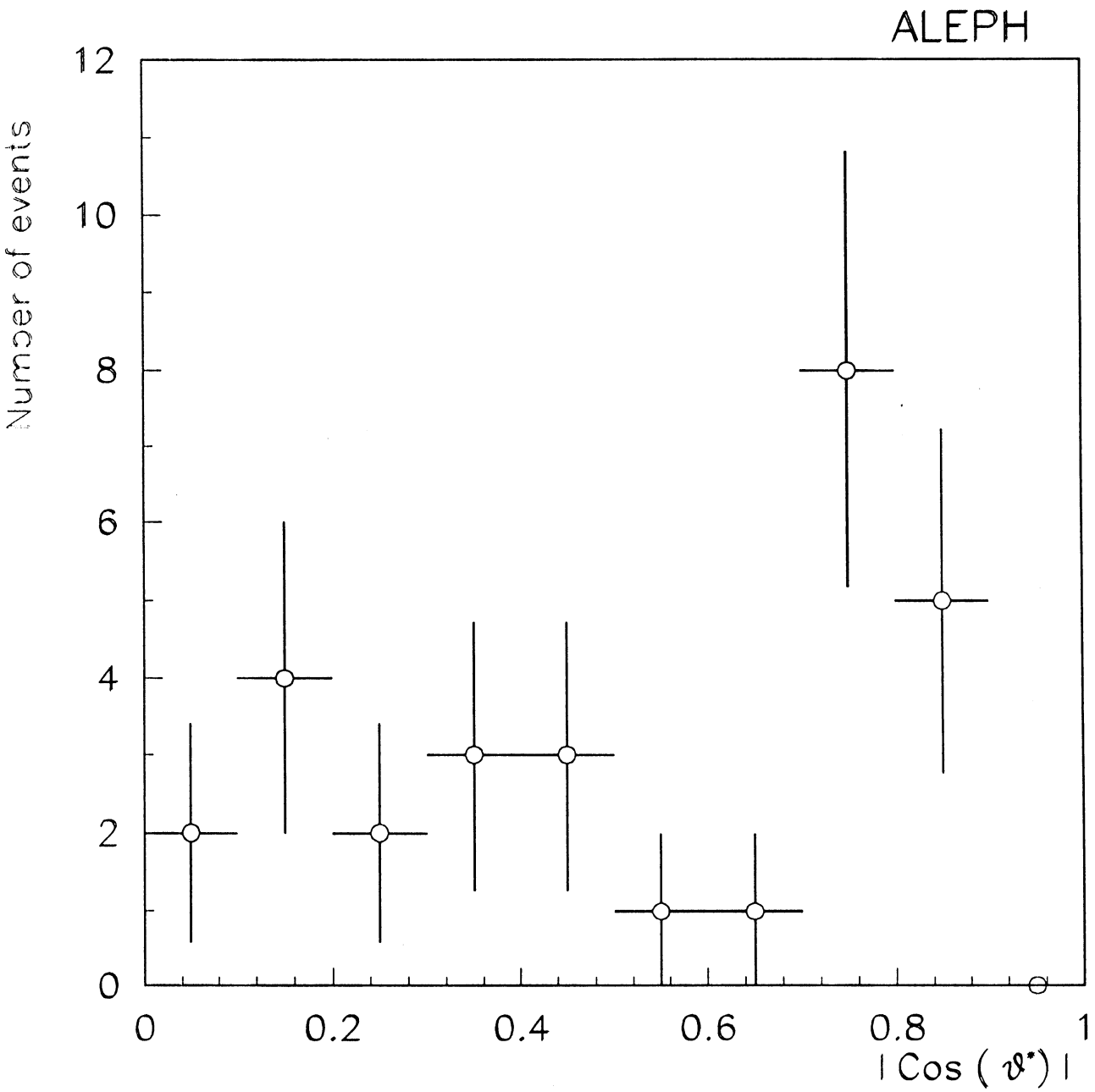

Fig. 17

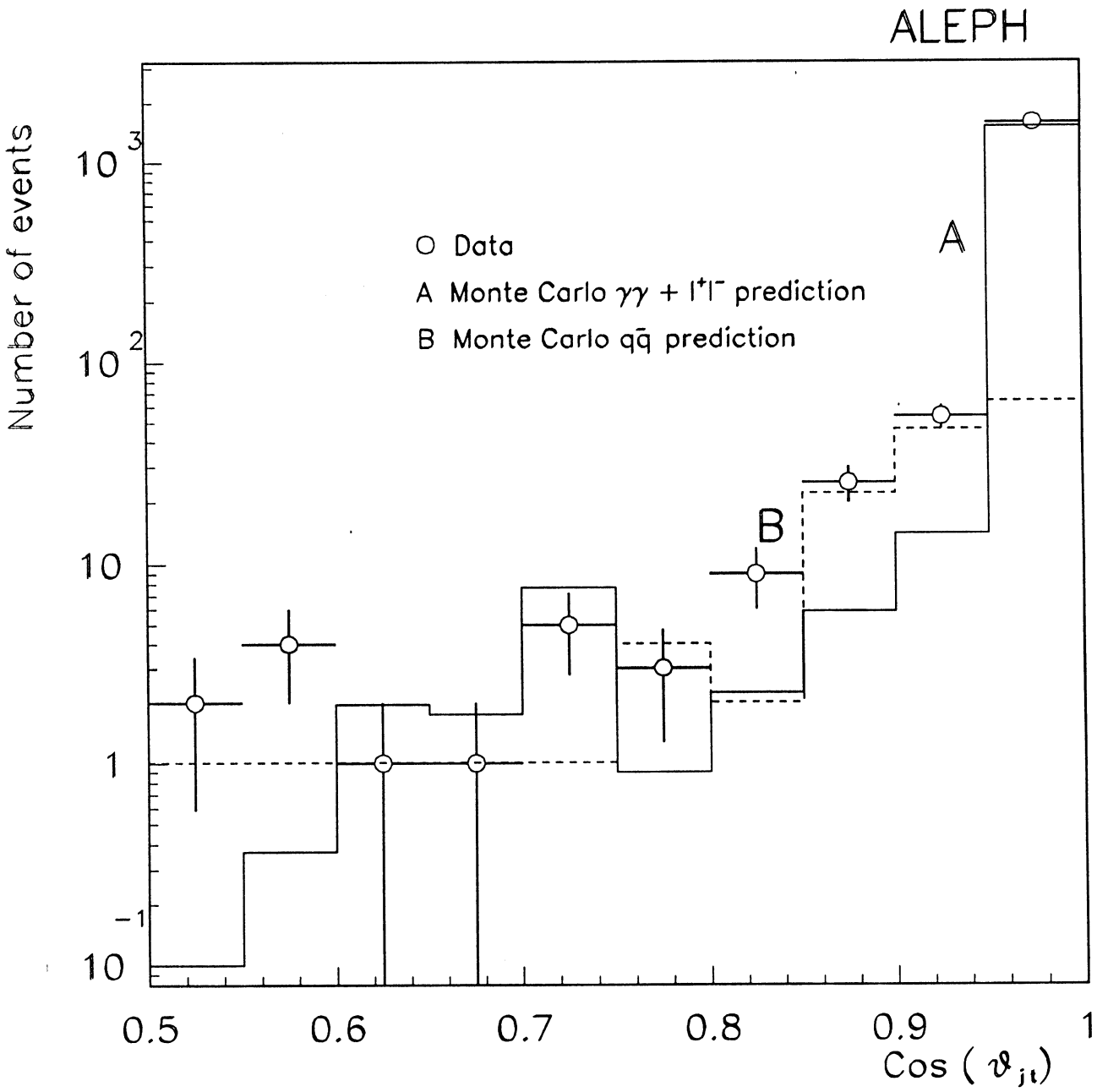
ALEPH
Number of events
10 3
10 2
10
1
-1
10
O Data
A Monte Carlo γγ + l+l- prediction
B Monte Carlo qq̄ prediction
A
B
0.5
0.6
0.7
0.8
0.9
1
Cos (ϑ jt)

Fig. 18

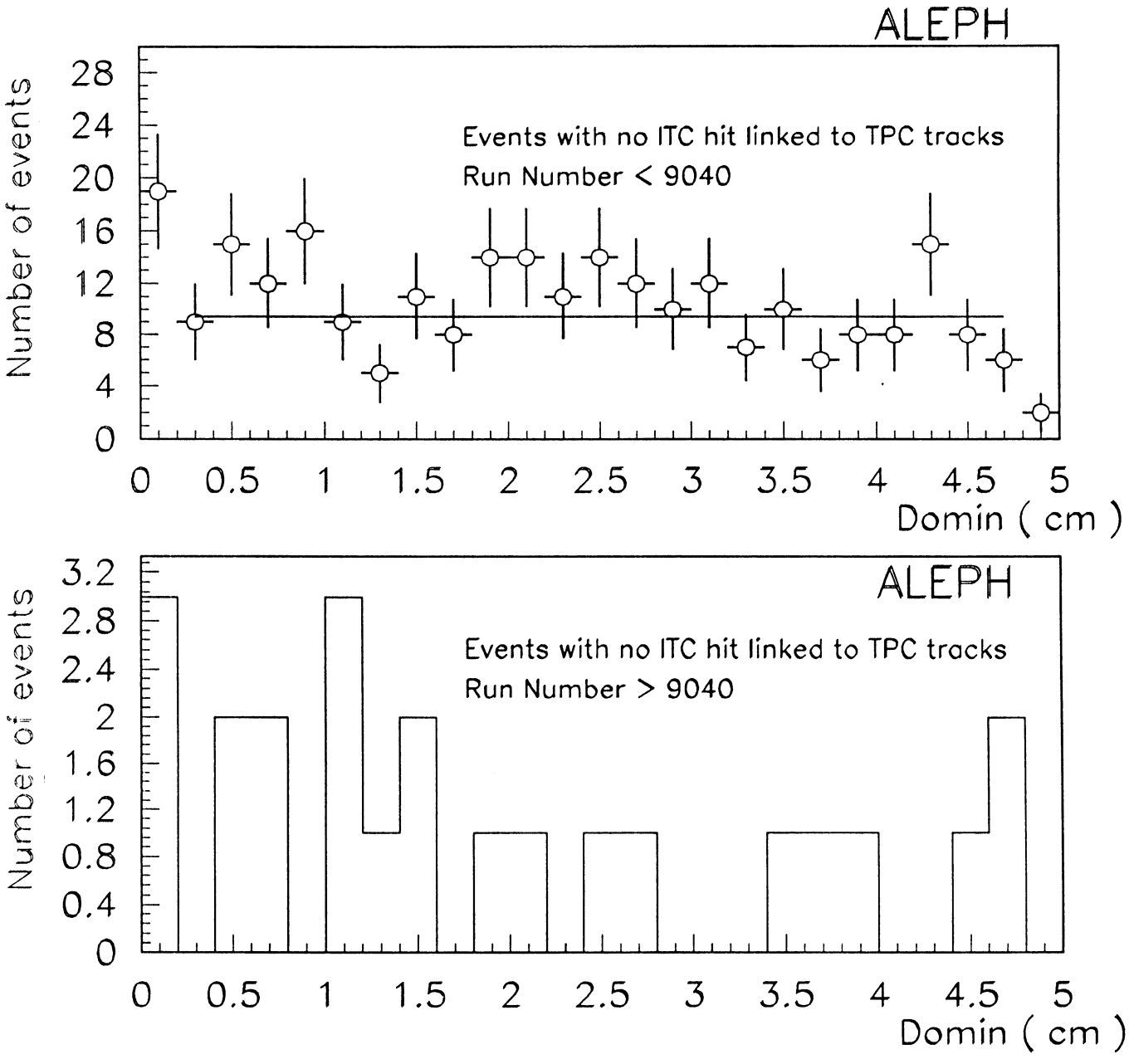
ALEPH
Events with no ITC hit linked to TPC tracks
Run Number < 9040
Number of events
Domin (cm)
ALEPH
Events with no ITC hit linked to TPC tracks
Run Number > 9040
Number of events
Domin (cm)

Fig. 19

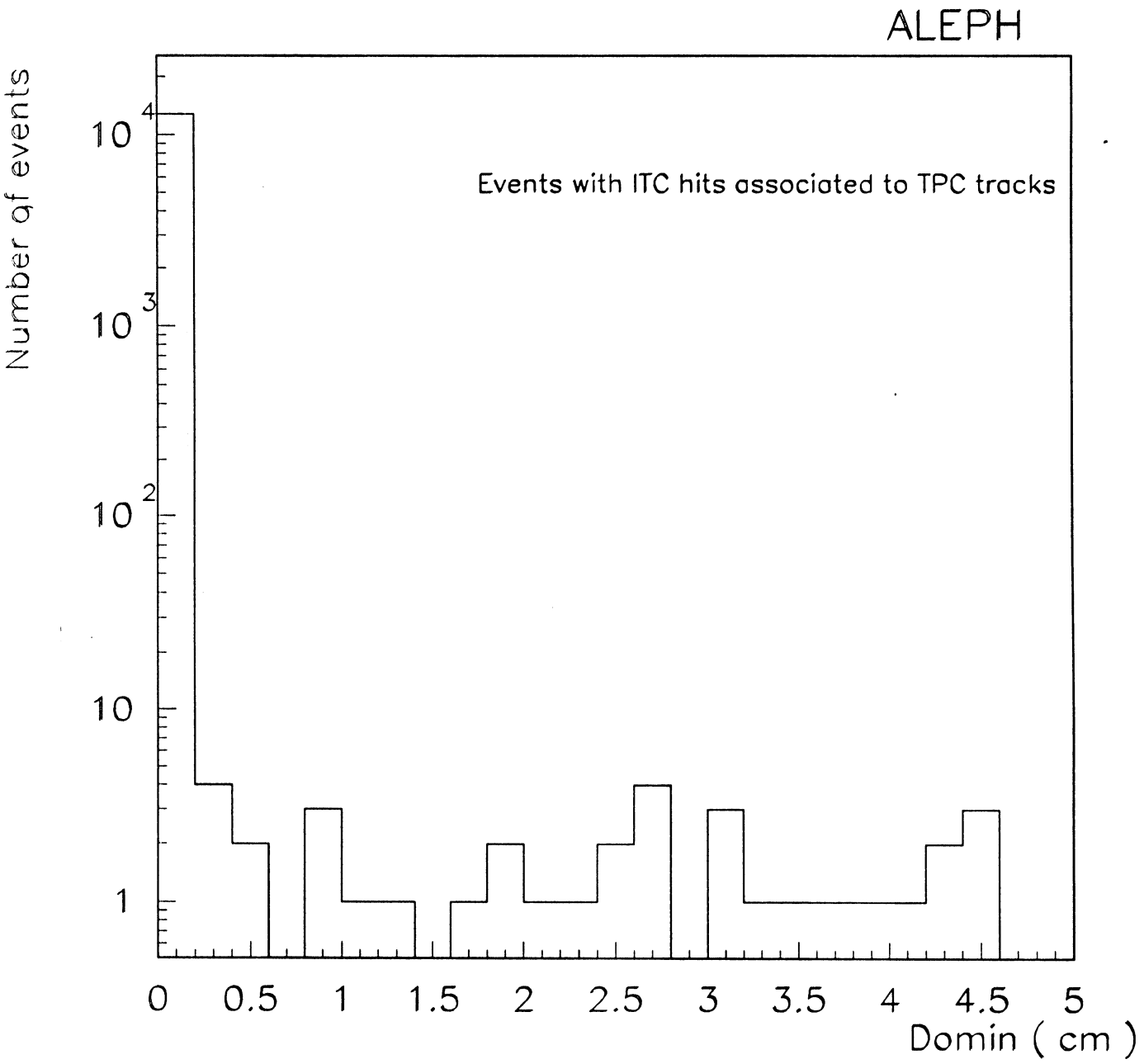
ALEPH
Events with ITC hits associated to TPC tracks
Number of events
10 4
10 3
10 2
10
1
0
0.5
1
1.5
2
2.5
3
3.5
4
4.5
5
Domin (cm)

Fig. 20

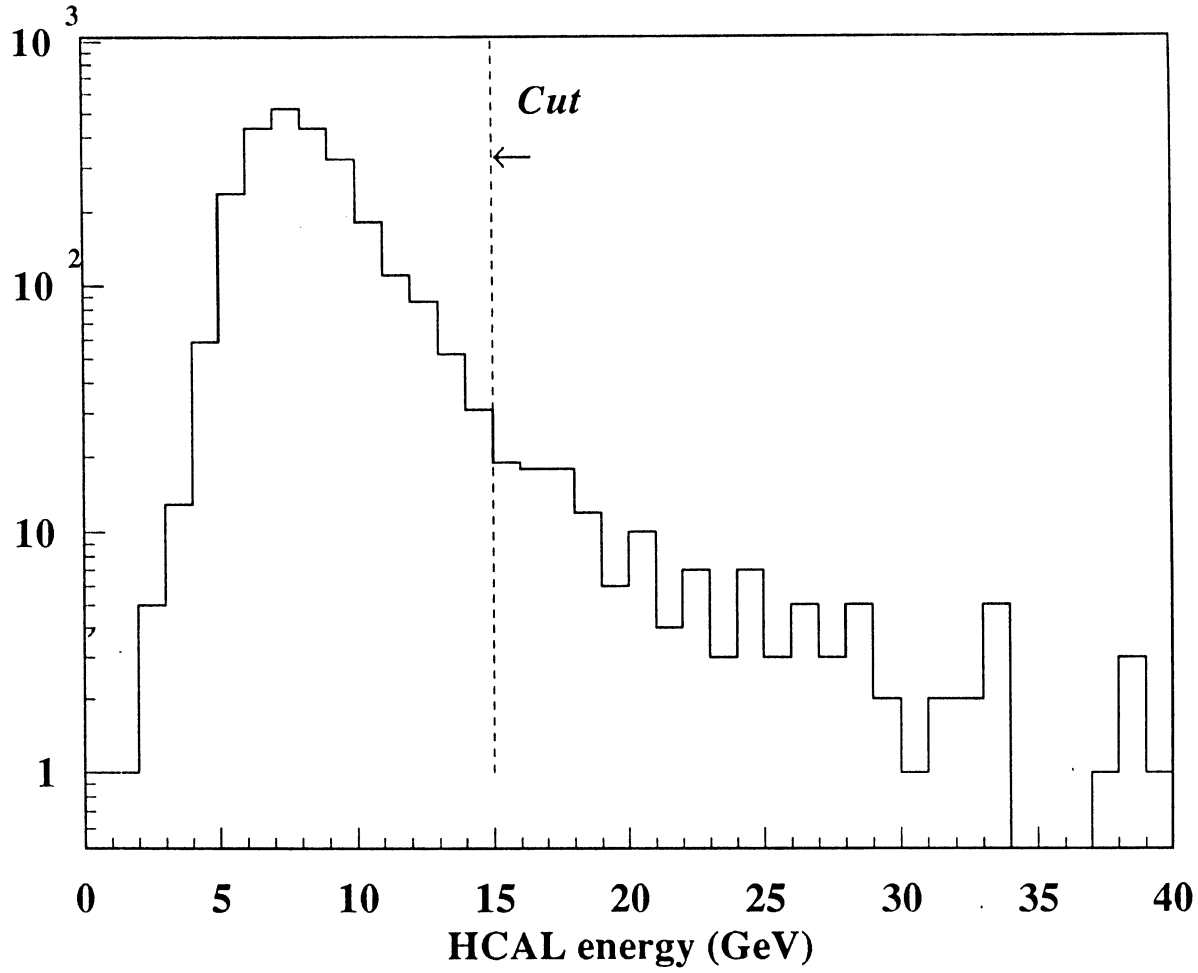
Cut
HCAL energy (GeV)

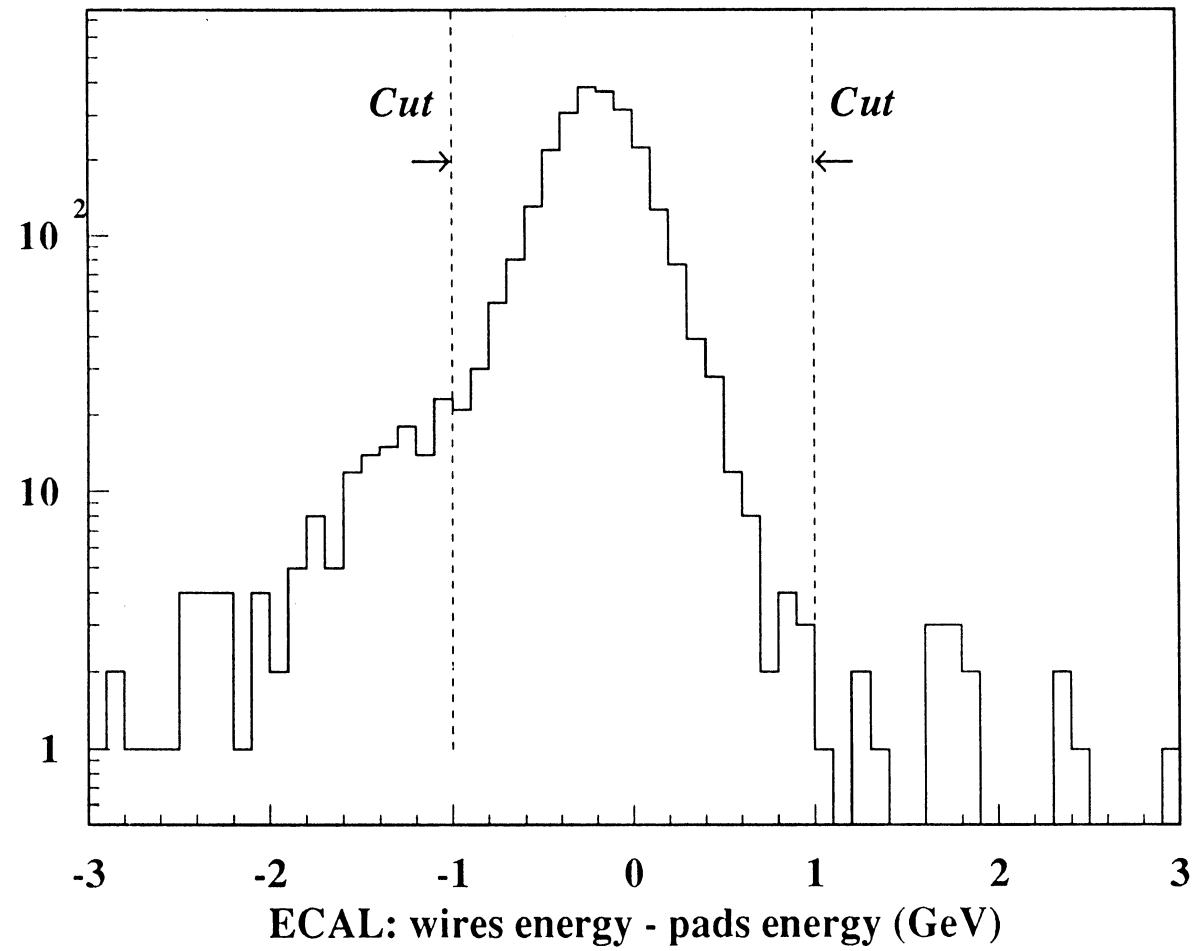
Cut
Cut
ECAL: wires energy - pads energy (GeV)

Fig. 21

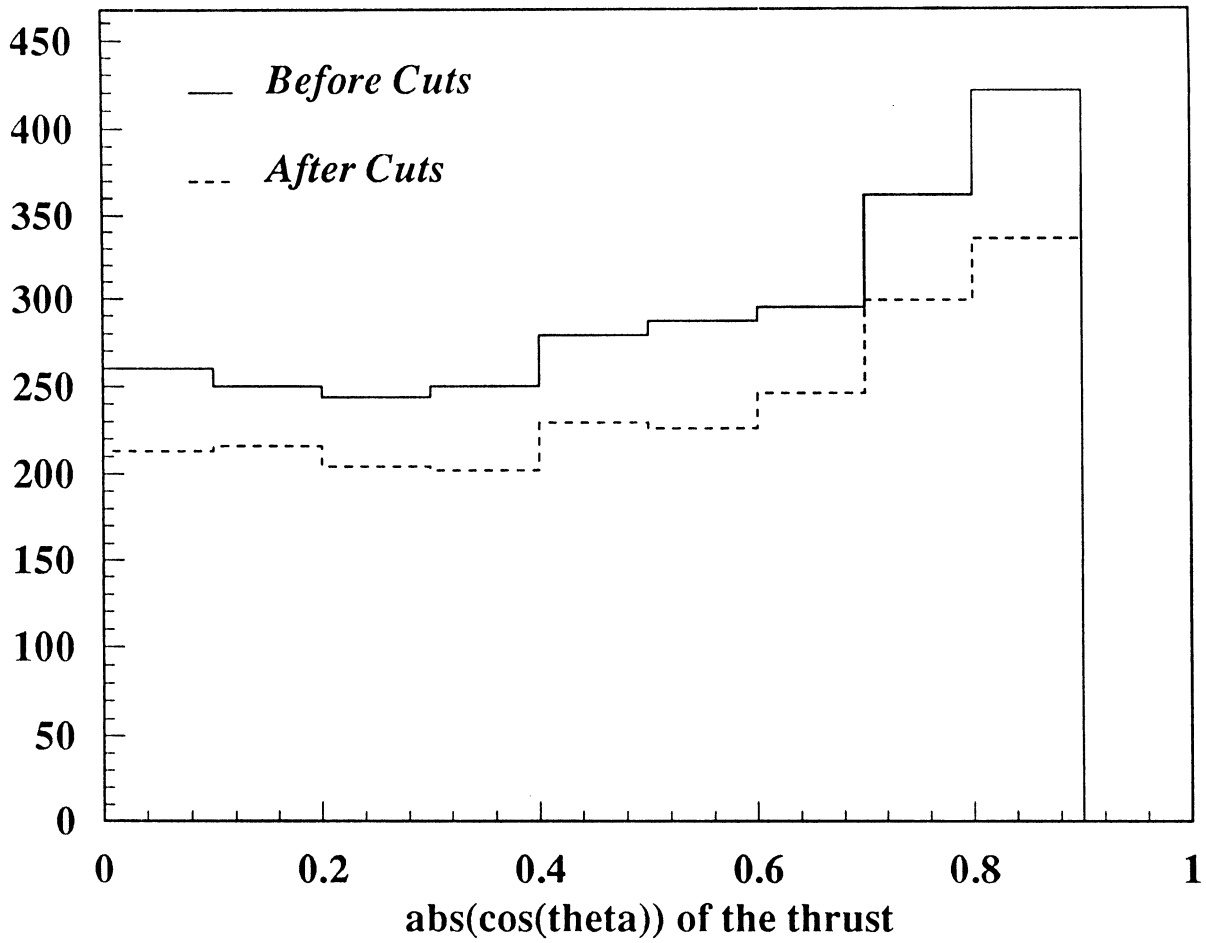
Before Cuts
After Cuts
450
400
350
300
250
200
150
100
50
0
0
0.2
0.4
0.6
0.8
1
abs(cos(theta)) of the thrust

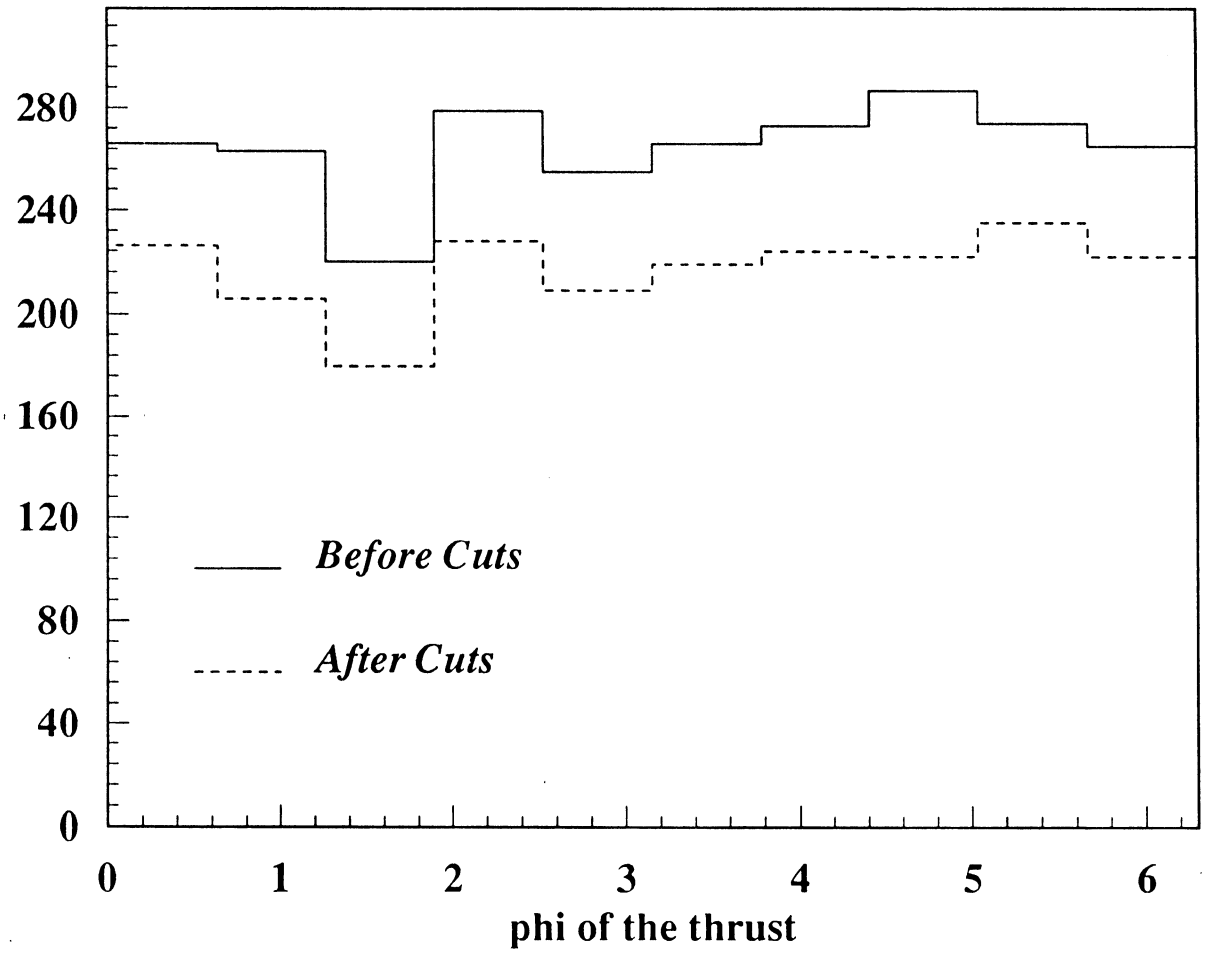
280
240
200
160
120
80
40
0
Before Cuts
After Cuts
0
1
2
3
4
5
6
phi of the thrust

Fig. 22

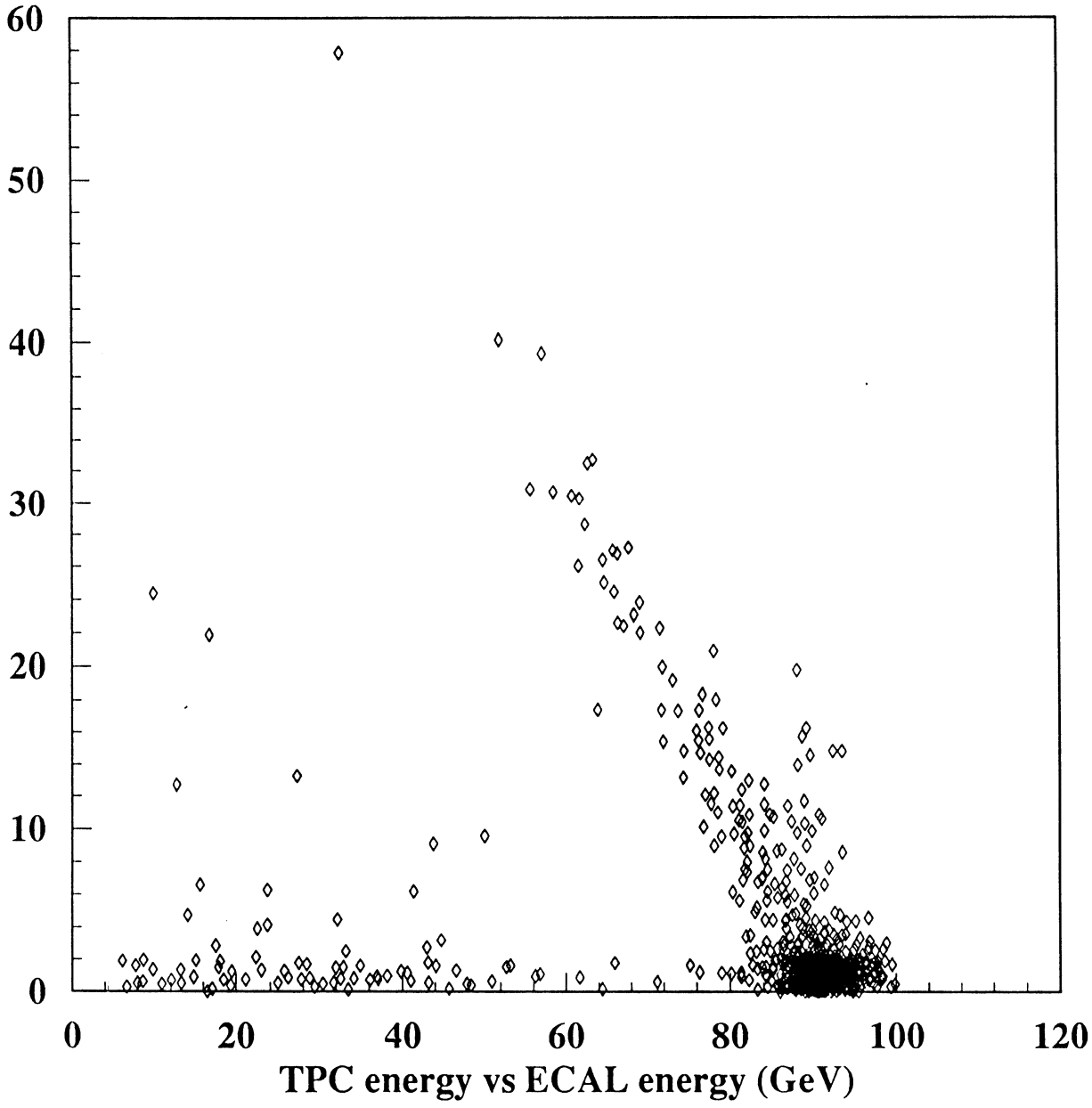
60
50
40
30
20
10
0
0
20
40
60
80
100
120
TPC energy vs ECAL energy (GeV)

Fig. 23

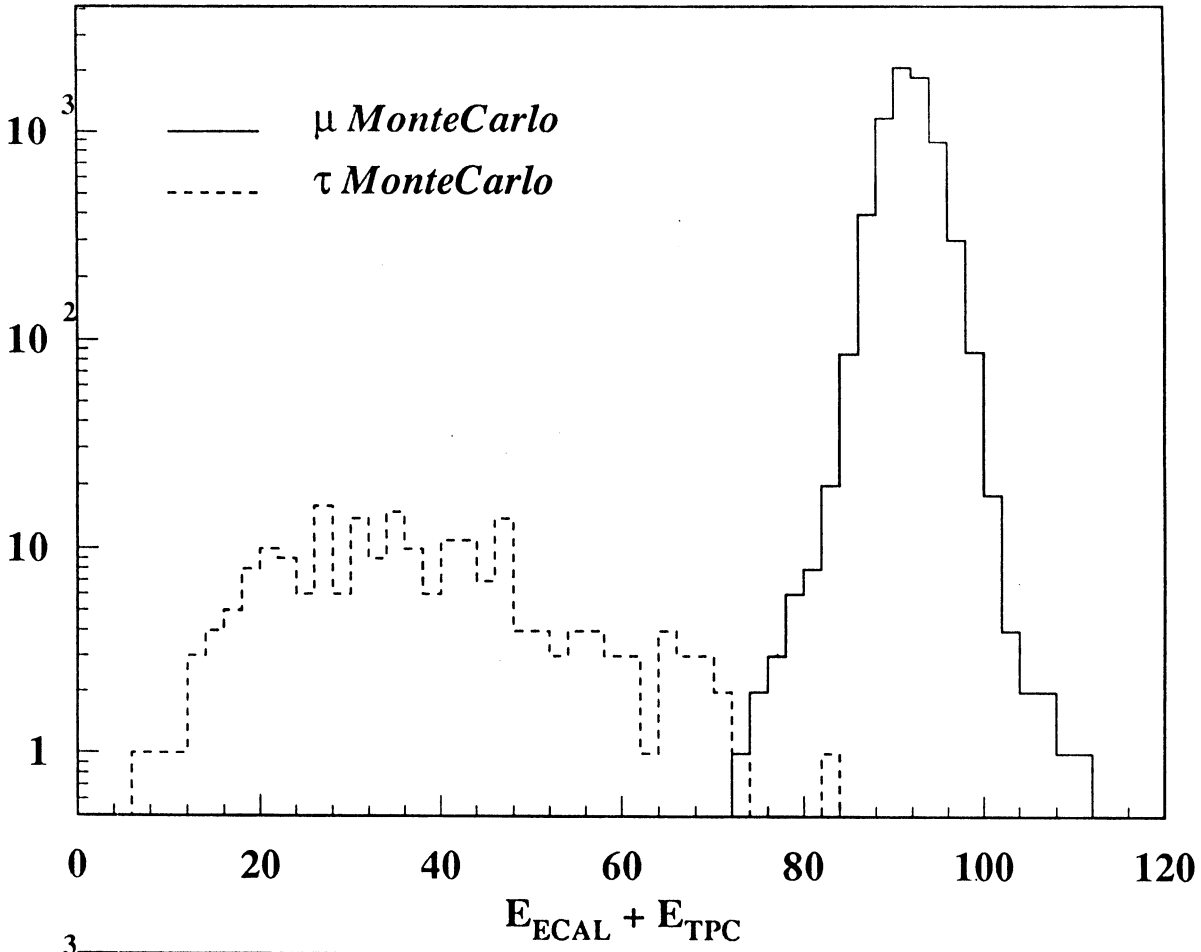
μ MonteCarlo
τ MonteCarlo
10 3
10 2
10
1
0
20
40
60
80
100
120
E ECAL + E TPC

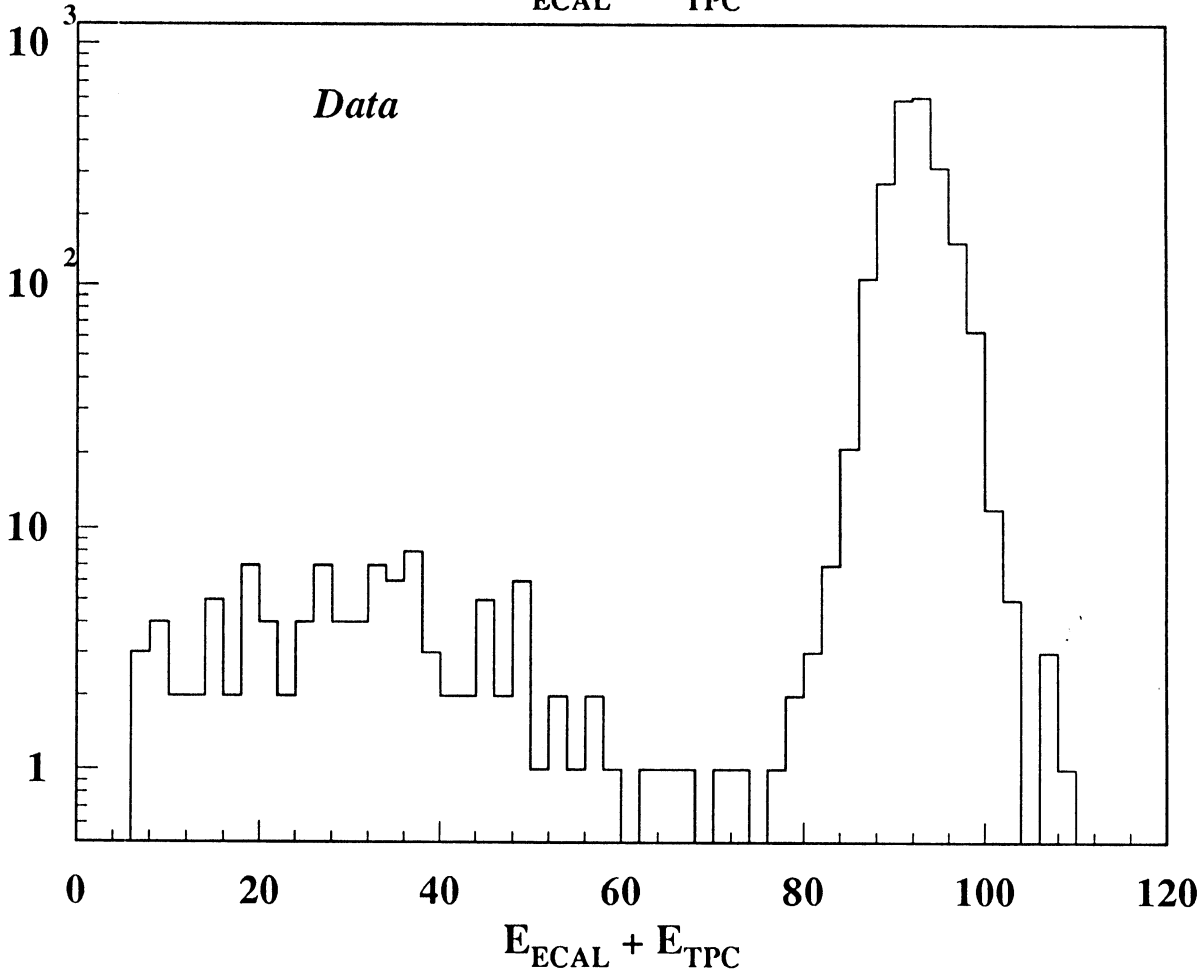
Data
10 3
10 2
10
1
0
20
40
60
80
100
120
E ECAL + E TPC

Fig. 24

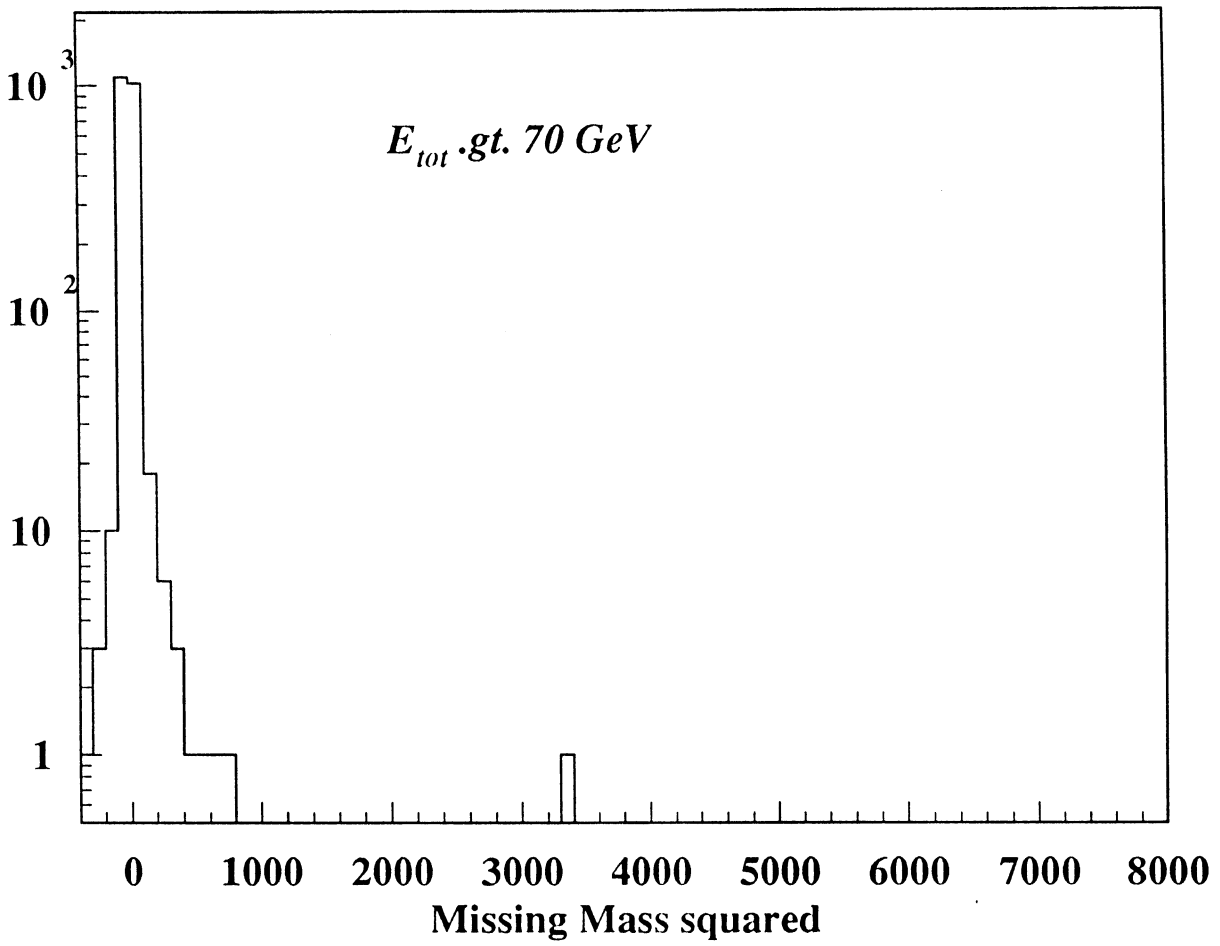
10^3
10^2
10
1
E_{tot} .gt. 70 GeV
0
1000
2000
3000
4000
5000
6000
7000
8000
Missing Mass squared

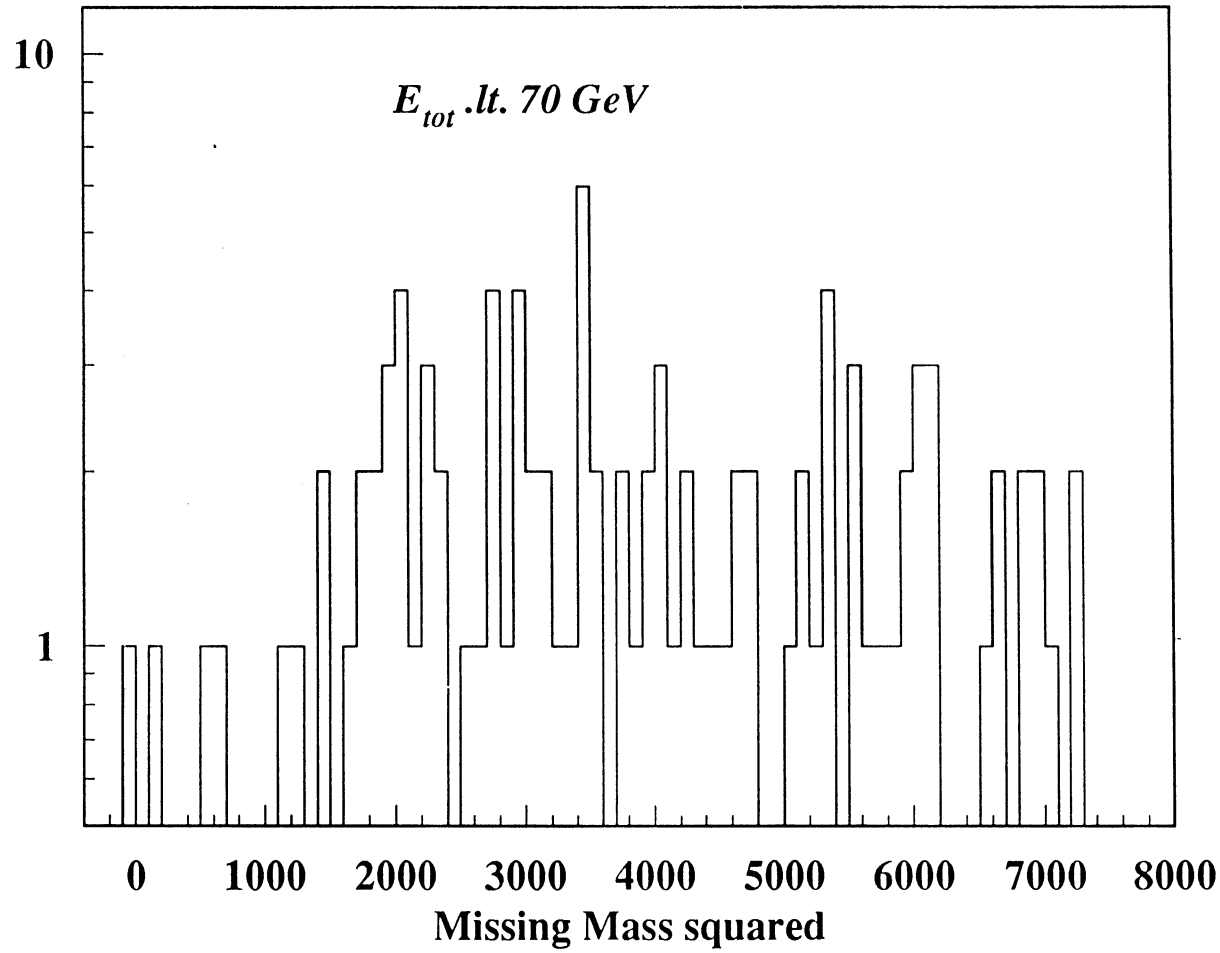
10
1
E_{tot} .lt. 70 GeV
0
1000
2000
3000
4000
5000
6000
7000
8000
Missing Mass squared

Fig. 25

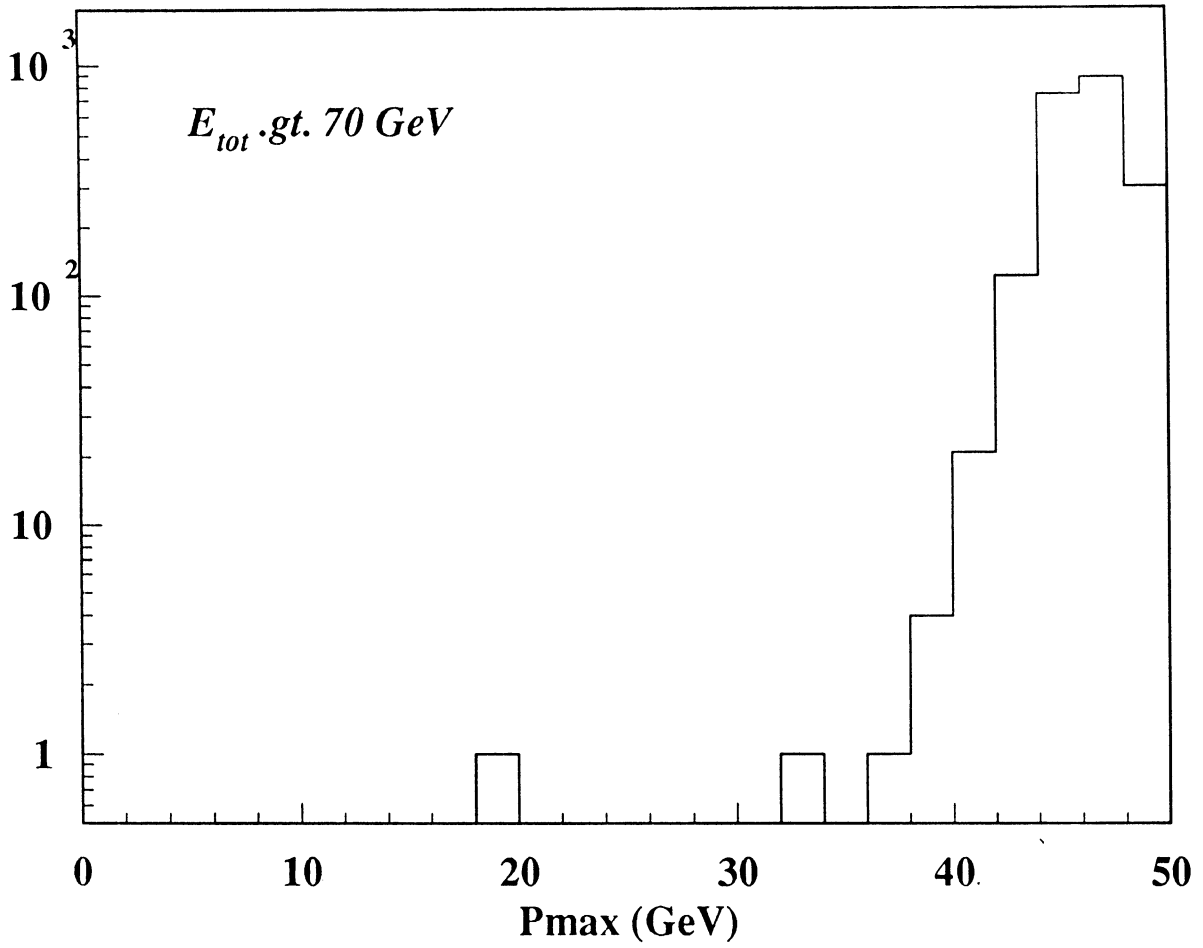
10^3
10^2
10
1
E_{tot} .gt. 70 GeV
0
10
20
30
40
50
Pmax (GeV)

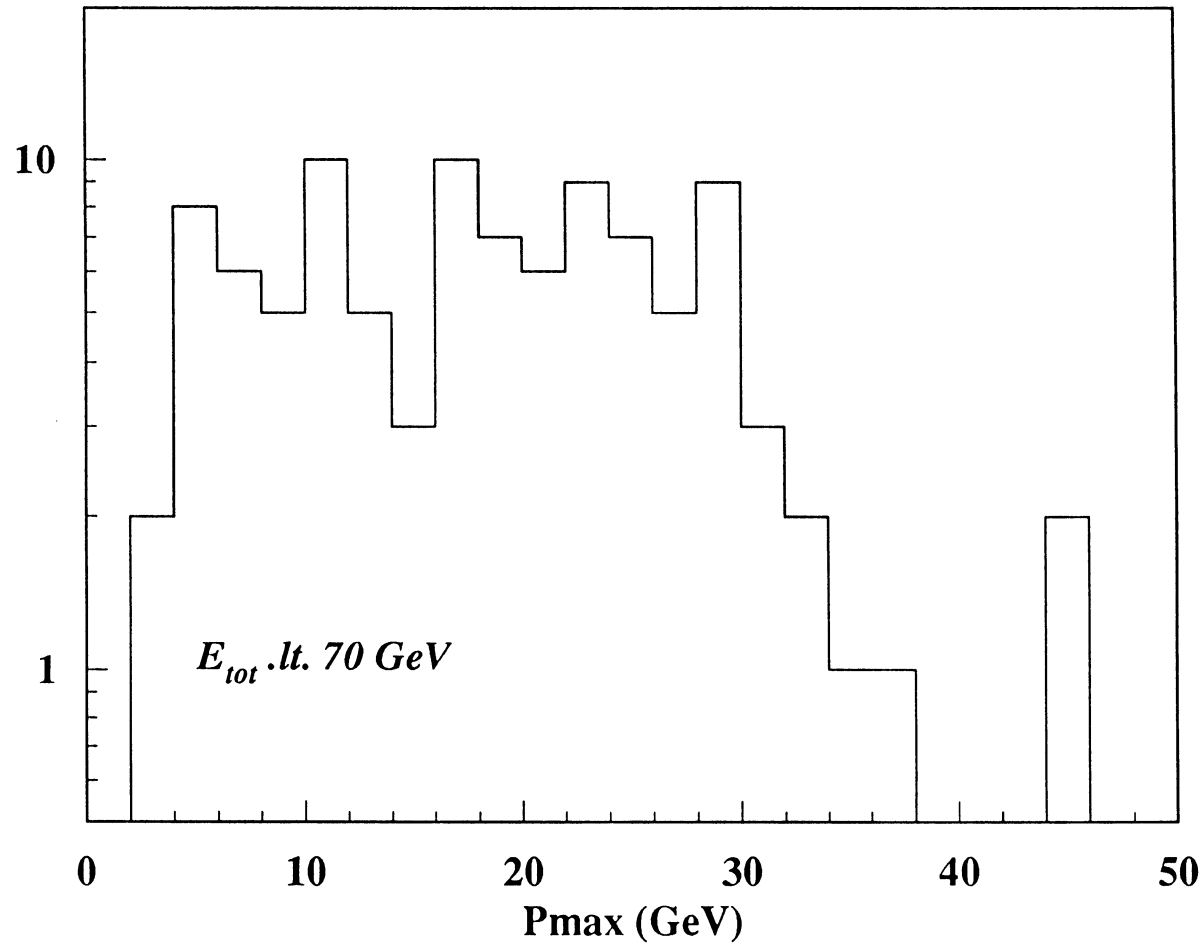
10
1
E_{tot} .lt. 70 GeV
0
10
20
30
40
50
Pmax (GeV)

Fig. 26

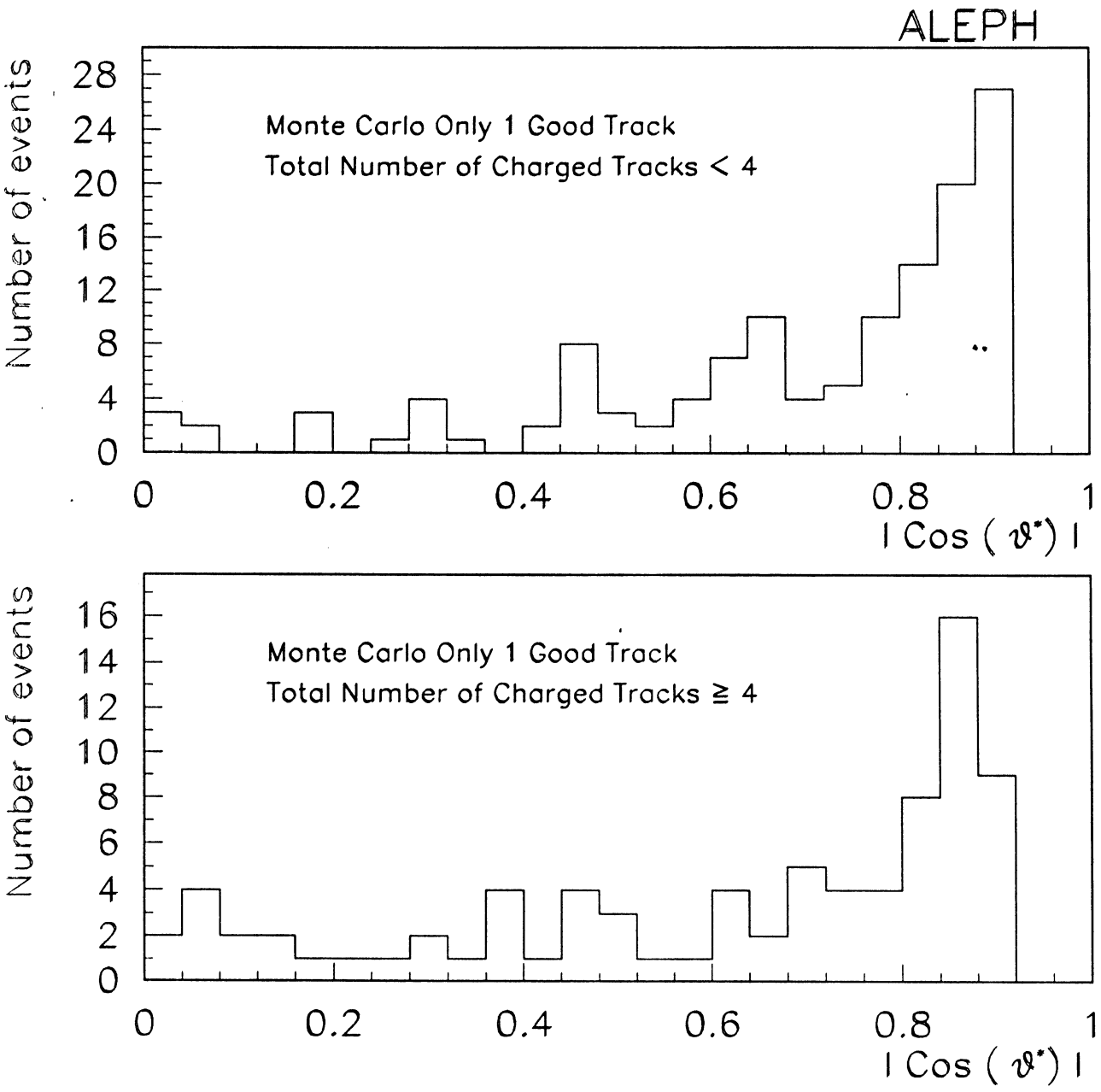
ALEPH
Number of events
28
24
20
16
12
8
4
0
Monte Carlo Only 1 Good Track
Total Number of Charged Tracks < 4
0
0.2
0.4
0.6
0.8
1
| Cos (ϑ*) |
Number of events
16
14
12
10
8
6
4
2
0
Monte Carlo Only 1 Good Track
Total Number of Charged Tracks ≥ 4
0
0.2
0.4
0.6
0.8
1
| Cos (ϑ*) |

Fig. 27

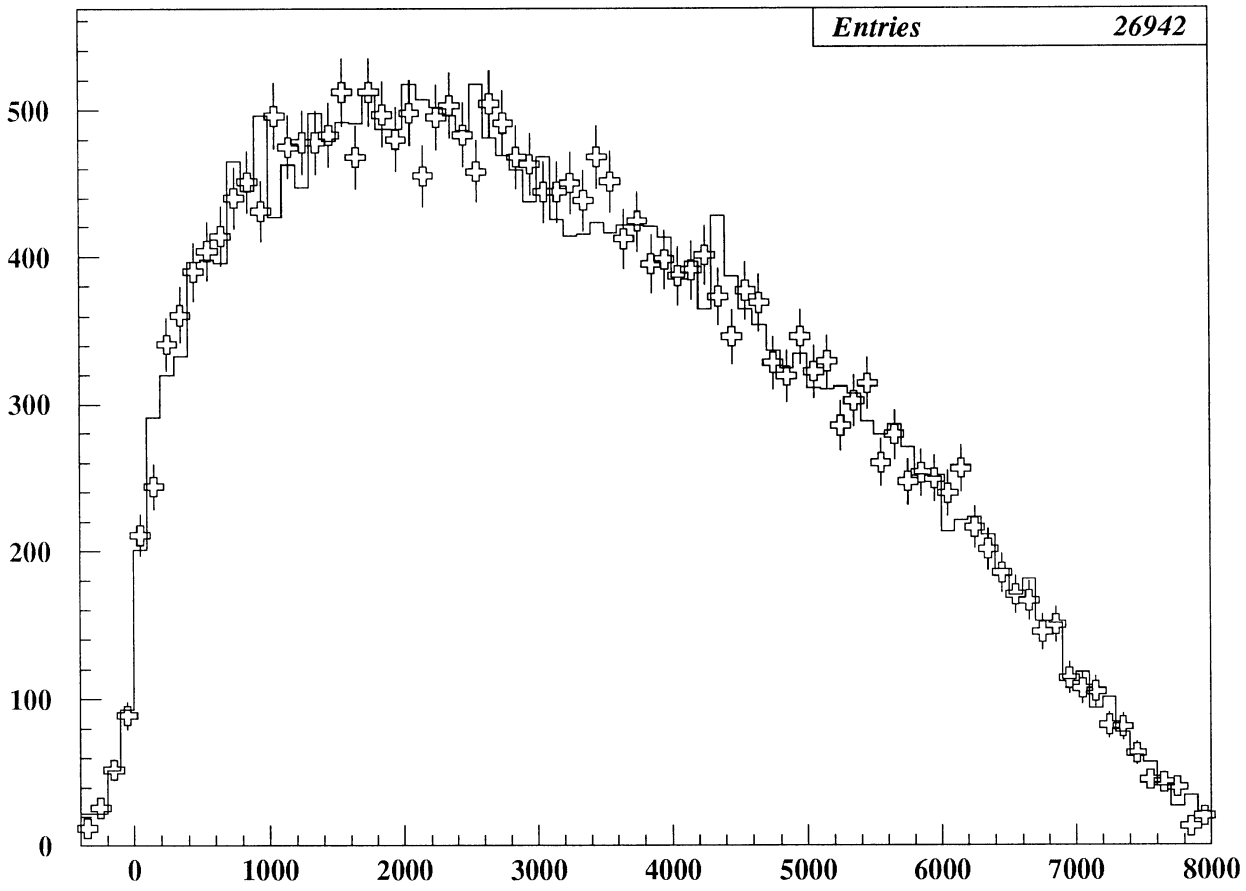
Entries 26942
500
400
300
200
100
0
0
1000
2000
3000
4000
5000
6000
7000
8000
(Missing Mass)^2

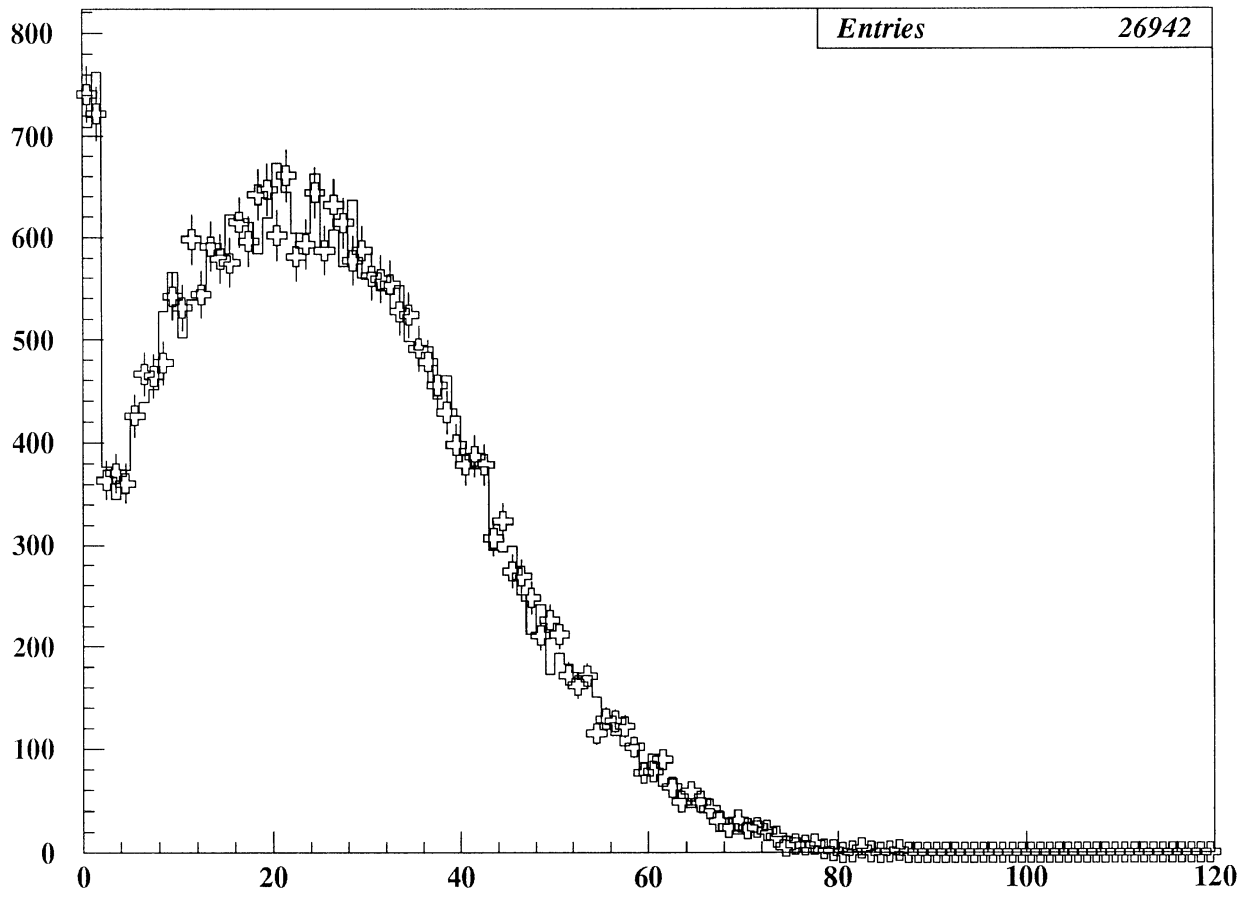
Entries 26942
800
700
600
500
400
300
200
100
0
0
20
40
60
80
100
120
Ecal wires energy

Fig. 28

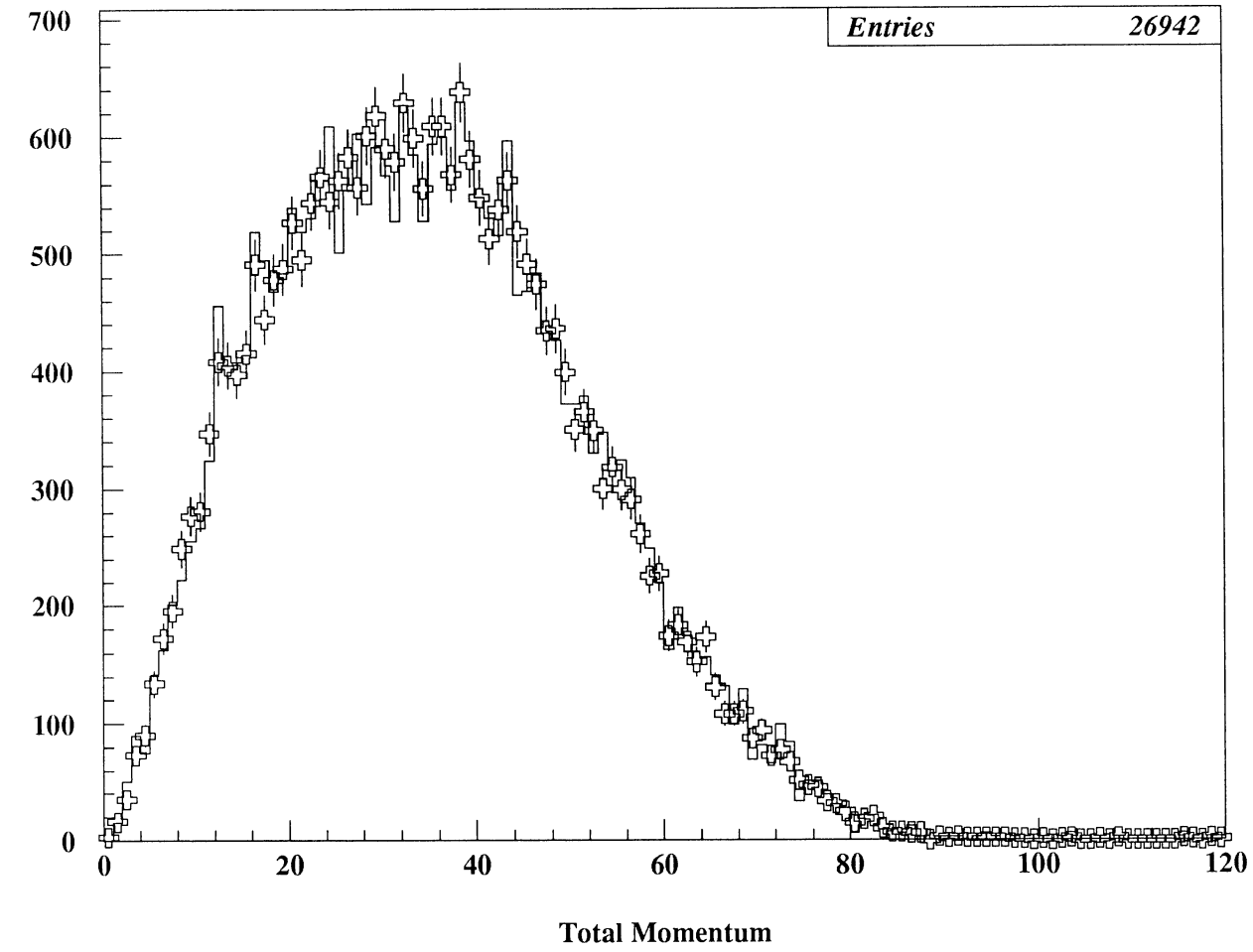
Entries 26942
700
600
500
400
300
200
100
0
0
20
40
60
80
100
120
Total Momentum

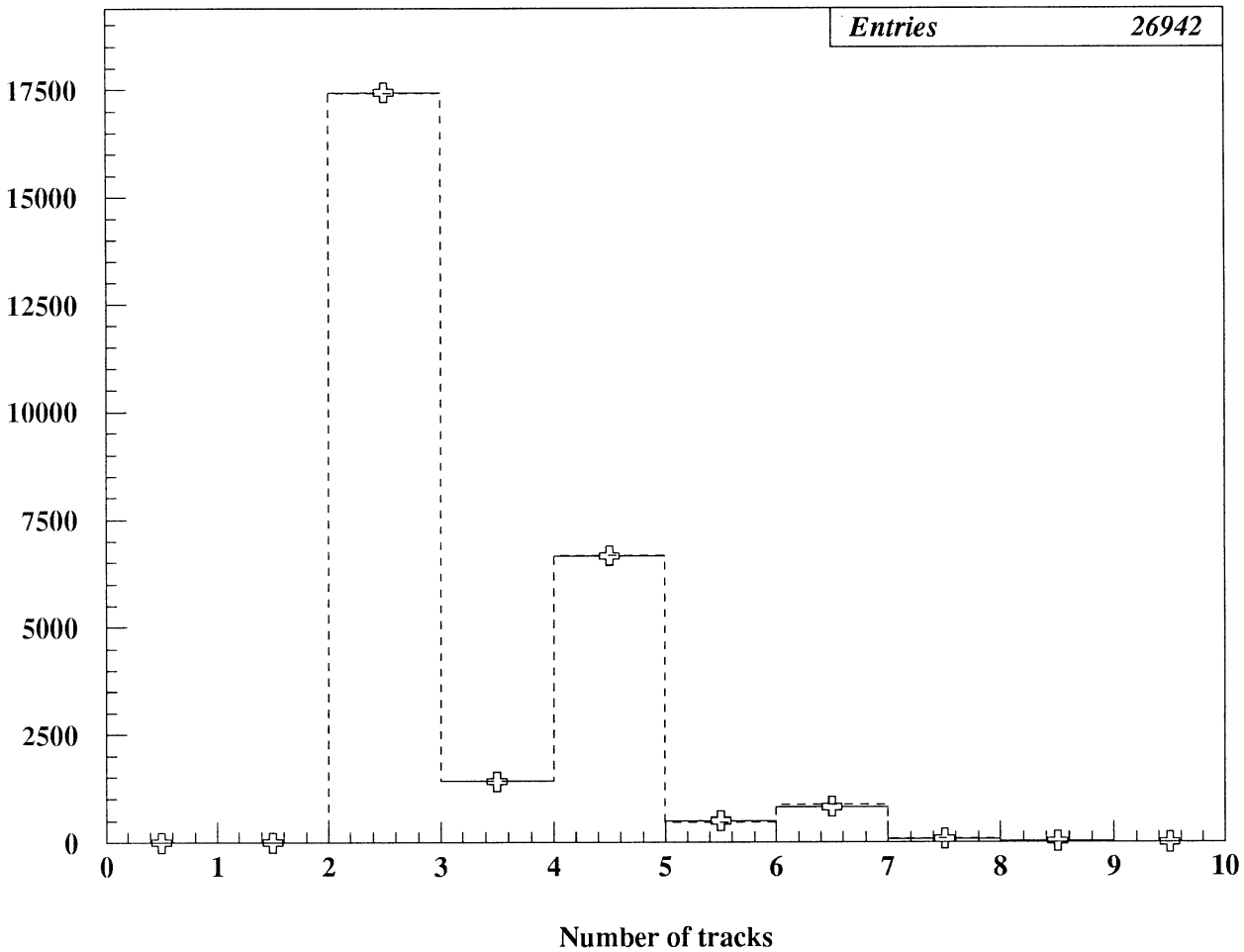
Entries 26942
17500
15000
12500
10000
7500
5000
2500
0
0
1
2
3
4
5
6
7
8
9
10
Number of tracks

Fig. 29

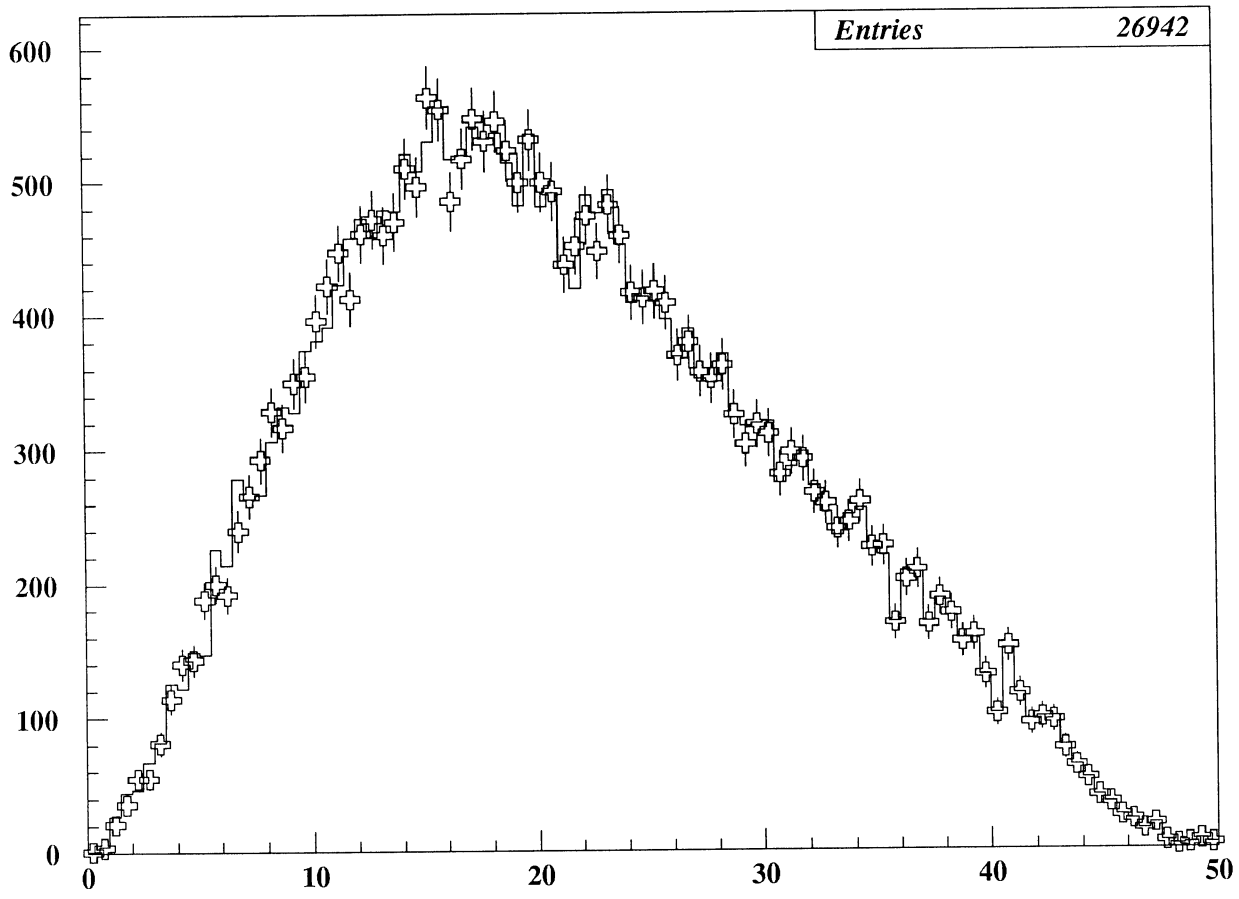

Maximum momentum

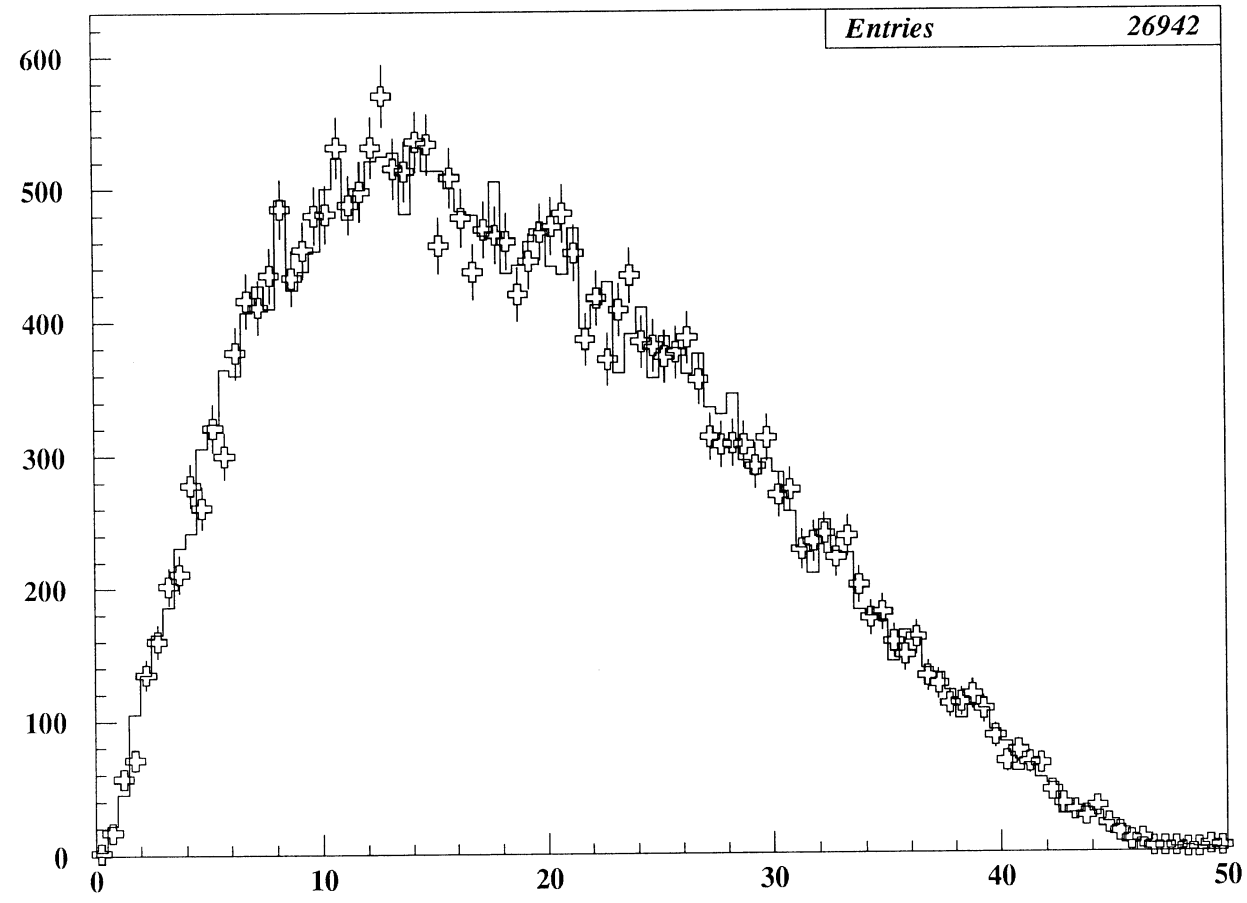

Maximum transverse momentum

Fig. 30

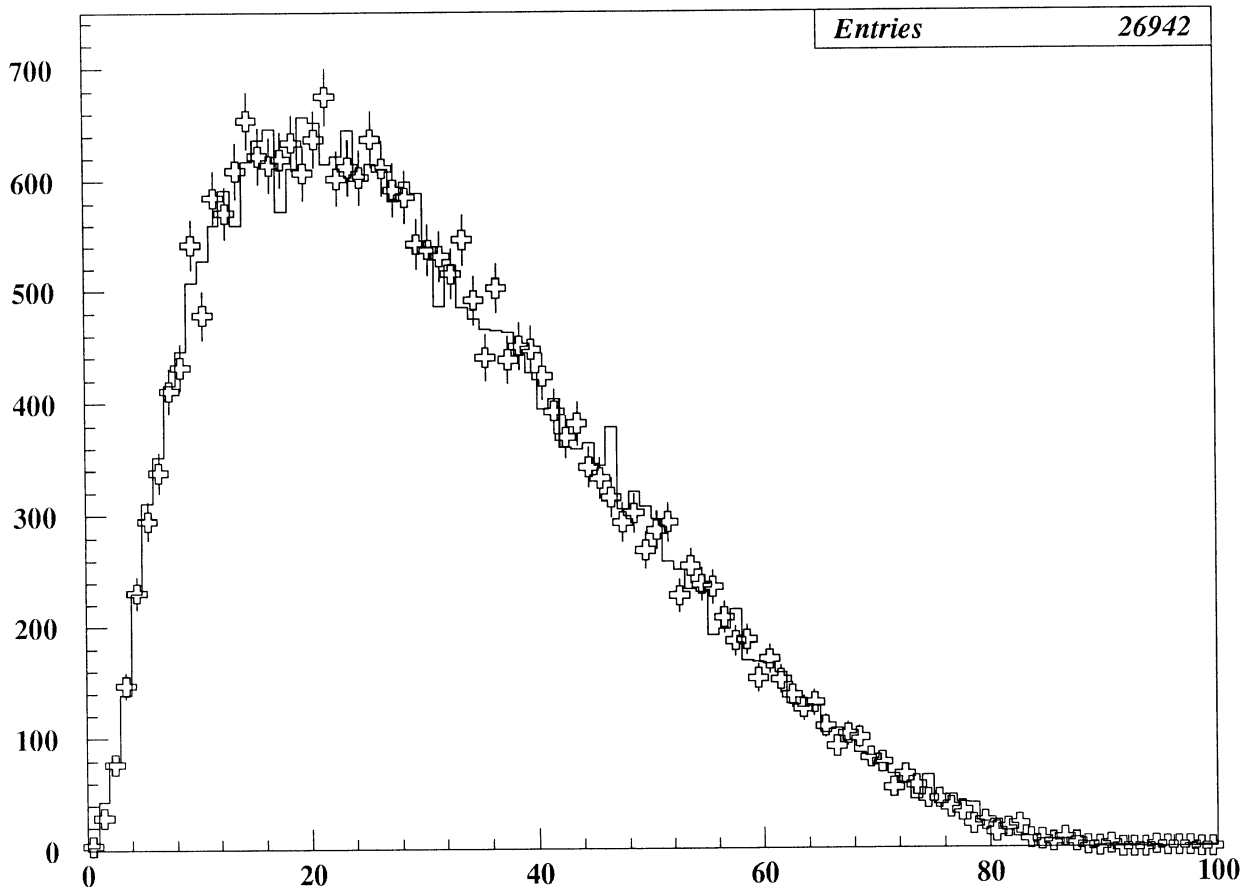

Invariant mass

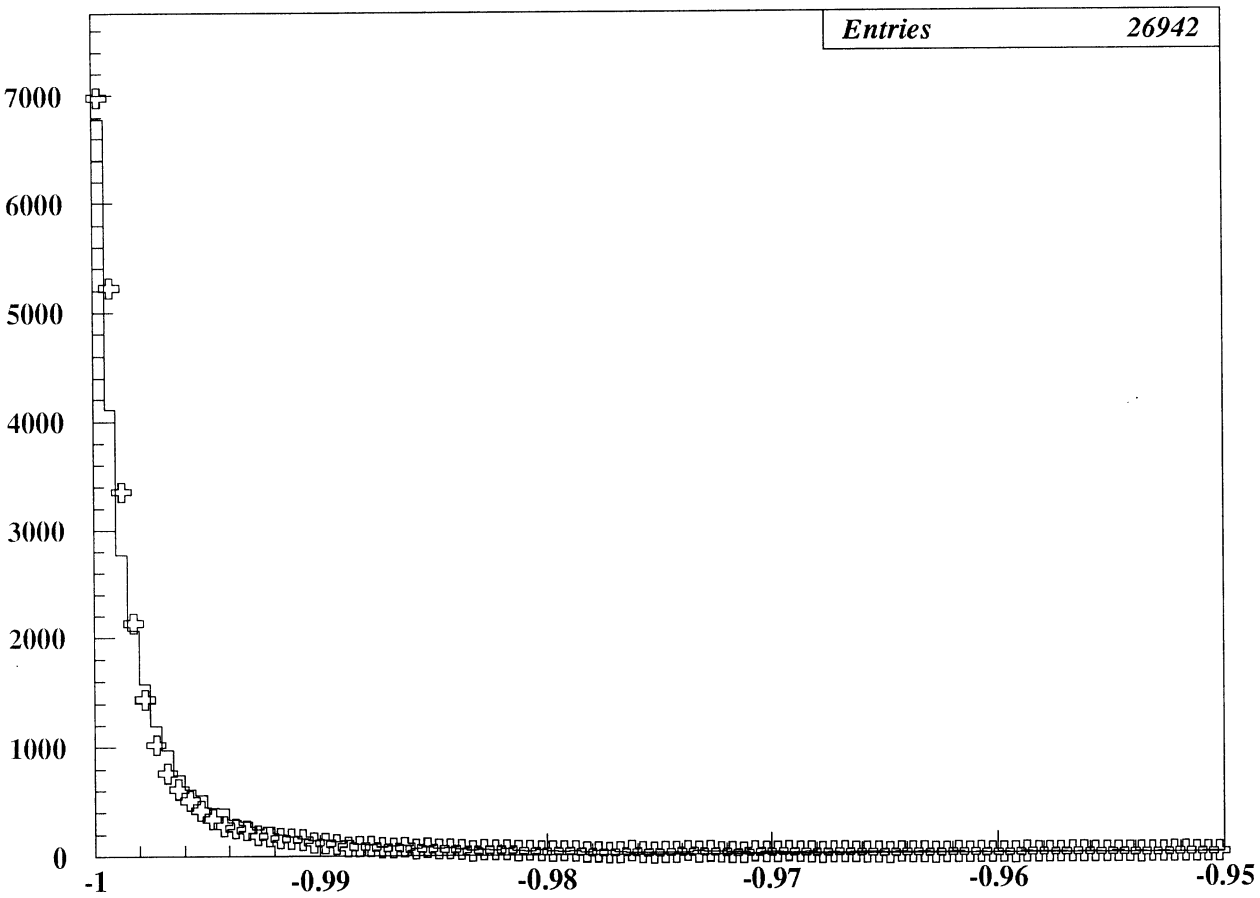

Acollinearity

Fig. 31

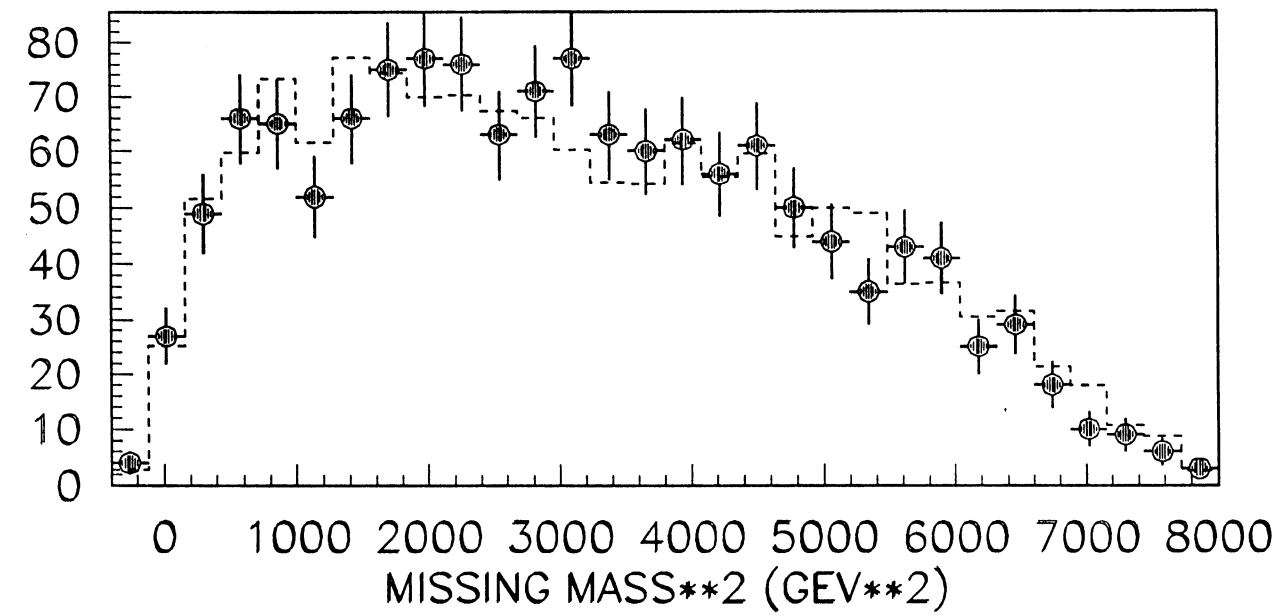
80
70
60
50
40
30
20
10
0
0 1000 2000 3000 4000 5000 6000 7000 8000
MISSING MASS**2 (GEV**2)

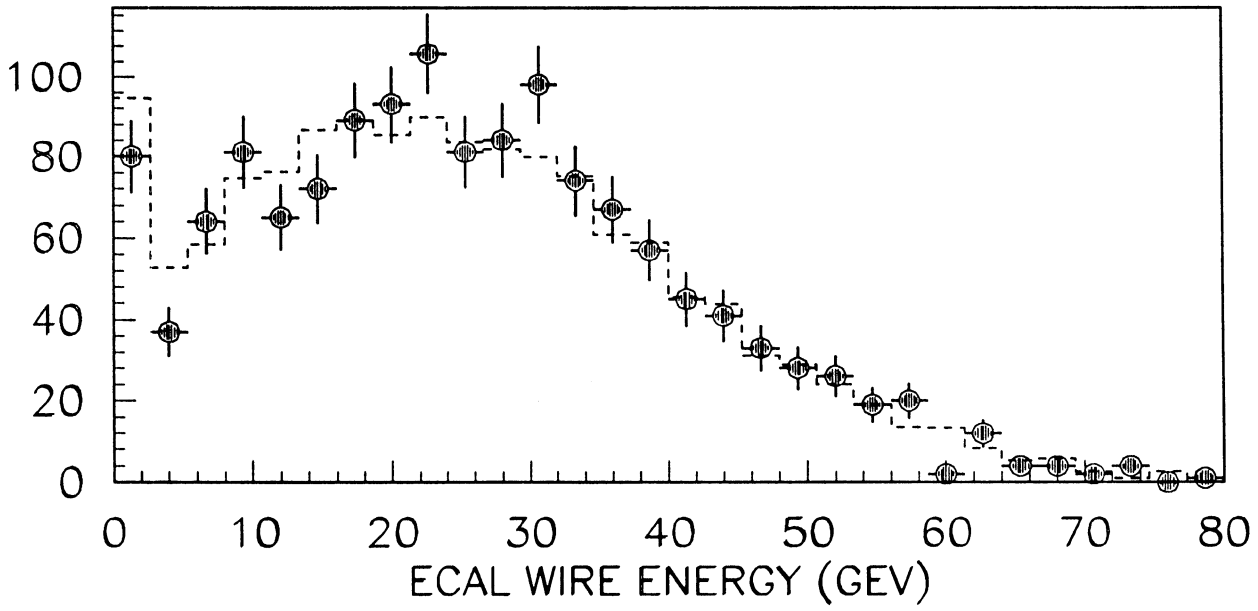
100
80
60
40
20
0
0 10 20 30 40 50 60 70 80
ECAL WIRE ENERGY (GEV)

Fig. 32

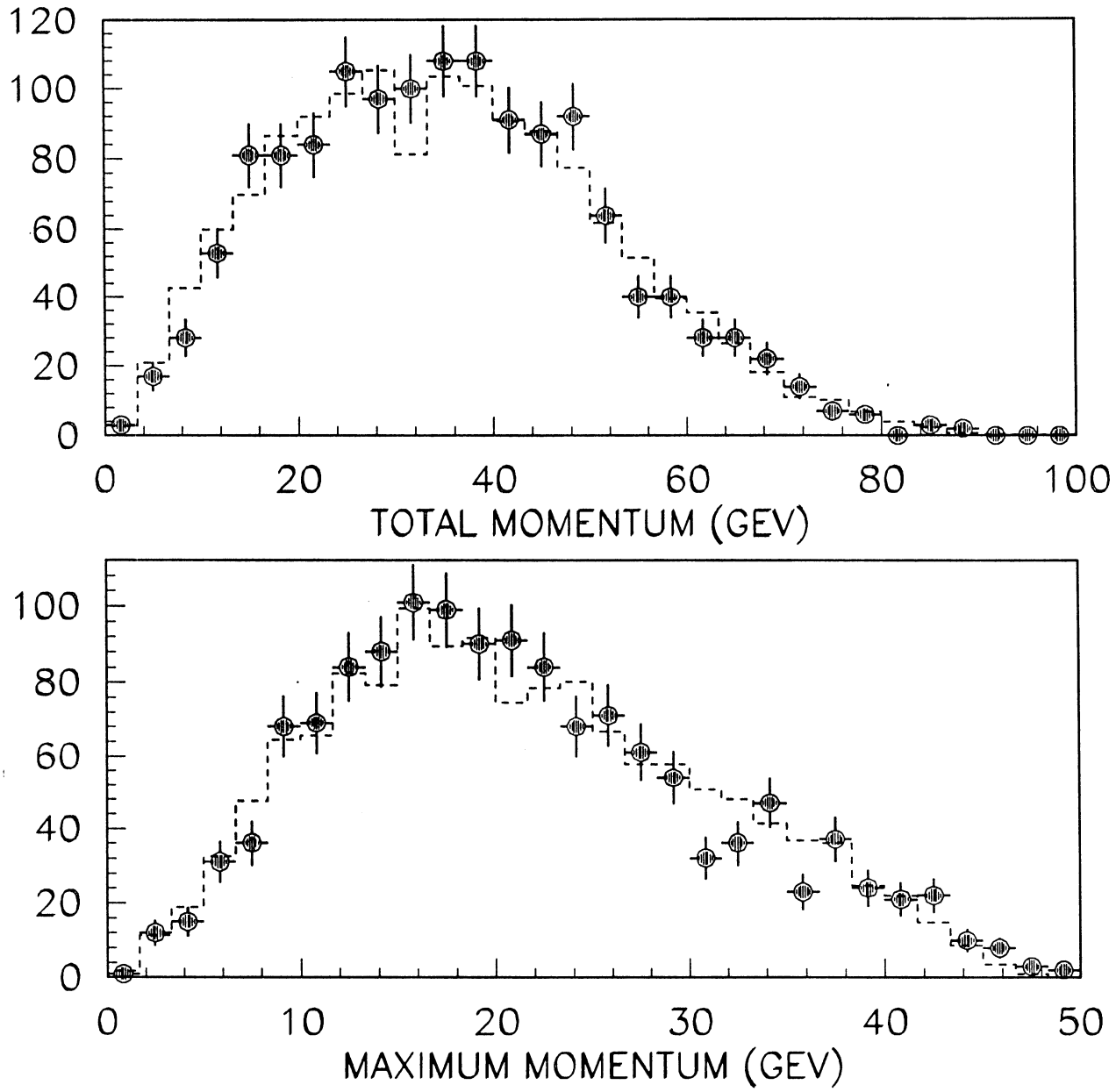
120
100
80
60
40
20
0
0
20
40
60
80
100
TOTAL MOMENTUM (GEV)
100
80
60
40
20
0
0
10
20
30
40
50
MAXIMUM MOMENTUM (GEV)

Fig. 33

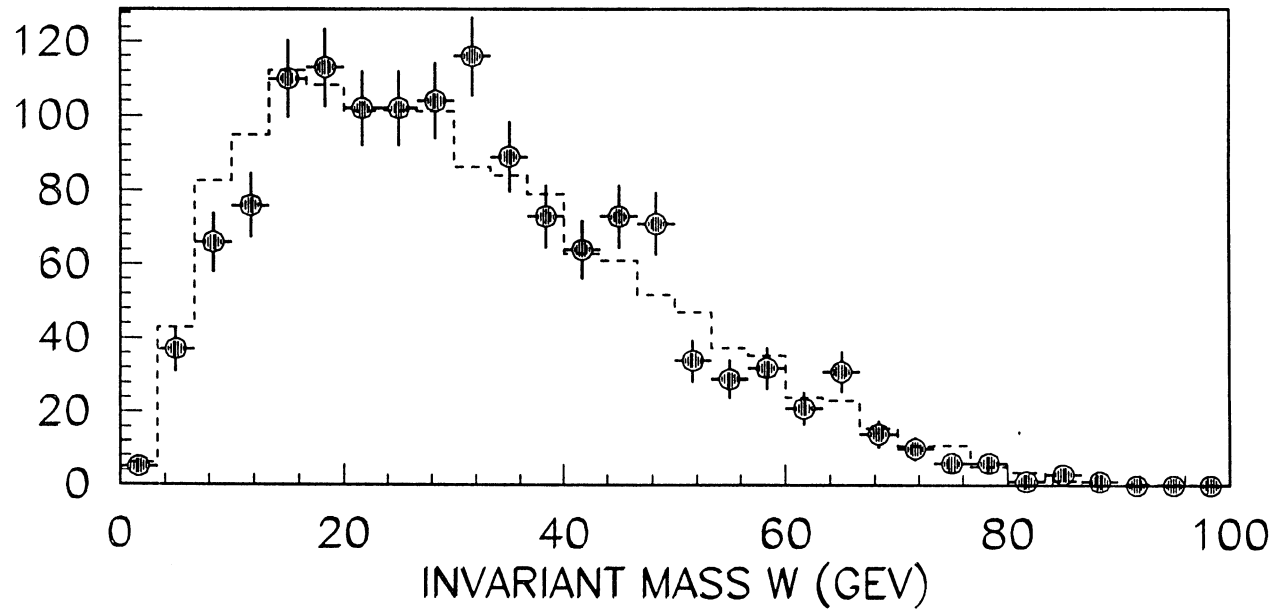
120
100
80
60
40
20
0
0
20
40
60
80
100
INVARIANT MASS W (GEV)

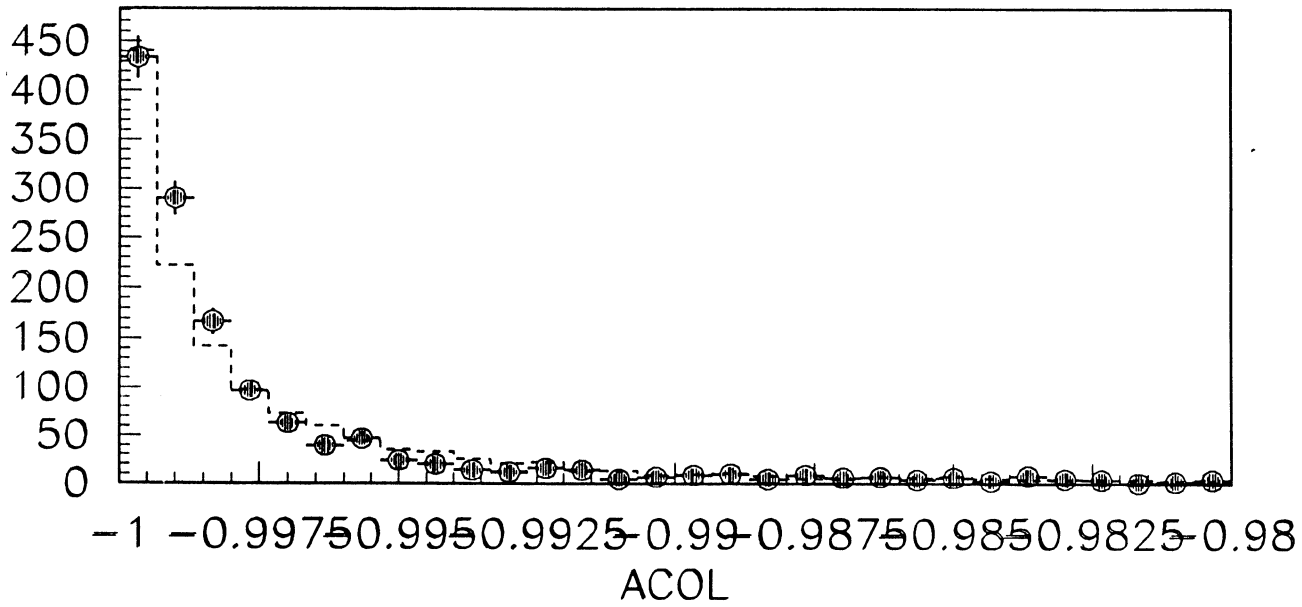
450
400
350
300
250
200
150
100
50
0
−1
−0.9975
−0.995
−0.9925
−0.99
−0.9875
−0.985
−0.9825
−0.98
ACOL

Fig. 34

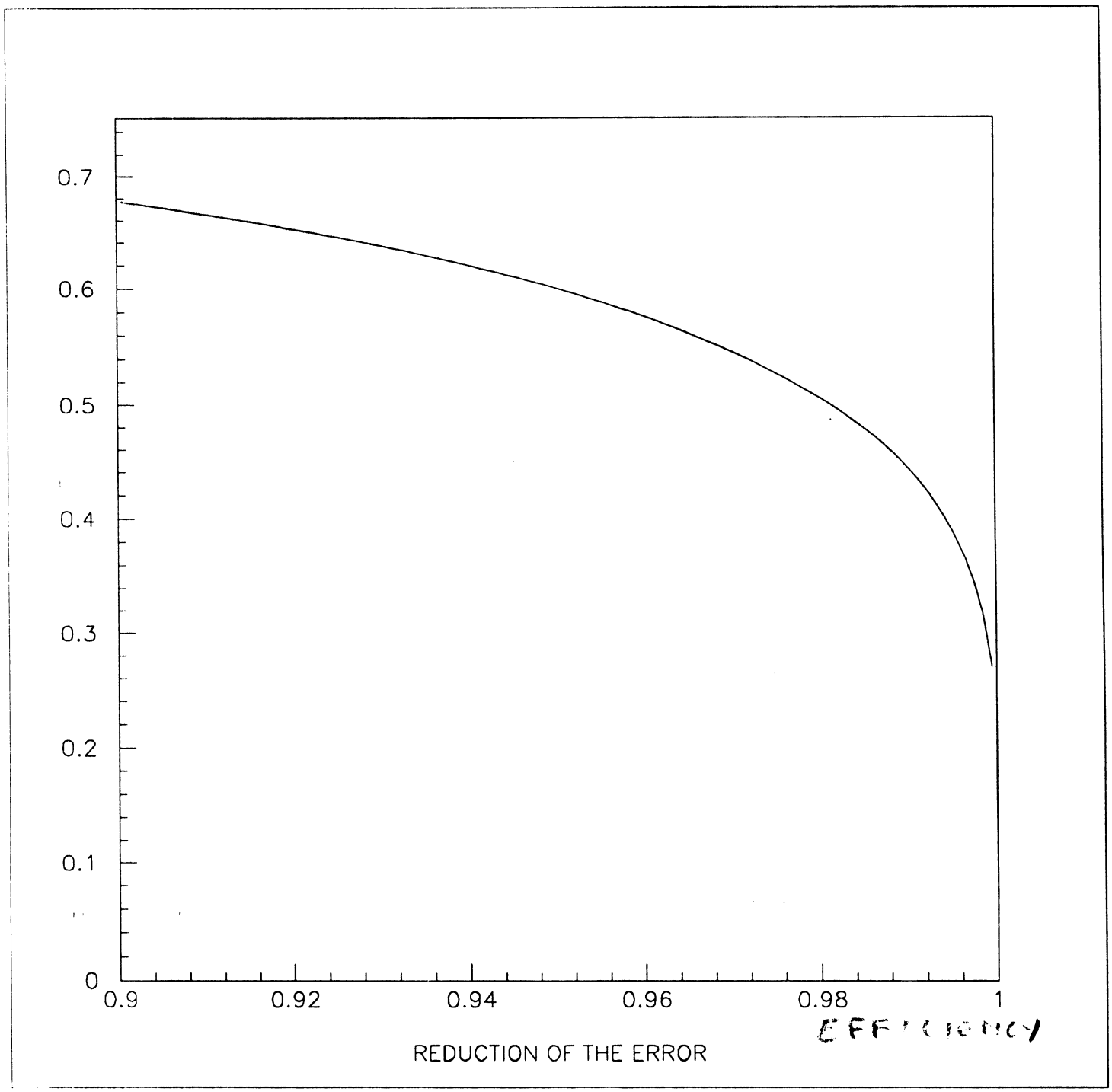
0.7
0.6
0.5
0.4
0.3
0.2
0.1
0
0.9
0.92
0.94
0.96
0.98
1
EFFICIENCY
REDUCTION OF THE ERROR

Fig. 35

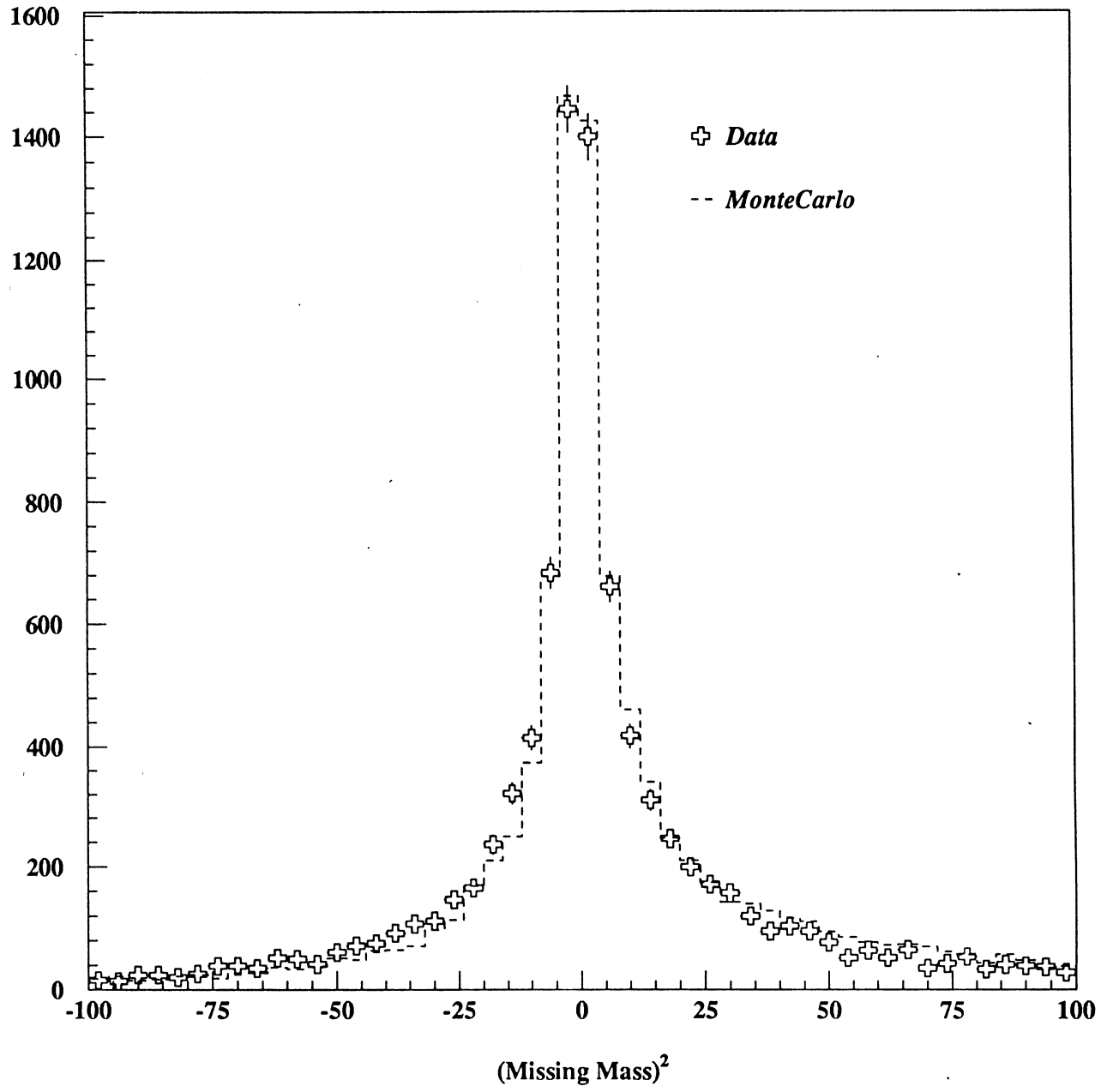
1600
1400
1200
1000
800
600
400
200
0
-100
-75
-50
-25
0
25
50
75
100
Data
MonteCarlo
(Missing Mass)^2

Fig. 36

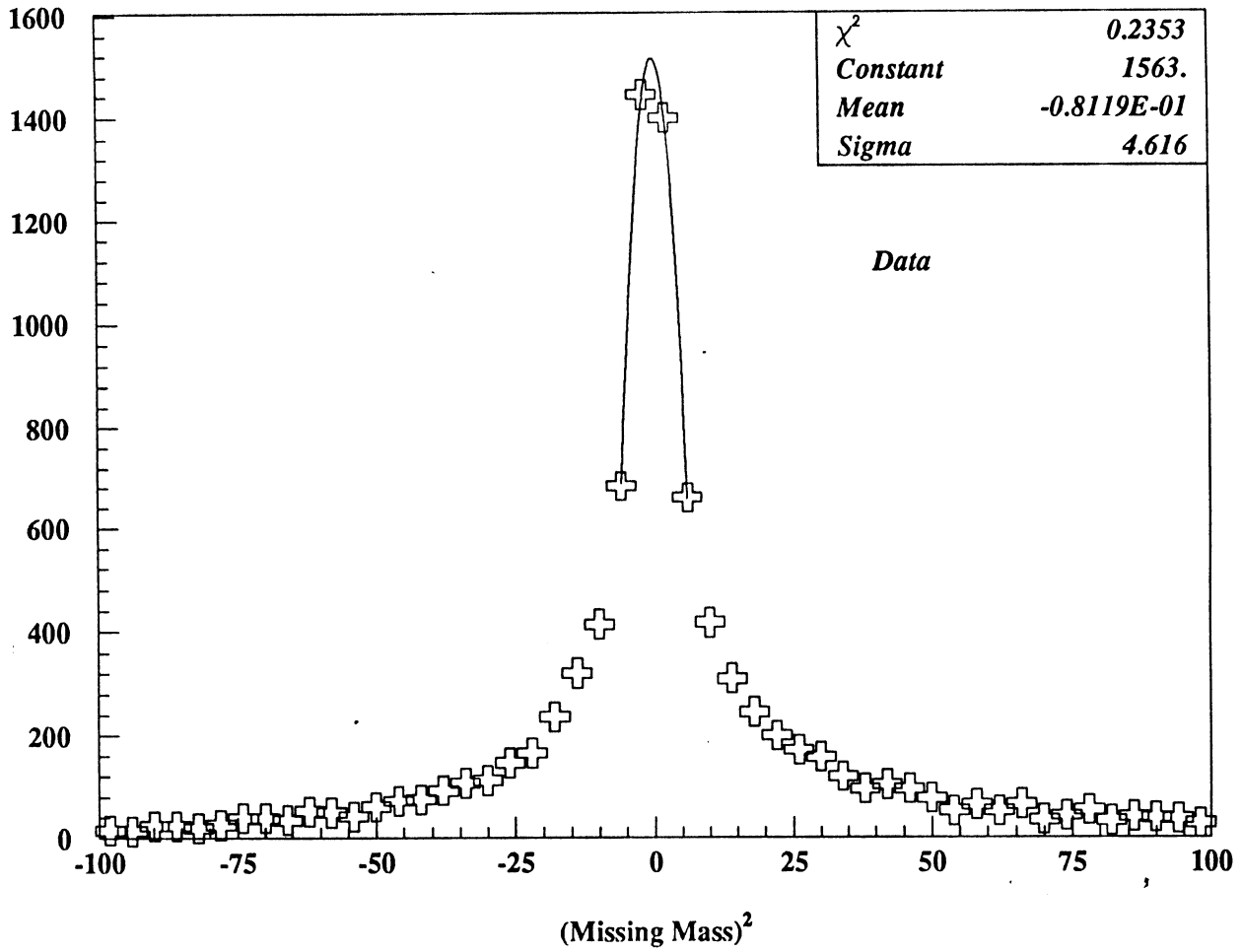
χ² 0.2353
Constant 1563.
Mean -0.8119E-01
Sigma 4.616
Data
1600
1400
1200
1000
800
600
400
200
0
-100
-75
-50
-25
0
25
50
75
100
(Missing Mass)²

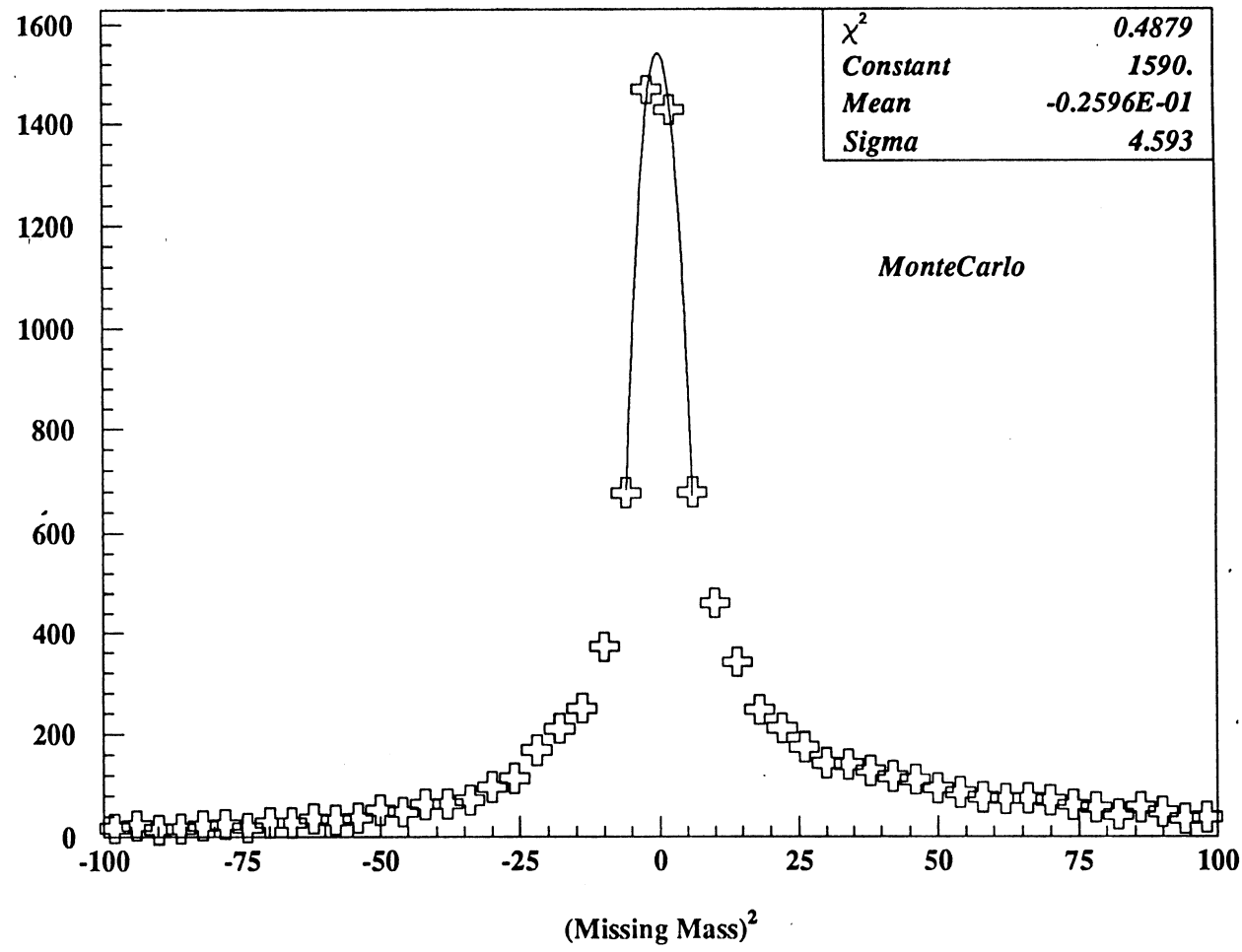
χ² 0.4879
Constant 1590.
Mean -0.2596E-01
Sigma 4.593
MonteCarlo
1600
1400
1200
1000
800
600
400
200
0
-100
-75
-50
-25
0
25
50
75
100
(Missing Mass)²

Fig. 37

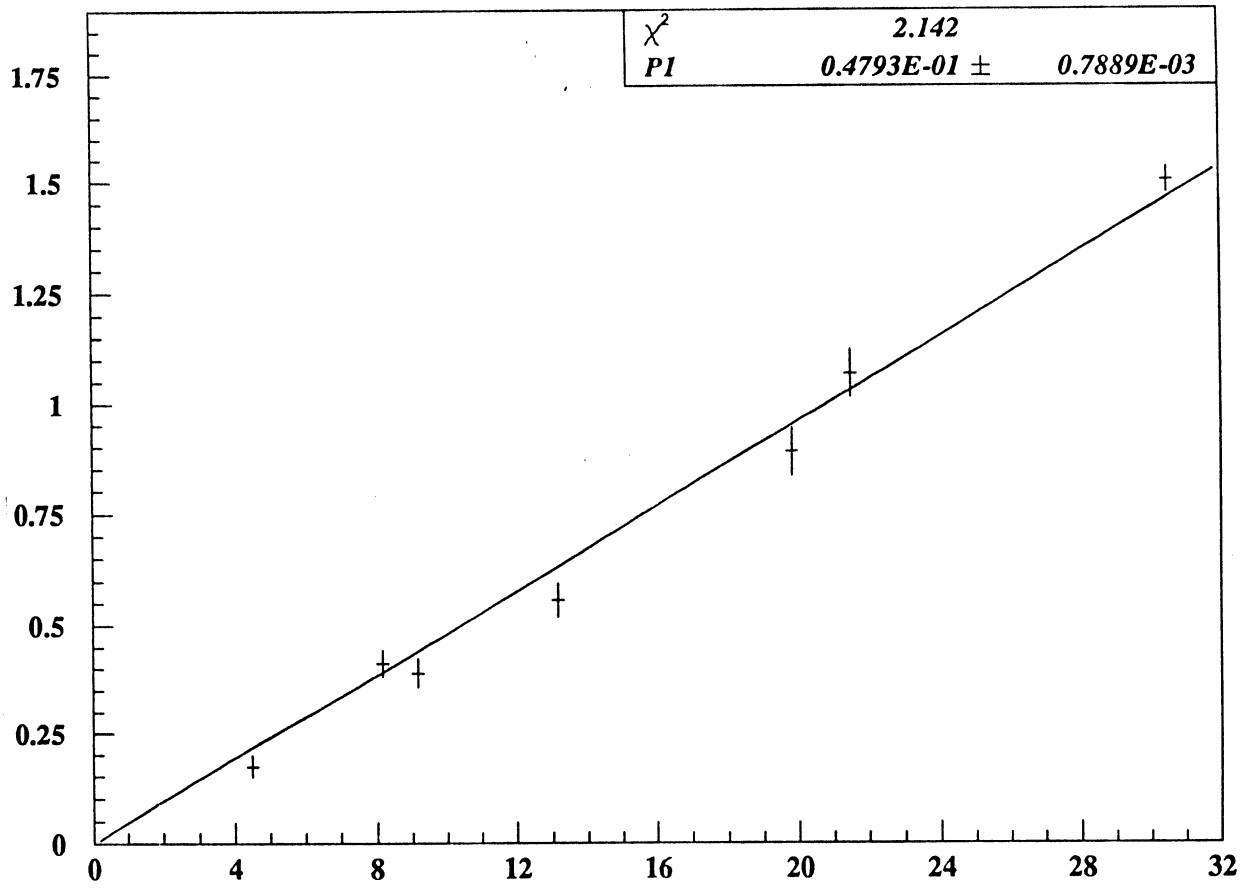

σ_{qq} vs $\sigma_{\tau\tau}$

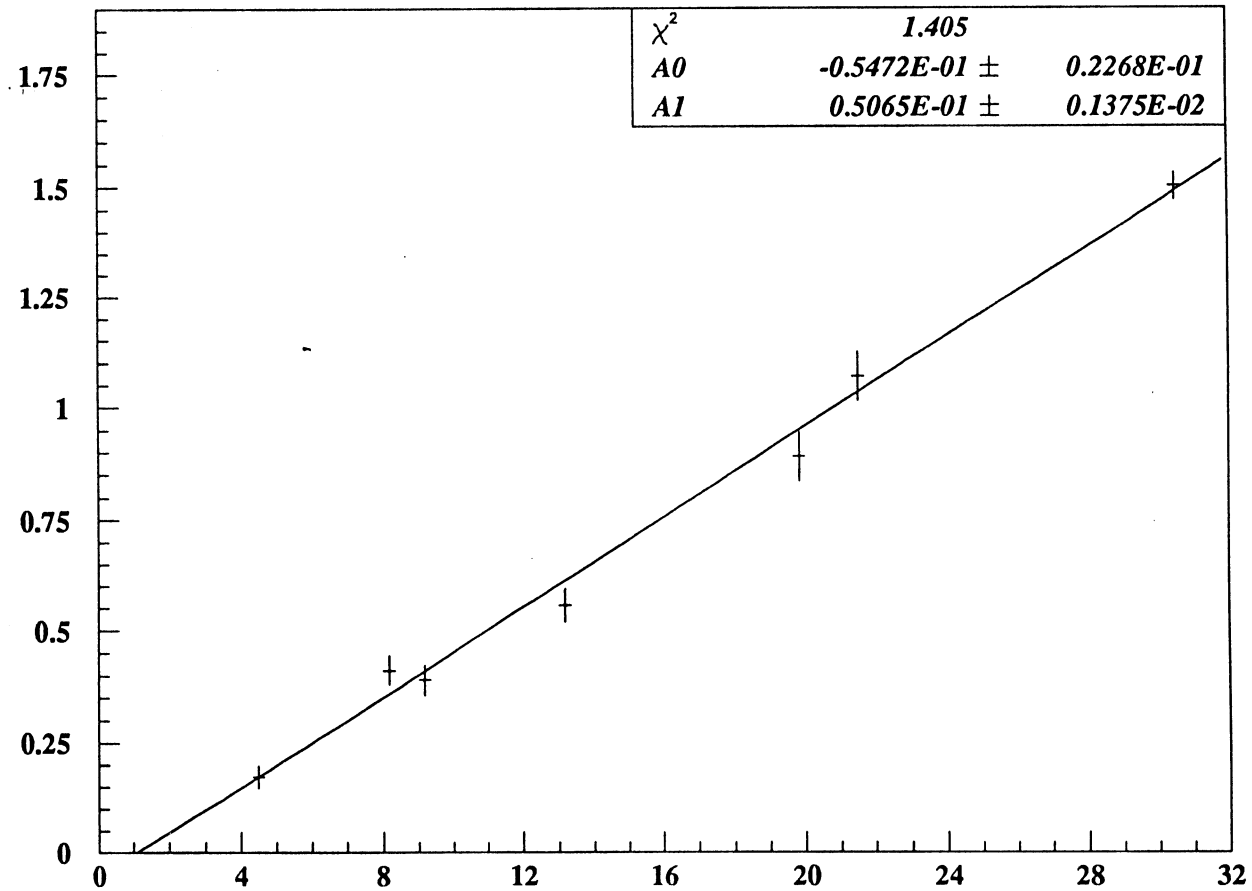

σ_{qq} vs $\sigma_{\tau\tau}$

Fig. 38

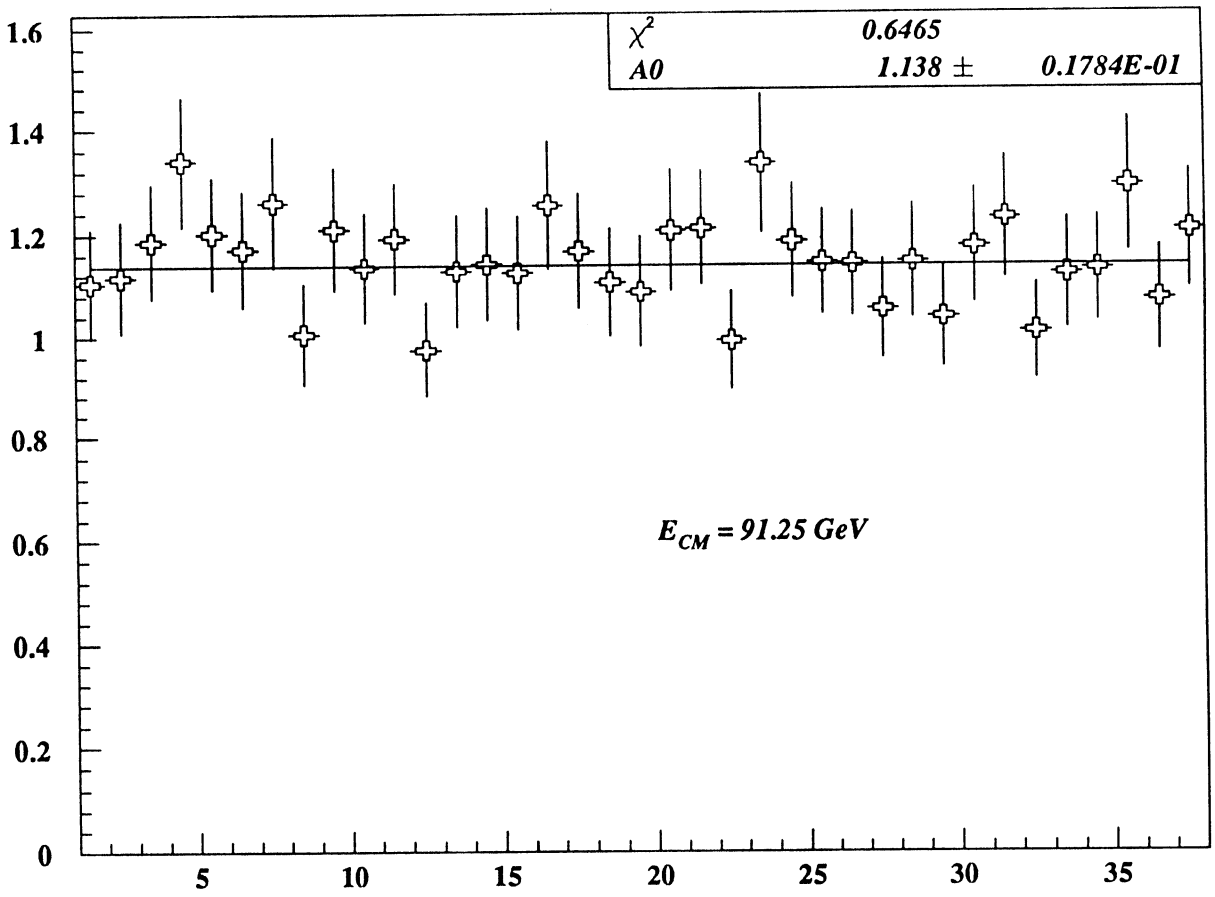

$\sigma_{\tau\tau}$ time evolution

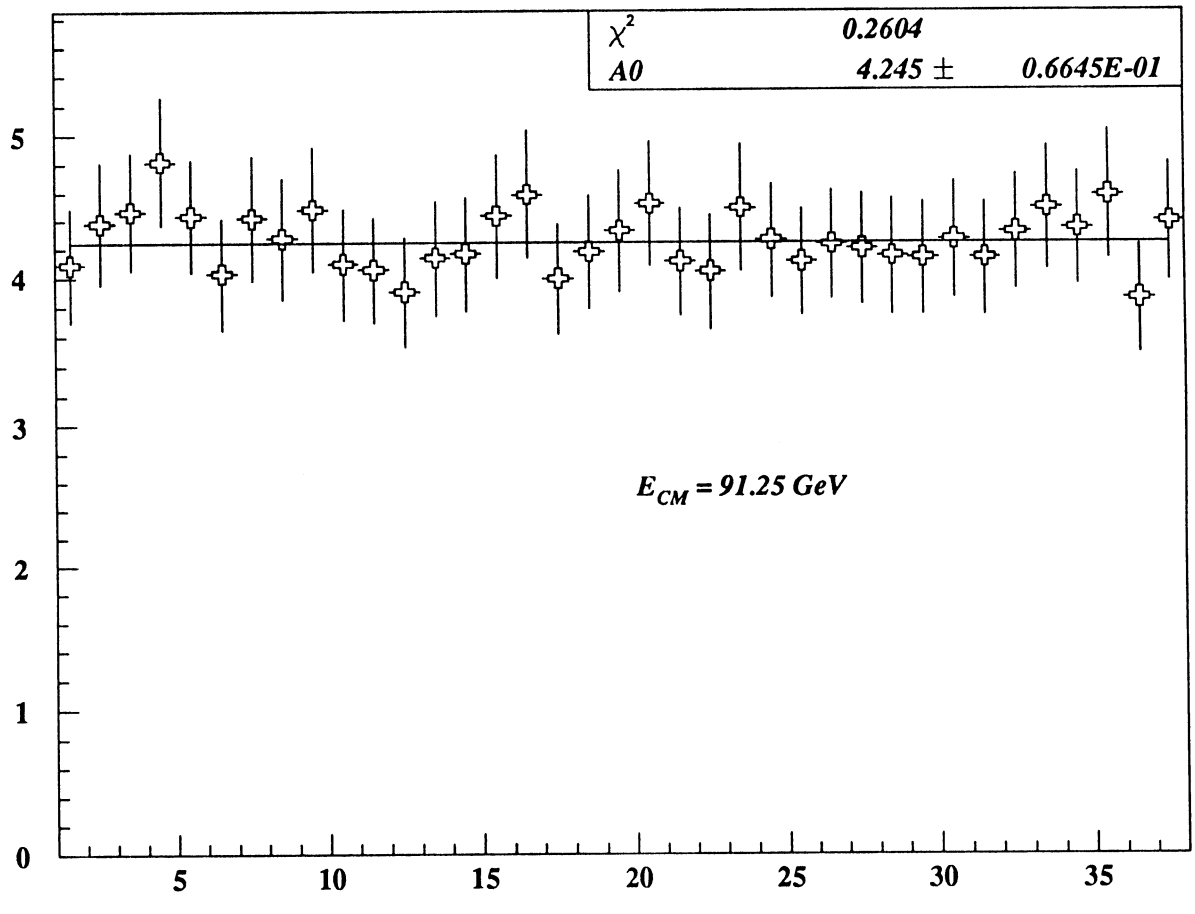

σ_{ll} time evolution

Fig. 39

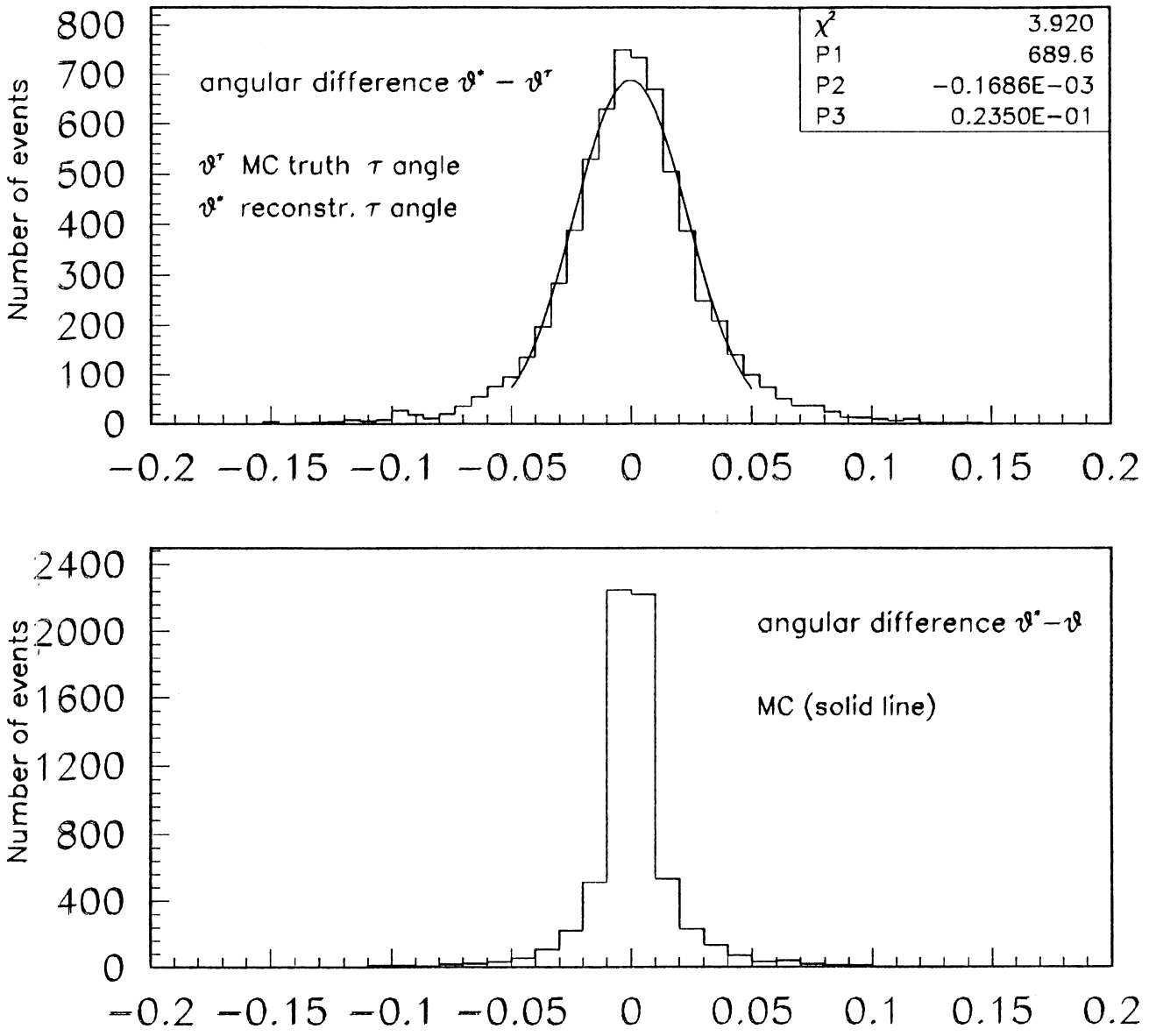
Number of events
800
700
600
500
400
300
200
100
0
angular difference $\vartheta^* - \vartheta^\tau$
ϑ^τ MC truth τ angle
ϑ^* reconstr. τ angle
χ^2 3.920
P1 689.6
P2 −0.1686E−03
P3 0.2350E−01
−0.2 −0.15 −0.1 −0.05 0 0.05 0.1 0.15 0.2
Number of events
2400
2000
1600
1200
800
400
0
angular difference $\vartheta^* - \vartheta$
MC (solid line)
−0.2 −0.15 −0.1 −0.05 0 0.05 0.1 0.15 0.2

Fig. 40

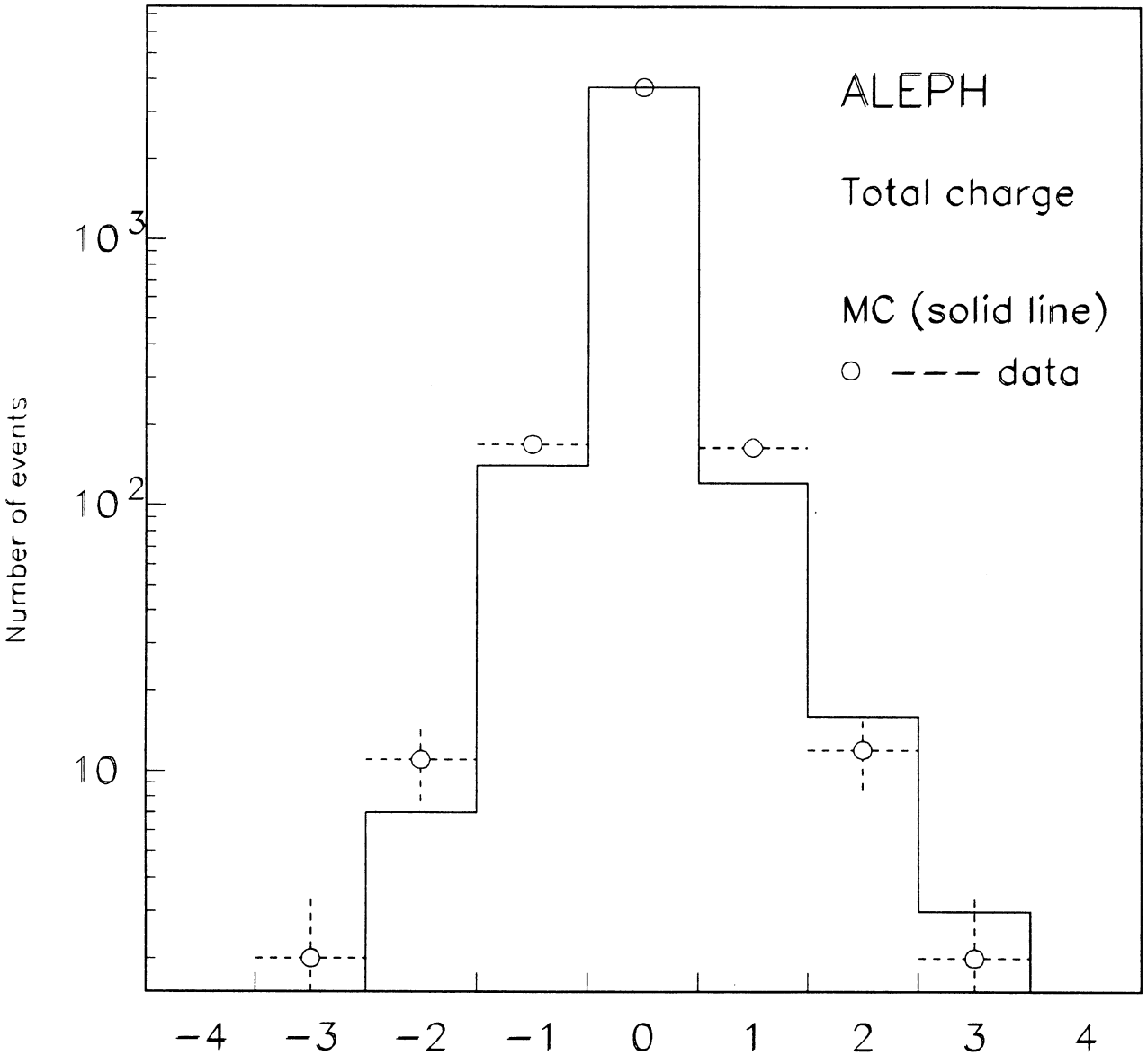
ALEPH
Total charge
MC (solid line)
data
Number of events
10 3
10 2
10
−4
−3
−2
−1
0
1
2
3
4

Fig. 41

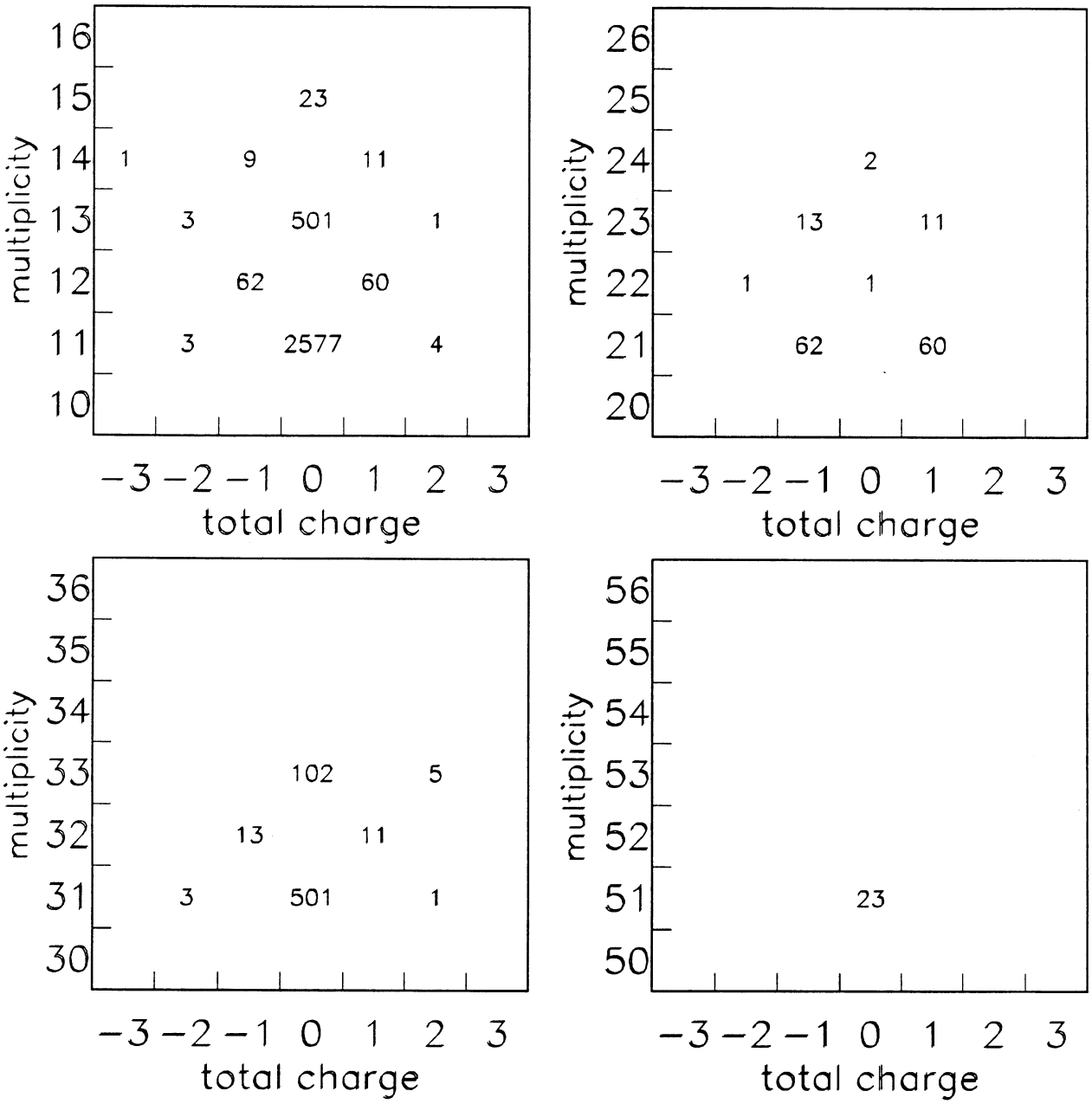
multiplicity
16
15
14
13
12
11
10
23
1
9
11
3
501
1
62
60
3
2577
4
−3 −2 −1 0 1 2 3
total charge
multiplicity
26
25
24
23
22
21
20
2
13
11
1
1
62
60
−3 −2 −1 0 1 2 3
total charge
multiplicity
36
35
34
33
32
31
30
102
5
13
11
3
501
1
−3 −2 −1 0 1 2 3
total charge
multiplicity
56
55
54
53
52
51
50
23
−3 −2 −1 0 1 2 3
total charge

Fig. 42

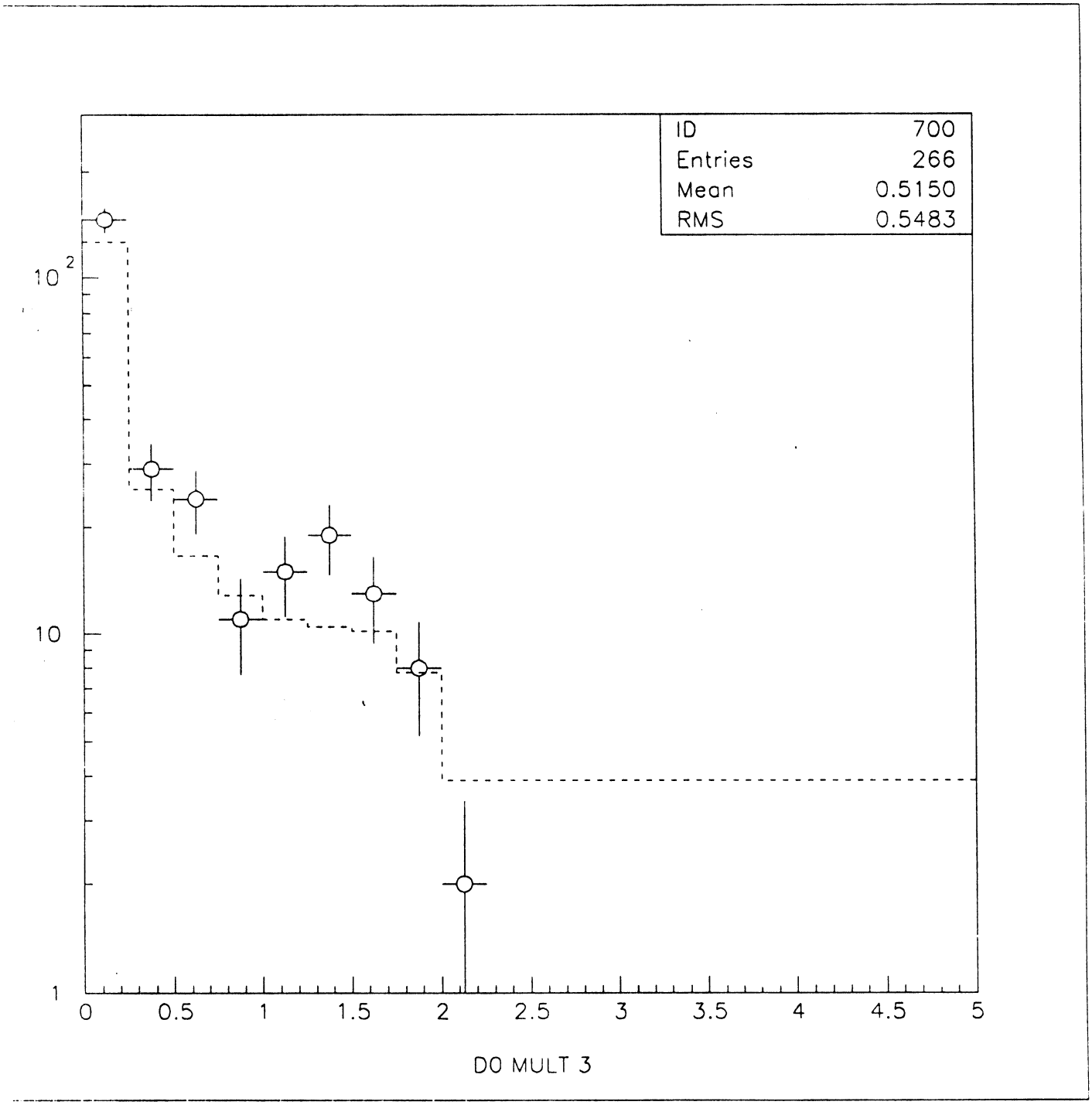
ID 700
Entries 266
Mean 0.5150
RMS 0.5483
10 2
10
1
0 0.5 1 1.5 2 2.5 3 3.5 4 4.5 5
DO MULT 3

Fig. 43

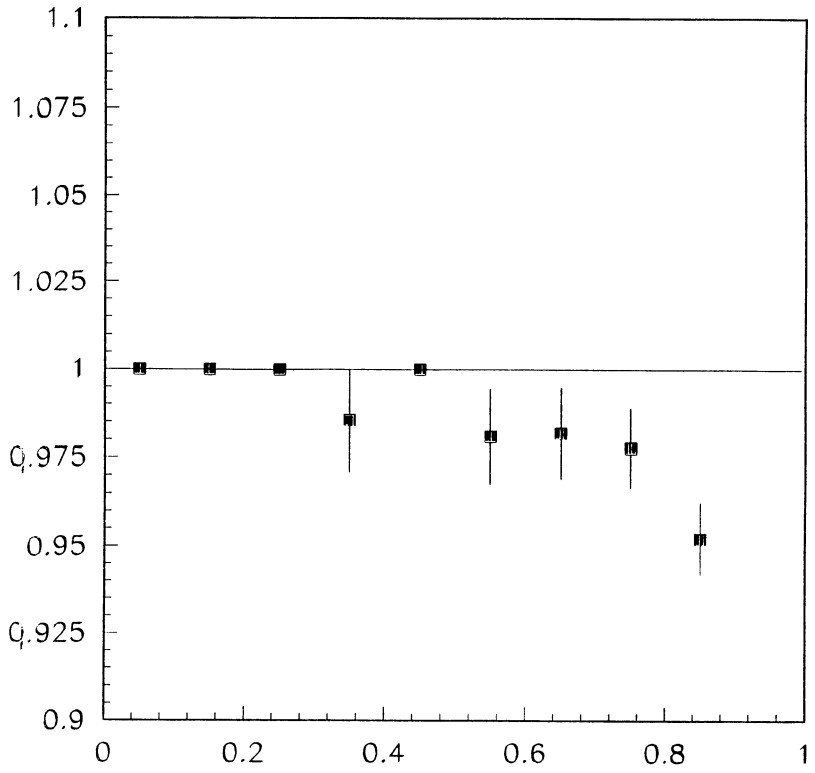
1.1
1.075
1.05
1.025
1
0.975
0.95
0.925
0.9
0
0.2
0.4
0.6
0.8
1

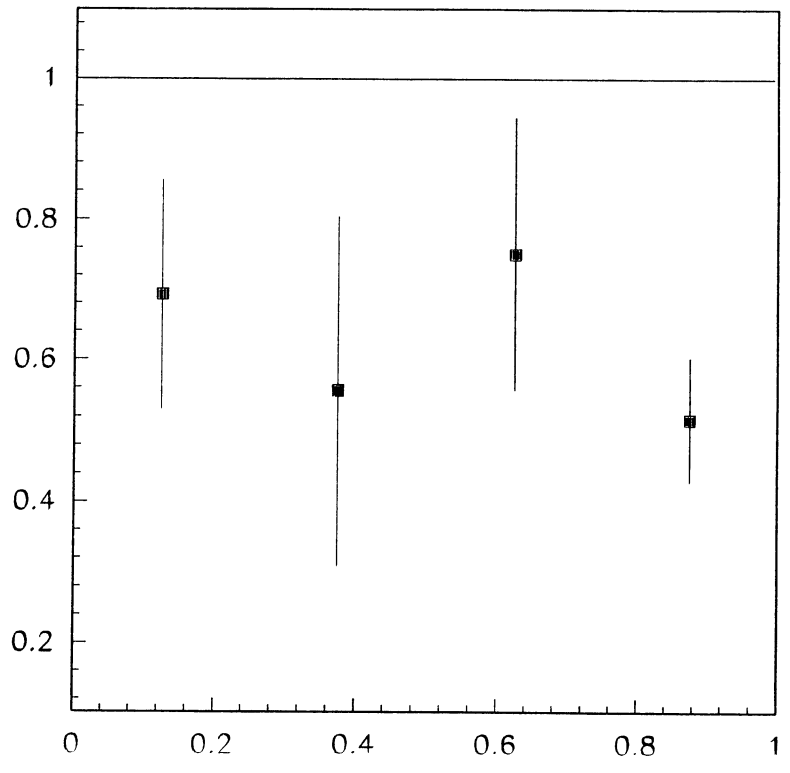
1
0.8
0.6
0.4
0.2
0
0.2
0.4
0.6
0.8
1

Fig. 44

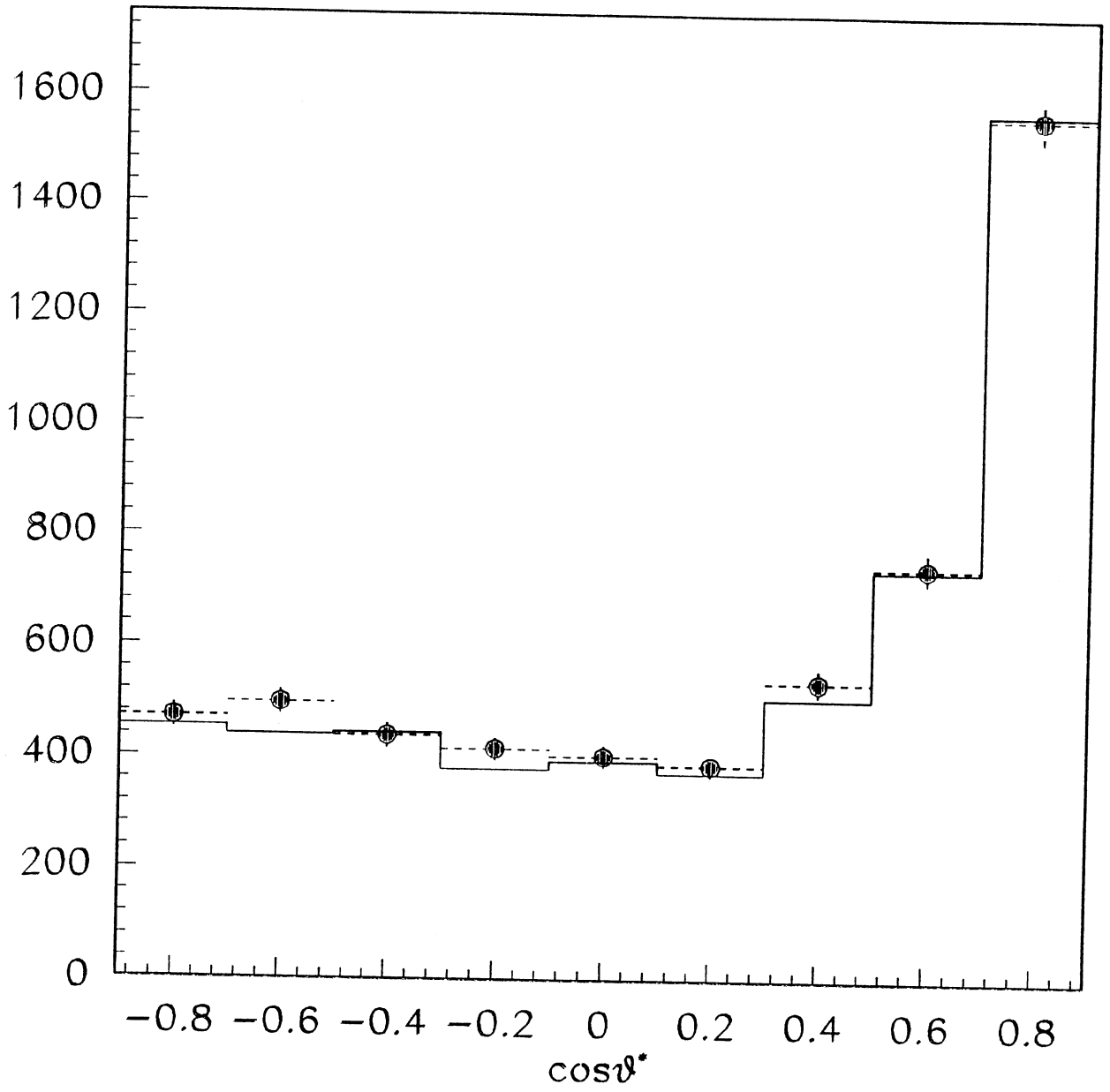
1600
1400
1200
1000
800
600
400
200
0
−0.8 −0.6 −0.4 −0.2 0 0.2 0.4 0.6 0.8
cosϑ*

Fig. 45

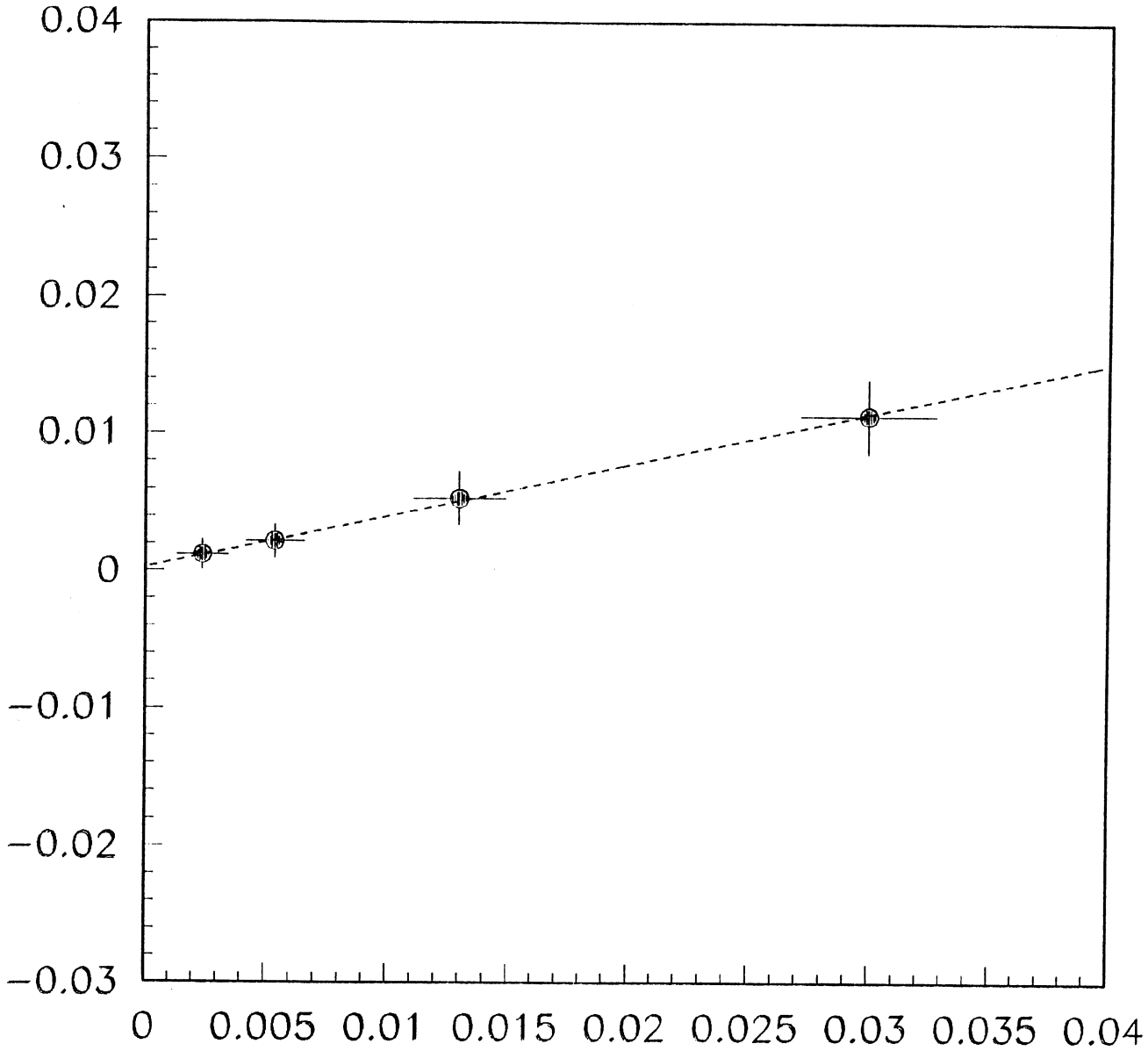
0.04
0.03
0.02
0.01
0
−0.01
−0.02
−0.03
0
0.005
0.01
0.015
0.02
0.025
0.03
0.035
0.04

Fig. 46

12-NOV-90 00:35:35

FCN	56.9844
1 a1	−0.97297
	+− 0.30311
a2	1.0000

cut in theta = 0.900
no. entries = 57

SQRT(s) = 88.280

asymmetry = −.364865
error = 0.113666

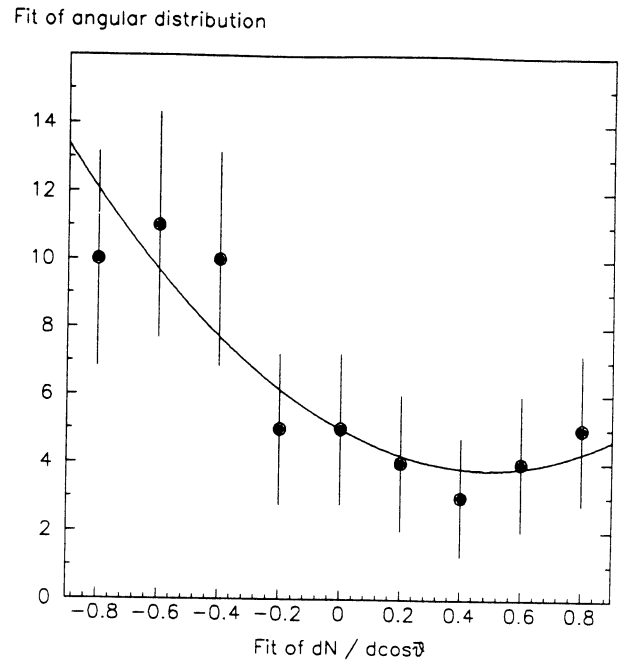

27-NOV-90 17:40:13

FCN	4442.09
1 a1	3.52778E−02
	+− 4.18113E−02
a2	1.0000

cut in theta = 0.900
no. entries = 3902

SQRT(s) = 91.280

asymmetry = 0.013229
error = 0.015679

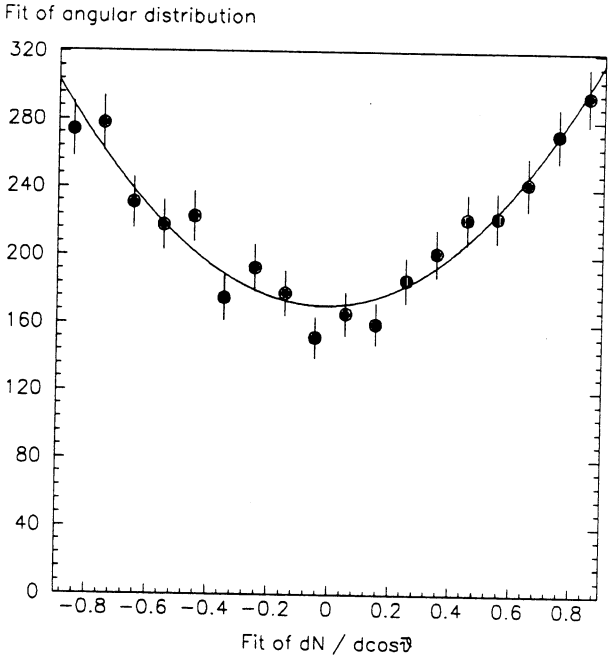

12-NOV-90 00:29:24

FCN	191.124
1 a1	0.70192
	+− 0.18307
a2	1.0000

cut in theta = 0.900
no. entries = 181

SQRT(s) = 94.280

asymmetry = 0.263219
error = 0.068652

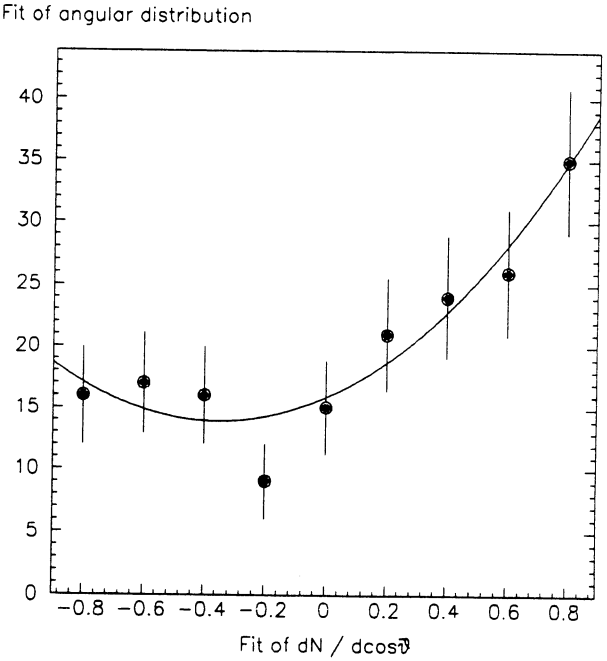

Fig. 47

29-NOV-90 22:51:55

FCN	4441.94
1 a1	3.55687E-02
	+- 4.24454E-02
2 a2	1.0444
	+- 3.87426E-02

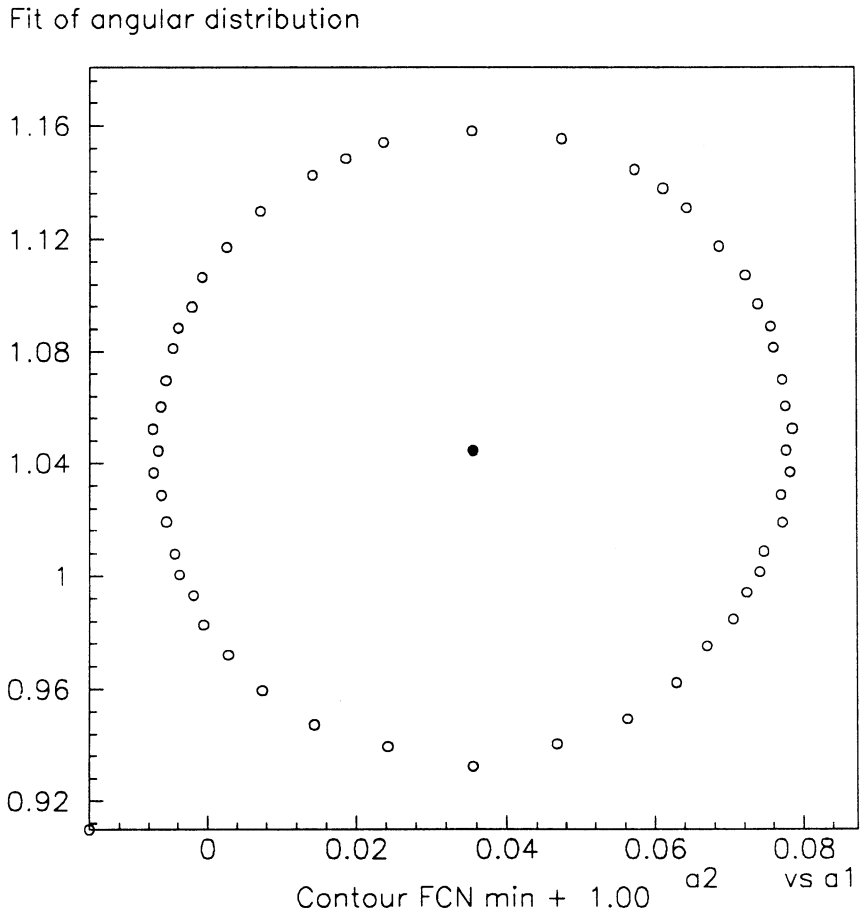

Fig. 48

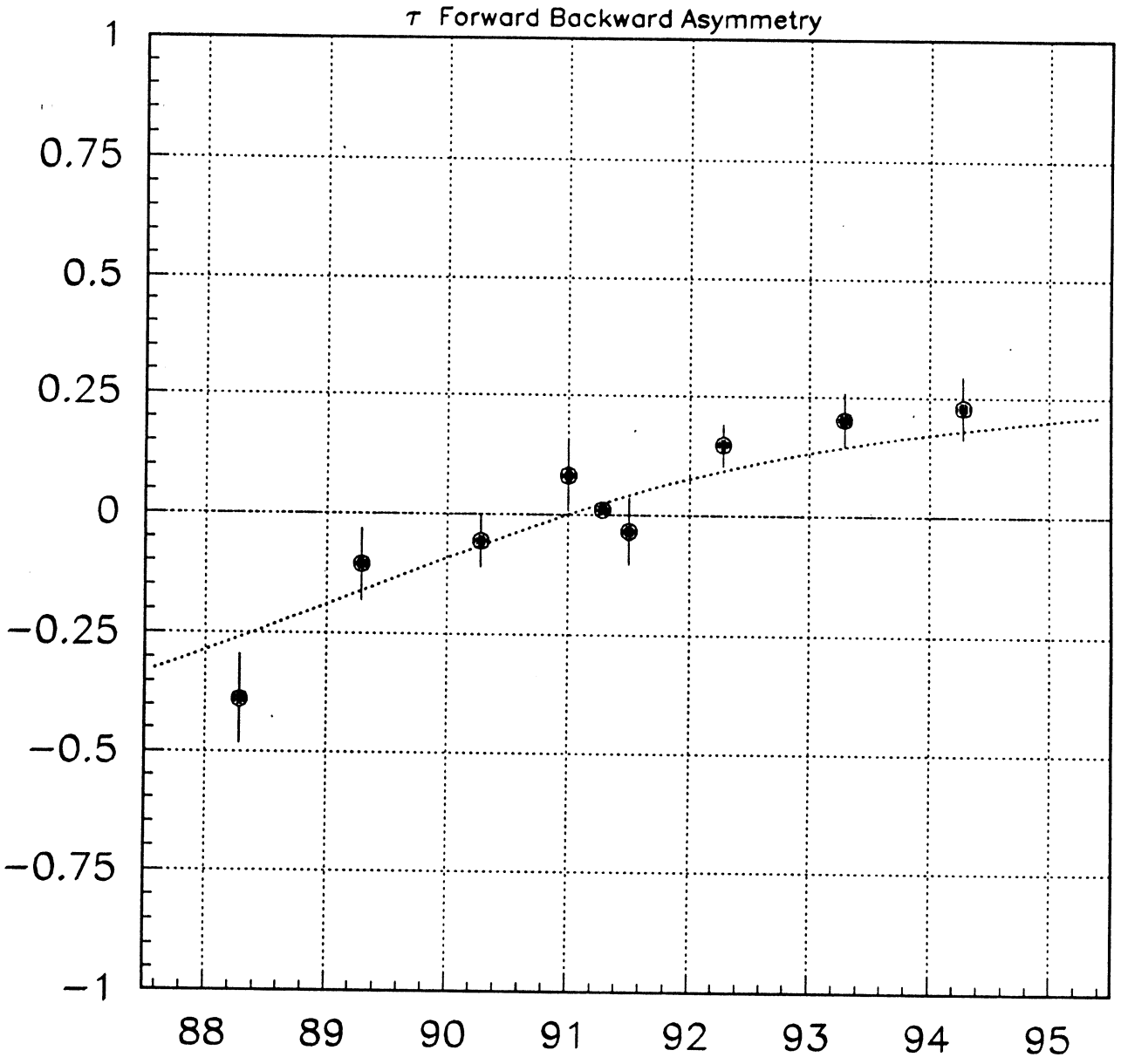
τ Forward Backward Asymmetry
1
0.75
0.5
0.25
0
−0.25
−0.5
−0.75
−1
88
89
90
91
92
93
94
95

Fig. 49

M C M L X X X I X
==========

88280
=====

Run	# lept.	# taus	luminosity
5154.	31.	4.	15.72
5155.	11.	1.	6.35
5156.	13.	4.	10.19
5382.	13.	3.	9.05
5383.	24.	3.	16.50
5384.	16.	3.	11.82
5385.	3.	0.	2.09
5871.	29.	4.	17.92
5875.	30.	9.	15.33
5876.	1.	0.	2.77
TOTAL	171.	31.	107.74

89280
=====

Run	# lept.	# taus	luminosity
5110.	6.	0.	4.10
5111.	23.	1.	13.30
5810.	52.	17.	26.96
5811.	2.	0.	1.78
TOTAL	83.	18.	46.14

90280
=====

Run	# lept.	# taus	luminosity
5060.	51.	11.	12.26
5061.	27.	5.	8.29
5062.	18.	2.	10.92
5063.	3.	1.	1.41
5519.	25.	4.	6.26
5520.	29.	8.	8.85
5521.	10.	2.	4.00
5527.	17.	1.	7.55
5532.	15.	6.	5.41
5533.	29.	5.	7.15
TOTAL	224.	45.	72.10

91000
=====

Run	# lept.	# taus	luminosity
5157.	37.	13.	7.26
5158.	42.	9.	8.62
5159.	41.	13.	7.37
5160.	29.	7.	6.88
5161.	9.	2.	1.89
5359.	42.	11.	9.00
5360.	48.	14.	11.15
5361.	5.	2.	1.32
5364.	32.	10.	8.17
5365.	36.	9.	7.71
5366.	20.	2.	4.65
5387.	25.	4.	8.85
5388.	17.	4.	5.56
5412.	24.	2.	7.64
5415.	25.	5.	4.80
5419.	22.	6.	4.16
5654.	19.	7.	4.61
5656.	5.	1.	1.63
5847.	36.	8.	9.91
5848.	42.	14.	9.42
5849.	41.	9.	9.91
5850.	8.	2.	2.68
TOTAL	605.	154.	143.19

91280
=====

Run	# lept.	# taus	luminosity
4981.	30.	7.	8.62
4982.	22.	3.	4.23
4987.	7.	1.	1.41
4988.	13.	4.	3.85
4989.	13.	3.	3.20
4990.	22.	3.	5.30
4991.	5.	2.	2.02
5166.	47.	20.	7.82
5167.	36.	13.	8.81
5168.	35.	7.	9.07
5169.	6.	2.	2.06
5328.	34.	6.	11.67
5337.	3.	1.	0.27
5502.	26.	1.	6.48
5504.	26.	7.	6.29
5505.	41.	14.	10.03
5506.	27.	10.	9.72
5507.	45.	12.	10.03
5659.	39.	9.	10.56
5660.	36.	8.	6.94
5666.	18.	4.	3.62
5795.	23.	4.	4.57
TOTAL	554.	141.	136.57

91500
=====

Run	# lept.	# taus	luminosity
5045.	2.	1.	0.35
5053.	18.	4.	3.27
5054.	1.	0.	0.96
5124.	37.	6.	7.19
5125.	48.	16.	9.19
5126.	24.	4.	5.11
5129.	33.	11.	6.27
5130.	23.	10.	5.38
5131.	40.	13.	10.65
5132.	5.	1.	1.12
5371.	20.	6.	5.04
5372.	31.	8.	9.38
5374.	4.	2.	0.92
5375.	19.	6.	3.46

APPENDIX

5512.	5.	3.	1.73
5513.	24.	7.	7.50
5514.	11.	1.	2.23
5516.	3.	0.	0.35
5517.	20.	3.	4.42
5820.	41.	6.	10.92
5821.	4.	1.	1.15
5823.	31.	10.	7.30
5824.	10.	1.	2.81
5825.	2.	2.	0.69
5826.	34.	8.	9.46
5827.	33.	10.	8.69
5828.	32.	7.	9.73
5829.	31.	9.	6.53
TOTAL	586.	156.	141.80

92280

Run	# lept.	# taus	luminosity
5000.	14.	4.	8.44
5001.	16.	3.	5.45
5002.	24.	6.	6.63
5170.	14.	2.	5.30
5171.	8.	2.	2.55
5173.	0.	0.	0.71
5175.	30.	6.	8.32
5176.	20.	6.	5.69
5509.	48.	13.	13.77
5510.	32.	7.	13.97
5511.	26.	10.	7.77
5906.	21.	7.	7.88
5907.	30.	12.	9.49
5908.	32.	13.	9.92
5909.	20.	4.	5.69
TOTAL	335.	95.	111.58

93280

Run	# lept.	# taus	luminosity
5075.	14.	0.	6.81
5076.	2.	0.	1.24
5077.	6.	1.	3.21
5078.	12.	2.	6.81
5657.	24.	10.	9.54
5658.	29.	5.	14.79
TOTAL	87.	18.	42.40

94280

Run	# lept.	# taus	luminosity
5145.	5.	0.	9.32
5146.	17.	8.	10.14
5147.	10.	1.	8.67
5831.	5.	2.	4.66
5842.	9.	3.	10.27
5843.	10.	2.	11.16
5844.	3.	1.	3.11
5883.	1.	0.	1.47
5885.	3.	1.	1.51
5886.	6.	2.	3.39
5887.	7.	1.	2.70
TOTAL	76.	21.	66.40

M C M X C

88280

Run	# lept.	# taus	luminosity
7393.	59.	7.	53.29
7394.	24.	1.	18.21
7681.	16.	3.	9.82
7682.	37.	2.	28.78
7684.	14.	0.	9.00
8011.	31.	4.	20.53
8013.	15.	1.	17.36
8359.	2.	0.	1.28
8361.	17.	4.	12.59
8363.	16.	0.	14.30
8364.	12.	0.	13.45
8365.	20.	1.	16.90
8366.	25.	8.	15.33
8367.	23.	4.	11.70
8680.	44.	10.	36.39
8681.	43.	7.	39.13
8682.	38.	4.	34.83
8683.	33.	2.	23.44
8960.	25.	1.	25.47
8970.	31.	5.	24.08
8971.	5.	0.	2.06
8972.	12.	0.	7.90
8974.	29.	2.	32.41
8975.	18.	2.	10.42
TOTAL	589.	68.	478.67

89280

Run	# lept.	# taus	luminosity
7346.	44.	8.	20.09
7347.	0.	0.	0.62
7410.	10.	1.	5.45
7412.	38.	7.	15.04
7413.	24.	2.	14.39
7414.	8.	0.	2.62
7415.	14.	2.	7.99
7416.	2.	0.	2.14
7588.	2.	0.	2.00
7589.	4.	0.	4.18
7590.	36.	7.	21.10
7649.	13.	3.	5.41

7966.	15.	1.	6.36
7967.	8.	4.	4.18
7970.	48.	6.	23.68
7971.	38.	8.	17.44
8157.	49.	4.	26.95
8158.	1.	0.	0.87
8161.	7.	1.	5.85
8163.	29.	6.	14.02
8610.	46.	7.	25.47
8611.	18.	4.	11.48
8613.	38.	4.	22.01
8880.	24.	7.	11.29
8885.	40.	6.	22.01
8886.	51.	4.	30.07
8887.	74.	8.	39.77
8888.	32.	5.	18.38
9078.	53.	11.	34.94
9079.	26.	8.	10.71
9083.	56.	13.	28.58
9084.	44.	8.	25.86
9085.	63.	13.	35.59
TOTAL	955.	158.	516.54

90280

Run	# lept.	# taus	luminosity
7252.	49.	13.	16.40
7253.	48.	12.	18.44
7254.	59.	15.	17.07
7255.	53.	12.	18.92
7256.	8.	2.	3.86
7534.	28.	4.	7.72
7858.	78.	10.	24.46
7859.	83.	23.	26.65
7860.	23.	5.	7.09
8115.	81.	15.	22.78
8118.	66.	15.	20.74
8119.	65.	14.	24.79
8120.	10.	3.	2.75
8121.	49.	16.	15.92
8122.	18.	1.	4.97
8124.	19.	5.	6.16
8489.	56.	19.	22.23
8490.	50.	9.	14.25
8493.	88.	13.	26.45
8494.	96.	20.	28.01
8495.	73.	19.	24.38
8496.	62.	17.	17.92
8803.	77.	16.	25.52
8804.	63.	16.	20.92
8805.	73.	8.	25.45
TOTAL	1375.	302.	443.85

91280

Run	# lept.	# taus	luminosity
6898.	14.	1.	4.20
6931.	19.	11.	4.12
6934.	80.	25.	18.33
6935.	24.	6.	4.43
6937.	38.	10.	9.47
6938.	2.	1.	0.76
6939.	37.	12.	8.13
6945.	21.	4.	8.55
6946.	7.	2.	1.95
6947.	49.	11.	14.66
6950.	30.	8.	7.18
6965.	42.	7.	8.06
6969.	33.	9.	6.95
6972.	78.	20.	17.15
6974.	68.	19.	18.67
6975.	30.	6.	10.42
6976.	2.	0.	0.69
6978.	19.	8.	3.40
7089.	56.	12.	13.67
7090.	11.	0.	1.72
7091.	8.	2.	1.30
7109.	9.	0.	2.75
7110.	106.	31.	18.67
7112.	21.	6.	4.70
7114.	27.	7.	7.45
7132.	34.	9.	5.15
7142.	32.	8.	5.19
7152.	48.	9.	12.07
7153.	8.	4.	2.25
7154.	29.	8.	7.71
7235.	56.	12.	13.87
7236.	8.	4.	1.11
7237.	60.	18.	15.58
7238.	54.	13.	12.11
7239.	20.	8.	4.16
7261.	57.	15.	10.35
7263.	7.	0.	1.64
7271.	18.	4.	2.67
7299.	95.	25.	19.21
7314.	23.	9.	7.26
7317.	28.	12.	6.03
7335.	76.	23.	17.34
7338.	90.	23.	17.57
7339.	80.	20.	14.86
7340.	45.	8.	10.05
7341.	4.	1.	1.11
7365.	28.	12.	5.84
7369.	44.	12.	9.47
7370.	40.	13.	9.05
7371.	30.	7.	6.49
7388.	23.	2.	3.47
7396.	84.	19.	20.20
7397.	79.	23.	18.64
7398.	84.	28.	19.70
7399.	11.	4.	2.44
7418.	64.	19.	15.50
7419.	7.	1.	2.37
7421.	35.	14.	7.60
7422.	50.	20.	13.33
7423.	65.	17.	11.91
7424.	28.	7.	8.21
7425.	18.	1.	5.04
7427.	20.	6.	4.54
7540.	30.	7.	9.09
7541.	47.	13.	13.06
7542.	62.	15.	12.49
7543.	62.	17.	11.42
7544.	31.	9.	7.06

7671.	67.	19.	18.86
7672.	17.	7.	4.51
7673.	14.	4.	3.32
7674.	54.	12.	11.53
7675.	16.	7.	4.39
7678.	20.	7.	4.09
7707.	11.	4.	2.44
7708.	34.	4.	5.23
7711.	94.	17.	20.35
7712.	60.	11.	18.48
7713.	34.	14.	7.33
7716.	36.	9.	5.96
7743.	94.	24.	23.75
7744.	82.	23.	20.43
7745.	67.	28.	15.12
7767.	68.	14.	14.82
7815.	29.	7.	8.13
7816.	9.	6.	1.76
7820.	5.	1.	0.50
7849.	97.	24.	19.44
7850.	79.	20.	19.21
7864.	35.	5.	7.87
7884.	61.	15.	14.78
7885.	74.	26.	18.87
7898.	83.	22.	18.10
7899.	7.	1.	3.21
7900.	89.	28.	20.47
7907.	94.	21.	24.21
7908.	15.	4.	3.82
7959.	85.	26.	19.09
7960.	101.	29.	23.25
7961.	42.	13.	12.41
7962.	43.	9.	11.15
7982.	61.	18.	16.23
7983.	75.	25.	18.14
7984.	65.	15.	17.03
8001.	1.	1.	1.07
8003.	56.	20.	14.59
8004.	43.	12.	9.28
8005.	72.	12.	15.73
8006.	61.	17.	16.23
8007.	12.	5.	3.32
8008.	4.	1.	1.68
8016.	59.	11.	13.17
8017.	8.	3.	1.57
8018.	52.	11.	17.30
8019.	72.	24.	16.15
8022.	61.	12.	18.37
8023.	17.	2.	2.10
8025.	1.	0.	0.95
8038.	60.	11.	13.52
8039.	84.	25.	17.87
8040.	30.	11.	8.82
8086.	64.	21.	16.23
8087.	68.	23.	17.00
8088.	68.	23.	17.07
8089.	27.	6.	4.47
8092.	9.	1.	2.60
8110.	80.	18.	18.68
8111.	78.	22.	17.07
8112.	68.	16.	18.68
8113.	57.	15.	11.99
8127.	87.	28.	19.78
8128.	103.	27.	20.51
8129.	4.	1.	0.99
8130.	92.	18.	20.55
8132.	22.	5.	5.00
8133.	41.	9.	12.83
8152.	62.	16.	14.01
8153.	26.	7.	6.19
8220.	16.	1.	3.97
8221.	1.	1.	0.76
8222.	45.	21.	8.21
8328.	41.	14.	8.90
8329.	36.	10.	5.88
8330.	16.	3.	2.86
8331.	42.	8.	9.89
8333.	34.	7.	9.24
8334.	61.	16.	13.03
8335.	35.	16.	11.15
8336.	23.	4.	4.81
8357.	21.	3.	7.52
8374.	16.	2.	3.74
8376.	46.	13.	13.14
8377.	67.	23.	13.86
8378.	18.	4.	6.68
8382.	82.	23.	16.34
8383.	65.	21.	16.23
8384.	59.	11.	13.10
8385.	18.	6.	5.73
8419.	49.	14.	8.29
8420.	36.	10.	9.74
8423.	3.	0.	0.57
8424.	16.	5.	4.39
8477.	77.	24.	18.67
8478.	18.	2.	4.51
8479.	25.	8.	7.14
8480.	30.	7.	6.95
8482.	85.	23.	20.47
8483.	85.	18.	19.51
8484.	89.	27.	18.67
8485.	42.	12.	8.86
8502.	82.	23.	22.45
8503.	104.	21.	23.48
8504.	103.	21.	23.33
8505.	92.	25.	24.90
8506.	23.	9.	4.73
8508.	45.	19.	9.16
8533.	8.	1.	1.41
8534.	3.	1.	0.53
8537.	123.	30.	23.87
8539.	46.	13.	13.71
8540.	3.	1.	0.92
8541.	79.	14.	20.39
8542.	4.	0.	1.22
8617.	34.	13.	6.76
8618.	84.	24.	19.17
8619.	55.	18.	11.34
8620.	18.	7.	5.61
8622.	88.	31.	20.89
8623.	18.	5.	4.16
8626.	70.	12.	21.65
8627.	38.	9.	9.05
8664.	97.	26.	19.02
8665.	82.	19.	21.00
8666.	40.	15.	9.16
8691.	75.	17.	19.95
8692.	83.	23.	20.41
8693.	72.	26.	17.12
8694.	54.	20.	13.80

8695.	109.	29.	19.53
8696.	25.	4.	5.62
8700.	72.	20.	20.29
8701.	41.	12.	10.85
8771.	68.	21.	16.92
8773.	77.	17.	17.38
8774.	37.	11.	9.47
8775.	115.	33.	21.31
8776.	16.	6.	3.67
8791.	73.	17.	19.24
8792.	88.	21.	21.19
8793.	85.	30.	20.28
8794.	98.	26.	22.60
8795.	89.	25.	22.30
8796.	93.	26.	20.43
8797.	70.	14.	18.94
8798.	7.	2.	2.41
8827.	33.	9.	5.69
8833.	71.	19.	16.76
8834.	98.	29.	22.41
8835.	88.	25.	22.07
8836.	91.	16.	21.53
8837.	24.	9.	6.26
8865.	63.	14.	15.31
8866.	41.	9.	10.23
8869.	83.	20.	16.53
8870.	71.	19.	20.50
8871.	94.	30.	20.77
8872.	88.	25.	22.64
8873.	97.	26.	21.53
8874.	104.	35.	24.63
8875.	95.	20.	23.75
8876.	20.	6.	6.41
8877.	42.	13.	9.47
8893.	71.	16.	16.72
8894.	70.	17.	18.21
8895.	78.	15.	16.65
8896.	75.	22.	19.32
8898.	91.	23.	21.27
8899.	102.	23.	22.64
8900.	101.	20.	22.49
8902.	2.	0.	0.46
8904.	105.	32.	24.55
8905.	93.	36.	24.32
8906.	33.	11.	10.19
8907.	129.	41.	22.98
8908.	2.	0.	0.46
8942.	14.	2.	4.16
8947.	67.	20.	19.89
8948.	35.	9.	9.74
8979.	90.	27.	22.03
8980.	79.	12.	22.15
8983.	79.	23.	19.78
8984.	108.	25.	19.86
8985.	65.	20.	15.27
8986.	85.	17.	22.34
8987.	72.	17.	13.63
9002.	112.	33.	24.51
9003.	40.	11.	8.32
9009.	83.	19.	21.37
9010.	91.	24.	21.18
9011.	106.	21.	20.91
9012.	89.	25.	23.74
9013.	57.	11.	12.06
9014.	98.	23.	23.43
9015.	22.	7.	3.74
9041.	83.	18.	21.65
9042.	116.	37.	22.41
9049.	15.	5.	4.93
9067.	125.	31.	24.51
9068.	118.	38.	25.39
9069.	107.	29.	24.93
9070.	82.	28.	23.06
9071.	92.	23.	23.97
9072.	99.	26.	22.29
9073.	52.	14.	13.70
9093.	67.	18.	18.63
9094.	6.	2.	1.30
9095.	82.	23.	18.40
9096.	77.	23.	16.57
9097.	61.	18.	18.25
9098.	54.	13.	12.71
9101.	30.	8.	6.49
9103.	14.	3.	2.44
9107.	87.	23.	17.49
9108.	28.	5.	5.57
9110.	79.	20.	22.18
9111.	31.	7.	9.89
9113.	89.	22.	17.83
TOTAL	15435.	4144.	3629.12

92280

=====

Run	# lept.	# taus	luminosity
7324.	17.	3.	5.47
7327.	29.	2.	9.75
7751.	43.	11.	11.79
7753.	49.	19.	19.74
7755.	13.	4.	3.18
8028.	27.	8.	9.99
8034.	46.	13.	19.46
8035.	66.	21.	20.44
8036.	22.	5.	9.36
8513.	63.	25.	24.81
8523.	75.	19.	25.16
8526.	10.	4.	3.89
8842.	29.	7.	10.26
8843.	7.	3.	1.81
8844.	72.	15.	26.69
8845.	81.	22.	26.49
8846.	49.	9.	14.31
8847.	74.	16.	25.39
8848.	15.	9.	4.99
8851.	79.	31.	26.73
8852.	52.	14.	15.96
8853.	77.	27.	27.44
8854.	76.	19.	27.83
8855.	75.	18.	25.12
8856.	40.	16.	15.37
9059.	82.	19.	26.45
9060.	61.	14.	21.11
9061.	75.	19.	27.28
9062.	74.	22.	28.73
9063.	91.	23.	24.33
9064.	39.	12.	12.22

TOTAL	1608.	449.	551.55

93280

Run	# lept.	# taus	luminosity
7224.	19.	5.	9.16
7225.	11.	3.	2.97
7226.	7.	0.	1.89
7228.	22.	6.	7.35
7402.	11.	4.	11.09
7405.	31.	8.	22.90
7406.	18.	3.	10.00
7407.	27.	5.	13.18
7548.	28.	9.	15.63
7549.	37.	9.	21.05
7550.	10.	1.	5.62
7551.	40.	8.	19.68
7910.	60.	17.	32.26
7911.	25.	4.	11.17
8137.	12.	5.	8.92
8635.	44.	11.	23.58
8636.	48.	12.	21.57
8637.	25.	5.	15.47
8638.	53.	12.	26.43
8639.	48.	10.	24.71
8640.	16.	5.	6.59
8642.	50.	10.	27.00
8643.	43.	12.	19.00
8645.	7.	2.	2.97
8646.	6.	2.	7.67
8649.	43.	5.	29.93
8651.	48.	18.	29.49
8652.	8.	0.	3.66
8653.	8.	5.	5.10
8658.	19.	3.	12.09
8989.	44.	13.	28.11
8990.	35.	7.	19.92
8992.	58.	15.	30.24
8993.	59.	15.	32.77
8994.	42.	8.	32.01
8995.	2.	0.	2.01
TOTAL	1064.	257.	593.19

94280

Run	# lept.	# taus	luminosity
7380.	28.	6.	18.08
7381.	1.	0.	1.11
7382.	8.	1.	6.31
7730.	28.	7.	18.40
7731.	10.	0.	8.69
7737.	2.	1.	2.66
7877.	43.	15.	33.69
7987.	48.	14.	33.57
7988.	31.	6.	21.03
7994.	26.	4.	20.12
7995.	9.	2.	4.67
8452.	31.	11.	24.22
8455.	5.	1.	1.84
8457.	21.	8.	16.27
8782.	40.	11.	32.63
8783.	36.	7.	29.26
8784.	40.	10.	25.94
8785.	4.	0.	4.71
8786.	0.	0.	0.66
8787.	17.	2.	23.28
8788.	13.	2.	7.62
8812.	21.	2.	15.08
8815.	33.	7.	32.87
8816.	35.	9.	24.67
8817.	46.	13.	36.52
8818.	13.	1.	9.39
9018.	48.	18.	39.71
9019.	24.	5.	19.59
9024.	53.	15.	39.79
9025.	53.	14.	38.93
9026.	43.	10.	39.63
9027.	10.	1.	6.11
TOTAL	820.	203.	637.05